PROGRAMME

FOR

ATMOSPHERIC WATER SUPPLY
(PAWS)

PHASE 2: 1987 - 1989

FINAL REPORT

VOLUME 2

Aircraft and radar measurements and cloud seeding experiments

Report to the
Water Research Commission
Pretoria, South Africa

by

G.K. Mather
CloudQuest (Pty) Limited

Griffith Morgan, Jr.
CSIR

March 1990

133/6/90

ISBN : 0 947447 62 8
Set No. : 0 947447 64 4

TABLE OF CONTENTS

LIST OF TABLES

LIST OF FIGURES

1.0 SUMMARY

The past 3 years have been important ones for the PAWS (Programme for Atmospheric Water Supplies), the research programme sponsored by the Water Research Commission to investigate the feasibility of augmenting the country's critical water supplies by cloud seeding. Some of the most important accomplishments of the past 3 years are listed below:

- completion of the 3rd season of the randomized cloud seeding experiment at Nelspruit and the initial analyses of the results

- the move of the project radar to Carolina, closer to the area where a successful technology is likely to be applied and the acquisition of a full season of radar data from the new site

- the development of cloud physics instrumentation, used for the first time at Nelspruit, which is capable of measuring the large quantities of water stored in the local clouds. The ability to discern between small water drops and ice crystals while flying at jet speeds means that the natural precipitation formation mechanisms can be revealed and documented. These measurements have led to the conviction that a successful rainfall augmentation technology must be based upon the ability to increase the efficiency of the natural rainfall processes

- developing the capability of measuring storm rainfall from a mobile platform. The WRC cloud base aircraft has been equipped with a laser probe which measures the concentration and size distribution of rain drops. These data, combined with measurements of vertical air motions, will produce accurate estimates of rain rates along the track of the aircraft through the sampled showers. Concurrent recording of reflectivities from the aircraft's radar will be used to supplement the probe measurements. It is hoped that successful development of this essential tool will obviate the necessity of an extensive surface network of recording rain gauges

- an expanding programme of collaboration with the Bethlehem Precipitation Research Project (BPRP). The resources (manpower, equipment and money) that can be focused on rainfall augmentation research is limited, therefore it is incumbent upon the participants in this vital field of research to make maximum use of the available resources

- the Berg-en-Dal workshop held in the Kruger National Park in August, 1989. This workshop, attended by notable overseas scientists, South African scientists working directly in the

field of weather modification, and leading advisors and administrators, was the most intensive examination of the National progress in weather modification to date. The recommendations that emerged from this workshop are of great value, and will significantly affect the future course of weather modification research in this country.

The following report is divided into three main sections:

- the seeding experiment
- aircraft measurements
- the project radar and radar measurements

2.0 THE NELSPRUIT RANDOMIZED SEEDING EXPERIMENT.

2.1 The third experimental season - 1986/87.

The randomized seeding experiment which was reported on in Volume I, III and IV of the PAWS Phase 1 Final Report for the 1983-1986 period (WRC Reports 133/1/88, 133/3/88 and 133/4/88 respectively) was continued for a third year, with one important new element, a double-blind procedure. The experiment was in other ways identical to the previous two years. We will present here a brief description of the double-blind procedures.

The seed/no seed decisions during the first two years of the Nelspruit seeding experiment were announced by the radar operator, who opened a series of sealed envelopes (prepared by the WRC in Pretoria) after the pilots had found a suitable target. To avoid possible biases arising from knowledge of treatment, a "double-blind" seeding technique was developed for the third year of the experiment. Neither aircrew nor radar operators were aware of the treatment until the analyses were complete.

The paired lists of randomized seed/no seed and sample/no sample instructions held by the WRC in Pretoria were sent to the CSIR, also in Pretoria. Here, the instructions on the two lists along with the case numbers were placed into a read only memory (ROM) which was then sent to Nelspruit. This ROM was installed in the Learjet's computer. A control system was built from which the case numbers were keyed into the computer. The computer then activated the seeding bins or not, depending upon the instructions in the ROM. No seed/no sample decisions were signalled by the illumination of an amber light on a control panel. This system in effect transferred seed/no seed decisions tasks from the radar operator, now blind as to treatment, to the computer. Keeping the aircrew blind was accomplished by building a skirt around the base of the seeding bins so that the mechanism driving the seeding system could not be seen. A loud undercarriage warning horn sounded when the pilot's seeding button was pressed, effectively masking the sounds of the seeding drive system and the noise of the dry ice pellets striking the exit chutes.

The output from the sensors in the dry ice chutes along with the case numbers and treatment were encoded on the instrumentation system's data tape. This information was not available during playback of the cloud physics measurements, but had to be decoded using separate software.

Since knowledge of treatment could have been gained by examining the contents of the dry ice seeding bins after landing, all dry ice was expelled on the descent after a mission by a dump switch on top of the control panel which activated both seeding drive systems and the horn.

2.2 The seeding experiment - a review

The Nelspruit randomized cloud seeding experiment was designed to test the hypothesis that there would be radar detectable differences between seeded and unseeded storms. Since the nature of any differences between seeded and unseeded storms was unknown, the experiment was designed to detect and to learn how best to measure such differences. This was the exploratory, but very important, facet of the experiment. For it was hoped that such differences, properly interpreted, would assist in the search for a rational seeding hypothesis that could be rigorously tested by physical measurements and a follow-on confirmatory experiment. With a clear understanding of the chain of events leading to rainfall increases, the anticipated responses would be specified prior to the commencement of a confirmatory experiment.

A storm tracking scheme had to be developed, since the experimental design required objective comparisons of storms. The software to carry out this task was developed and tested for two seasons prior to the commencement of the experiment. It was during these tests that the experimental unit was chosen; the isolated multicell convective storm. Seeding trials led to the selection of dry ice as the seeding agent.

The experimental design is detailed in Volume III (WRC Report No 133/3/88). Only a brief review will be given here. The experiment was a three-way randomized design; clouds that were:

- seeded and sampled	(50%)
- not seeded, but sampled	(25%)
- not seeded and not sampled	(25%)

The no seed category was split into two because of the concern that aircraft produced ice crystals (APIPs) might contaminate the experiment. Pilots, scrambled by the project radar and directed to the storm of interest received treatment instructions from the radar operator only after declaring the storm in question an acceptable experiment.

The experiment progressed for two seasons without any changes in design. It was during this period that the following data stratifications were developed

- storm volumes at decision time had to be equal to or less than 750 km^3. This was adopted because the storm tracking scheme occasionally tracked squall lines, only a small part of which was the experimental storm

- average storm track positions had to be contained within an annulus 10 to 80 km radius from the radar

- storms had to be growing in a thermodynamic environment in which the ratios of cloud base temperature to buoyancy at 500 mb ratios were 2.0 or greater. This stratification was first developed from an examination of cloud physics measurements and served to roughly separate those clouds that were likely to develop coalescence products (drops) at around -10°C from those that were not. It was only after the end of the second experimental season that this stratification was applied to the radar data, with exciting results, some of which will be shown later.

At the end of the second season, the experiment was carefully reviewed, and a suggestion to conduct an "in house" experiment for the third season was implemented. Those track properties that had apparently responded to treatment for two seasons and were therefore expected to respond in a third were published in Table 3.4 in Volume III of the PAWS Phase I report, (WRC 133/3/88) before the commencement of the third season. The outcome of this very important exercise is reviewed below.

2.3 Statistical analyses

The following updates the analysis of the seeding experiment contained in Volume III, section 3 of the PAWS I report (WRC 133/3/88) with the addition of a third season of data.

(a) The "in-house" experiment

It was felt at the end of the second experimental season that sufficient experience had been gained to declare an "in house" confirmatory experiment. This was done by stating those radar-derived storm track properties which were expected to respond in a third season of experimental seeding.

The storm tracks were analysed in precisely the same manner as in the previous two seasons and the same stratifications were applied in the statistical analyses. Case tracks were accepted whose:

- storm volumes at decision time were less than 750 km^3
- average tracks were between 10 and 80 km from the radar
- environmental T_{ccl} /buoyancy at 500 mb ratios(measured
- by the Learjet sounding) equalled or exceeded 2.0.

Table 2.3.1 shows the track properties listed in Table 3.3, Vol. III as well as their associated "p" values for:

- 1984/85 season
- 1985/86 season
- 1984/5 and 85/86 combined
- 1986/87 season
- all three seasons combined

Table 2.3.1 Significance (p) levels of various track properties, season 84/85, 85/86 and 84/85, 85/86 combined; 86/87 and 84/85, 85/86, 86/87 combined.

PROP NO.	84/85	85/86	Combined	86/87	Combined
0 to 10 min					
98	76	97	97	83	98
0 to 20 min					
66	87	79	93	84	98
155	95	94	100	84	100
160	80	89	93	88	93
164	86	100	100	98	100
0 to 30 min					
32	90	84	(94)	78	(92)
50	89	71	88	97	98
65	82	81	(93)	85	(85)
66	93	77	95	93	99
71	89	77	90	80	95
72	96	83	96	87	99
121	90	75	90	75	95
149	72	86	89	79	93
155	82	83	91	84	99
164	74	97	98	91	100
165	75	52	89	82	98

Again the test statistic is either the arithmetic or the geometric mean of the track property considered.

The values for the combined seasons indicate that all but two of the "p" values have either stayed the same or increased with the addition of the third (86/87) season. Circles indicate those "p" values that have decreased.

(b) Ten minute "time window" analyses

An analysis of 10 minute time intervals after decision time (0 to 10, 10 to 20 etc) was carried out on all case tracks. This exercise appears to be particularily sensitive in terms of revealing some of the physical changes that accompany the seeding.

The results of this analysis are listed in Table 2.3.2. All track properties listed here have achieved a "p" value of 95% or greater (5% or smaller). There appears to be a physically realistic chain of events that is being revealed by these statistics.

0 to 10		10 to 20		20 to 30		30 to 40	
PROP NO	DESCRIPTION	PROP NO	DESCRIPTION	PROP NO	DESCRIPTION	PROP NO	DESCRIPTION
93	$\frac{\text{Mean Mass}}{\text{Rain Mass}}$ - above C.O.	71	P_F @ 3° - Persis	35	Mass Time Integral	23	Depth - Persis
94	Centroid - MROI	72	P_F @ 3° - M.R.	36	Mean Mass	67	P_F @ 3° - Mass
95	Centroid - Persis	85	Precip H_2O - M.R.	65	P_F @ 3° - Max	68	P_F @ 3° - Mean
101	Z x Centroid - MROI	145	$\overline{Z}$ above C.O. - Persis	83	Precip. H_2O Time Integral	112	Centroid - Persis
105	Z x Centroid - Persis	152	H_{max} 45's - Persis	*94	Centroid - MROI	113	Centroid - M.R.
106	Z x Centroid - M.R.	154	$\overline{dBZ}$ = f(Ht) - MROI	119	Z_{max} - $\overline{MAX}$	*156	Ht Z_{max} - Mean
155	Ht Z_{max} - MROI			121	Z_{max} - $\overline{MEAN}$	160	" " - M.R.
164	$\overline{Mass}$ = f(Ht) - MROI			125	Z - $\overline{MAX}$	223	% Area = f(dBZ) - $\overline{MIN}$
				126	Z - $\overline{MEAN}$		* "p" value of 5% or less
				133	Z_{3e} - $\overline{MAX}$		
				135	Z_{3e} - $\overline{MEAN}$		
				140	$Z_{c.o.}$ - $\overline{MAX}$		
				142	$Z_{c.o.}$ - $\overline{MEAN}$		
				147	H_{max} 45's - MAX		
				*155	Ht Z_{max} - PERSIS		
				201	% Vol = f(dBZ) - $\overline{MEAN}$		
				202	" - $\overline{MAX}$		
				222	% Area = f(dBZ) - $\overline{MAX}$		

Table 2.3.2 Track properties analysed in 10 minute time blocks after decision time. Each listed track property had a "p" value that equalled or exceeded 95%.

0 - 10 minutes: Seeded storms are showing very strong increases in reflectivity aloft. This could be a dynamic reaction (the sudden release of latent heat increasing the updraft which is now capable of bringing more mass aloft, or alternatively, holding precipitation already forming aloft longer), or a microphysical response (an increase in the number of growing precipitation embryos aloft) or a combination of the two. Statistically, it is a very strong result. Properties 94, 98, 101, 106 and 164 (5 out of 8) have achieved "p" values of 98 percent or better.

10 - 20 minutes: This is the least active time slot judged by number of storm properties equalling or exceeding "p" values of 95 percent. It is between 10 and 20 minutes that we see the first sign of a change in rain flux at cloud base (71 and 72). Also seen is a change in the rate of precipitation generation, increasing in the case of the seeded storms (88). The other properties continue to indicate higher reflectivities aloft in the seeded storms (145, 152, 184).

20 - 30 minutes: Prior to this time slot, all but one of the radar detected changes between the seeded and unseeded storms have shown up in the persistence, max ratio or maximum rates of increase statistics. Now changes are seen in the maximum and the mean values, and most of these show up in the reflectivity (Z_e) measurements.

30 - 40 minutes: The flurry of activity shown in the previous time slot is largely over. However, it is satisfying to note that the seeded storms are now producing significantly more rain than their unseeded counterparts (properties 67 and 68).

A plot of the "p" values of all the track properties used in this time window analysis is shown in Fig. 2.3.1. The -10 min to 0 min histogram of "p" values is close to a uniform distribution. As time progresses from 0 to 10, 10 to 20 and 20 to 30 minutes, the distribution becomes more and more skewed to the right (positive "p" values). By 30 to 40 minutes, the distribution is again approaching a uniform distribution. The seeding rates shown in Fig. 3.3.0, of Report WRC 133/3/88 should be kept in mind when viewing these histograms. While this analysis is more qualitative than quantitative it is highly suggestive of a system receiving an input pulse, then after a lag, settling back to its original state.

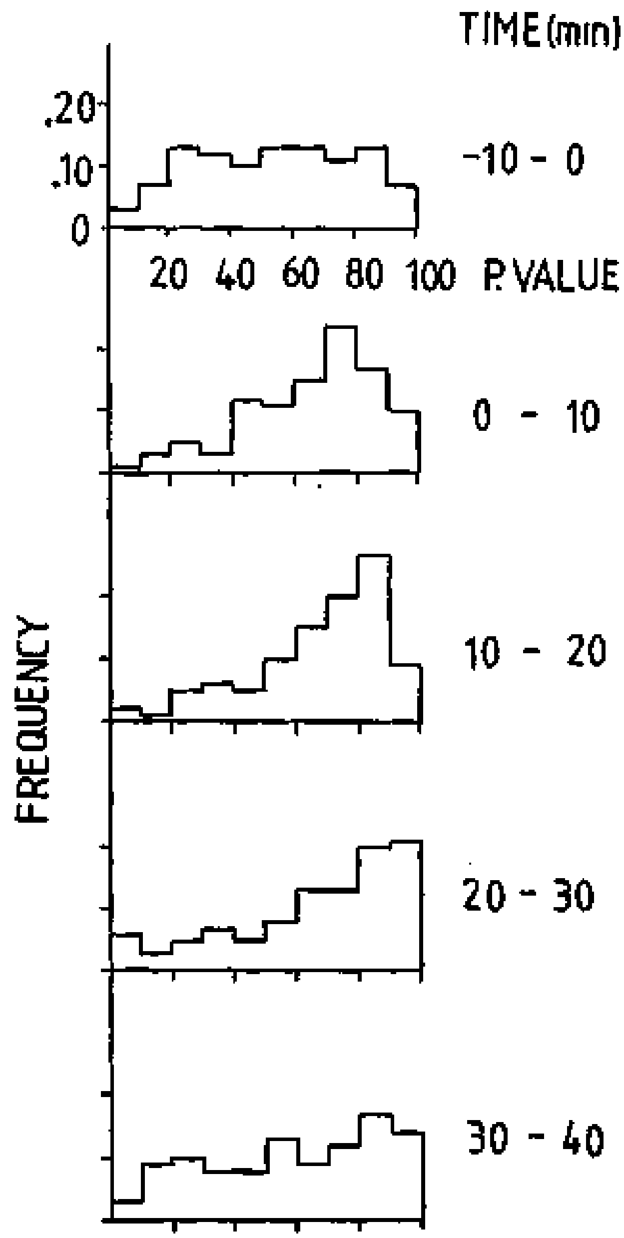

Fig. 2.3.1 Frequency histograms of the "p" values of track properties in ten minute time slots from decision time.

(c) The microphysical partitioning of the experimental data

This is perhaps one of the most important results of the 3 year experiment since it implies that those storms with a high probability of developing supercooled drops at around -10°C appear to be showing the strongest response to glaciogenic seeding. In review, the microphysical measurements in the Nelspruit clouds often reveal the presence of large (>1 mm diameter) drops at -10°C, indicating the presence of an active coalescence mechanism. It was discovered that the absence or presence of coalescence products at -10°C could be roughly defined by a ratio of the cloud base temperature to cloud buoyancy at 500 mb. The cloud base temperature is defined by the temperature at the convective condensation level (T_{ccl}) and the buoyancy at 500 mb is measured by the difference between a pseudoadiabat through the T_{ccl} and the environmental lapse rate (ΔT_{500}). When the ratio of the two ($T_{ccl}/\Delta T_{500}$) equals or exceeds 2.0, the probability is high that precipitation is forming via a condensation-coalescence process.

After the second season of the seeding experiment, this observation was applied experimentally to stratify the radar-acquired storms, eliminating those storms from the analysis which were unlikely to develop precipitation via the coalescence process. The results were dramatic. Many of the radar-measured variables that are believed to indicate a seeding effect showed marked increases (decreases) in probability levels. Table 2.3.3 which contains the full three seasons data set, illustrates this result.

Table 2.3.3 Results using the cloud base temperature/buoyancy ratio to stratify the radar data from the seeding experiment.

Stratification - Range 10 - 80 km,
- Volume at decision time: 0-750km^3

Minutes Mean	-10 to 0	0 to 10	10 to 20	20 to 30	30 to 40
Rain flux	4	-3	-12	-18	17
Storm Volume	1	-3	-15	-11	8
Storm area	2	-4	- 8	- 6	15%
<u>Cases</u>					
Seed	47	51	49	47	38
No seed	60	63	62	61	52

Stratification - Range : 10 - 80 km
- Volume at decision time: 0-750 km^3
- $T_{ccl}/\Delta T_{500}$: > 2.0

Minutes Mean	-10 to 0	0 to 10	10 to 20	20 to 30	30 to 40
Rain flux	27	17	17	32	76*
Storm volume	20	17	19	26	42*
Storm area	16	7	10	16	43* %
<u>Cases</u>					
Seed	38	40	39	38	31
No seed	47	49	47	47	39

*Significant at 0.05 or better

All percentages calculated from : $\frac{\text{Seed - No seed}}{\text{No seed}} \times 100$

Compared to the increase recorded during 0 to 10 minutes after decision time, the percentage increase in average rain flux from seed storms over that from no-seed storms has almost doubled by 20 to 30 minutes and more than quadrupled by 30 to 40 minutes after decision time. The percentage increase in storm volumes has just doubled over the same time interval. This suggests an increase in the efficiency of the rainfall process in the seeded storms. The relative increase in mean rain flux between 20 and 30 minutes can largely be accounted for by increases in 3 degree reflectivities, i.e. seeded storms producing more rainfall per unit area than their unseeded counterparts. By 30 to 40 minutes the fourfold percentage increase in rain flux of seeded versus unseeded storms is coupled with a similar increase in storm area.

The division of the storm case tracks into 10 minute time windows as in Table 2.3.4 produced additional insights. Perhaps the strongest apparent response to seeding (largest difference between seed and no seed storm tracks) occurs in the first 10 minutes following seeding in the radar-observed distribution of storm mass with height.

Table 2.3.4 Differences between radar-observed maximum rates of increase in mean storm mass with height; seed versus no seed storms.

Mass=f(Height)	-10 to 0	0 to 10	10 to 20	20 to 30	30 to 40min
Max. rates of increase	10	129*	66*	-10	3
Max. rates of decrease	-9	6	11	57*	8 %

*Significant at 0.05 or better

(d) Summary

In summary then, this statistical analysis of radar-derived storm track variables shows:

1. In the first 10 minutes after decision time, an increase in height of the centre of gravity in seeded storms.

2. This increase persists to 20 minutes after decision, showing up in the higher reflectivities detected aloft in the seeded storms.

3. The big changes between the seeded and unseeded storms at the surface (3 degrees) show up between 20 and 30 minutes. The observed increases in rainfall at first appear to be almost entirely due to an increase in radar reflectivity at 3 degrees.

4. By 30 to 40 minutes after decision time, the seeded storms are producing 76 percent more rainfall than the unseeded storms and cover 43 percent more area.

The chain of events apparently revealed by these statistics does not violate any physical principles in terms of permissible time rates of change. What is not clear is whether the changes are brought about through "dynamic" or "static" changes in the seeded clouds. Increases in the height of centres of gravity of the seeded storms in the first ten minutes suggest a dynamic reaction; more rainfall per storm area (greater rainfall efficiency) evokes the static concept of seeding-induced rainfall increases.

At this stage, the feeling here is that the observed reaction is a combination of both reactions. Support for this assertion must come from additional cloud physics measurements.

2.4 Confirmatory experiment

(a) Introduction

The new confirmatory seeding experiment at Nelspruit differs in two major aspects from the first experiment. The radar has been relocated to Carolina and the previous 3 way randomization has been reduced to a 2 way scheme; seed and sample versus no-seed/no sample. The latter change was brought about because of the suspicion that aircraft-produced ice particles (APIPs) were affecting the no-seed/sample storm category.

The design of the confirmatory experiment is contained in Appendix I of this report. This plan was slightly altered because of the roughness of the runway at Carolina, which prevented routine landings at this airport with the cloud base aircraft. Radar operators were required to drive to Carolina on "go" and "standby" days, leaving Nelspruit at 09:00 a.m. This decision was implemented by generating an earlier forecast.

A total of just 27 experiments were conducted during this first season. The season was remarkable for its lack of the usual convective activity.

(b) Results

While 27 experiments are not enough to produce statistically significant results, nevertheless, the data to date are examined for any trends that may be emerging at this early stage of the experiment.

Of the 27 experiments, just one was rejected because of doubts about the track of the test storm. All the other storms were accepted as valid experiments. Figure 2.4.1 shows the average location of the tracks of the 26 experimental storms from Carolina (the centre of the plot).

Selected overall seed versus no-seed storm track properties are compared in Table 2.4.1 for all cases and those cases in which the cloud base temperature/500 mb buoyancy ratio equalled or exceeded 2.0. The same trend shows up here that was noted in the first experiment; an increase in the percentage differences and statistical significances of the seed versus no-seed differences when cases with a cloud base temperature/500 mb buoyancy ratio of less than 2.0 are eliminated from the analysis.

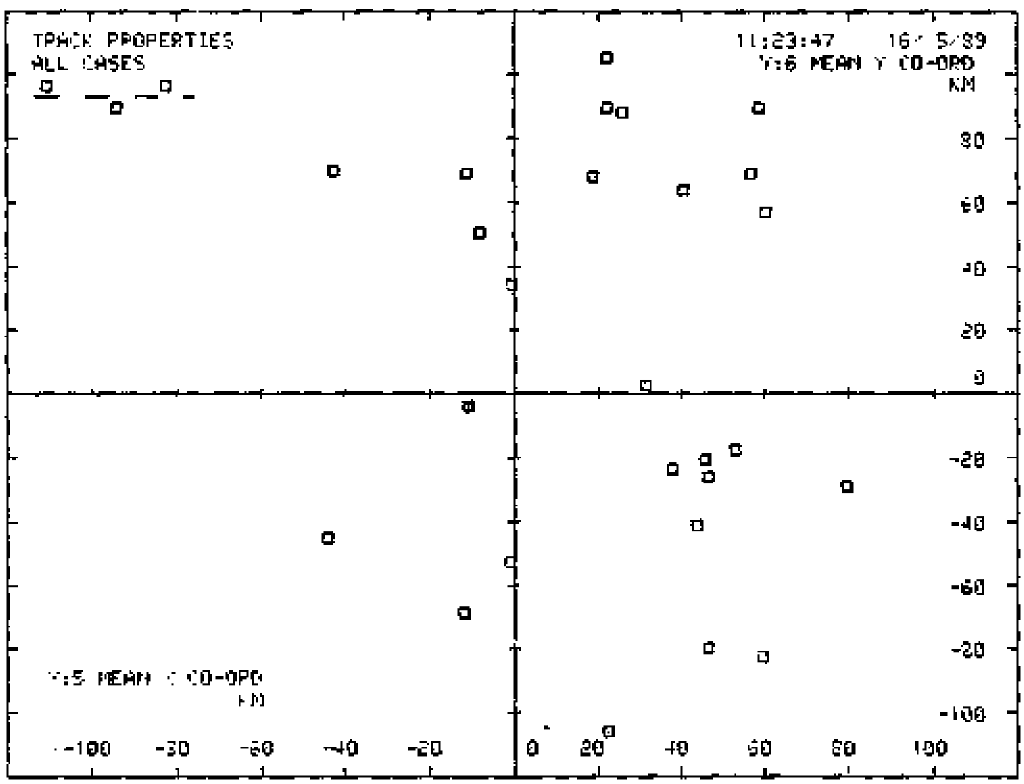

Fig. 2.4.1 Average positions of storm tracks accepted as experiments, 1988/89 season. The figure is centred on the Carolina radar.

Table 2.4.1 Seed versus no seed comparisons for selected storm track properties for all cases and for those in which cloud base temperature/500 mb buoyancy ratios equal or exceed 2.0.

	ALL TRACKS S=15, NS=11		$T_{CB}/\Delta T_{500}$ > 2.0 S=11, NS=7	
	Means *Difference	p value	Means Difference	p value
TRACK PROPERTY	%	%	%	%
ECHO TOP - MROI **	- 17	22	19	75
MEAN VOLUME	- 8	41	4	56
MEAN AREA	15	68	24	80
RAIN MASS	12	58	24	67
MEAN RAIN FLUX	15	63	20	70
dBz = f(Ht) MROI	- 7	37	28	80
dBz = f(ht) MROD ***	- 18	23	18	80
DURATION	- 1	48	13	66

$$* \quad \frac{\text{SEED - NO SEED}}{\text{SEED}} \times 100$$

** Maximum rate of increase

*** Maximum rate of decrease

Care should be taken in interpreting any results from the experiment at this stage. Experience has shown that 100 valid cases (roughly 50 seed, 50 no seed) are required before the statistical results stabilize. Until this stage in the experiment is reached, results at 25 cases could easily be reversed with the addition of another 25 to 50 cases.

(c) Reasons for suspension

At the recent Berg-en-Dal workshop (August, 1989) it was pointed out that no matter how often an experiment is repeated and a statistical result obtained, the result of the experiment will not be fully accepted until the physical mechanism driving the observed (statistically significant) change is understood. It was agreed that the confirmatory seeding experiment at Nelspruit should be suspended and all efforts concentrated on developing a seeding hypothesis.

3.0 AIRCRAFT MEASUREMENTS

3.1 Estimates of precipitation embryo densities using measurements from an aircraft radar.

(a) Introduction

The growth of precipitation in mixed phase (water and ice) convective clouds is usually attributed to one of two processes: ice crystal growth by vapour diffusion followed by riming growth as graupel, or the growth of drops by condensation and coalescence, which then freeze and continue to grow by riming into high-density graupel particles. An understanding of which process dominates in a region should be a prerequisite of serious attempts to alter (augment) local precipitation.

Determination of the approximate densities of particles whose images are gathered by 2D laser imaging probe in cloud physics measurement programmes would provide valuable information on the origins and growth habits of particles. Supercooled water drops and recently frozen drops that are undergoing rapid growth by riming should have distinctly different densities from ice crystals that are just beginning to rime, although their 2D images may appear quite similar; this should be especially so in the early stages of their riming growth.

Measurements made in vigorously growing convective clouds at around -10^{o}C by the Nelspruit cloud physics Learjet have failed to detect ice crystals at the early stages of precipitation growth in the local clouds. Rather, round images of either graupel, or supercooled or recently frozen drops are observed (Mather et al., 1986). Recently, estimates of the densities of these particles have been made by comparing equivalent radar reflectivity factors measured by an on-board radar to reflectivities calculated from the 2D-C images over a range of densities. The best match is taken as an estimate of the average particle density.

Since the difference in reflectivity between a water drop and an equivalent ice sphere is about 7 dB, this method should also be capable of resolving any ambiguities about the phase (liquid or ice) of the observed particles.

This section describes the instrumentation used in these determinations, then gives examples of measurements made in fresh cloud turrets which illustrate how the system is used and also indicates the approximate particle size ranges over which the measurements appear to be valid.

(b) Measurements

The manner in which the 3 cm on-board radar is used to make reflectivity measurements is similar to a system previously used by Dr. Ray Booker (unpublished). Characteristics of the aircraft radar are as follows:

Make	: Radio Corporation of America, Primus 30A
Pulse length	: 2.25 µs
PRF	: 107.5 HZ
Frequency	: 9.375 GHZ
Power	: 8 kw
Beam width	: 8^{o} (all planes)

A 30 MHZ logarithmic receiver was added after the radar mixer.

The one-way attentuation through the aircraft radome was measured at 2 dB and the beam-width in both planes at 8^{o}. The antenna gain was measured using a standard 3 cm gain horn and a power meter. The receiver was calibrated by using a signal generator and a wave guide adapter to insert a signal in front of the receiver. The calibration was calculated from the output of the logarithmic receiver. All test equipment was calibrated on a regular basis.

Prior to cloud penetrations, the radar antenna is locked facing forward (approximately zero degrees azimuth and elevation with respect to the aircraft flight path) by a switch on the instrumentation console. A single radar range gate 1800 m ahead of the aircraft is sampled 10 to 11 times each tenth of a second. The peak reflectivity during this period is recorded and 10 of these estimates are then averaged to produce one second reflectivity estimates. Since the aircraft radar beam width is 8.0^{o}, and the radar pulse length is 2.25 µs, each second of reflectivity value represents a sample from a volume of about 1.7×10^{8} m^{3} of cloud air.

The recorded signal can be pictured as a reflectivity profile through a horizontal cylinder of cloud about 250 m in diameter.

The 2D-C particle image data are processed in a manner very similar to the methods used at the University of Wyoming. Standard artifact rejection techniques are used to eliminate "streakers", zero images, images with gaps and invalid time words (Cooper, 1978). Sample volumes are determined using the "particle weighting" technique (Heymsfield and Baumgardner, 1985) developed at the University of Wyoming by W A Cooper, which adjusts the particle concentrations by

$$\text{Factor} = \frac{32}{32 + X} \qquad (1)$$

where X is the horizontal number of diodes occulted by the imaged particle. This particle weighting technique reduces the computed concentrations of the larger particles.

For radar reflectivity computations, circular images are assumed, which is adequate for most of the particles encountered in clouds around Nelspruit; thus X as described above is assumed to be the particle diameter. Also, particles whose diameters exceed 30 diodes (1.05 mm) are truncated to 30 diodes. These particles are then included in the 30 diode bin when computing radar reflectivities.

For each one second of 2D particle data, 5 reflectivities are computed assuming that the acquired images were:

- water drops (density = 1 g cm^{-3})
- graupel, with densities of 0.2, 0.4, 0.6 and 0.8 g cm^{-3}

Reflectivities are computed from:

$$Z_e = \sum n D^6 \qquad (2)$$

where Z_e is reflectivity (mm^6 m^{-3}), n is particle concentration (m^{-3}) and D is the diameter (mm) of the particle, or in the case of the graupel computations, the diameter of a water equivalent sphere. For the graupel reflectivity computations (2) is multiplied by 0.224 which is the ratio of the dielectric factor of ice to water (Smith, 1984).

When the data are displayed, the radar signal is lagged by the distance to the radar range gate (1800 m) divided by the true airspeed averaged over the run (in this case by about 12 seconds), to bring the radar and 2D probe measurements into spatial congruence.

(c) Results

The measurement system described above has been in use for more than two seasons (1985 to 1987). We will attempt to summarize our experience with this system by presenting five representative case studies.

First, some general comments about the following figures are in order here. Each shows a record of 2D images from traverses through fresh active cumulus turrets at around the -10°C level. Each record (one line from left to right) is a full buffer of image data which is recorded and displayed at a maximum rate of 1 per second. The time bars (vertical lines) separating each frame are 1.12 mm long. The reflectivities calculated for different assumed particle densities and the recorded radar signals along with a panel showing pertinent microphysical measurements (time histories) for each cloud pass are displayed below the images. Since the radar pulse duration is about 2 μs and the aircraft velocity is close to 150 m/s the reflectivities computed from the 2D images are averaged over 2 second intervals (each microsecond of pulse duration equals 150 m in range). Averaging is not used when image buffers take longer than 1 second to fill. This helps to smooth the reflectivities calculated from the 2D images. The calculated equivalent radar reflectivities, Z_e, are averaged, then converted to dBz.

(i) Small images, maximum diameters less than 1 mm.

Fig. 3.1.1 shows 2D images recorded towards the end of a long pass through convective elements rising on the flank of a multicell storm. With images as small as these, it is often difficult to determine whether they are crystals or water drops. Here, the comparison of the radar and computed reflectivities indicate a reflectivity-weighted average particle density of between 0.6 and 0.8 g cm^{-3}. Averaging over 2 seconds results in sample volumes of between 3 and 10 litres, still a long way from the volumes sampled by the radar. Sample volume can be increased to about 35 litres by summing the 2D images for the complete pass. This has been done by summing the counts in each size category, calculating a Z_e and then summing these Z_e over all 32 size ranges. These pass-averaged reflectivities are shown in Fig. 3.1.1. The radar signal lies close to the average computed from assuming an average particle density of 0.6 g cm^{-3}.

Fig. 3.1.2 shows a pass through a cloud containing high concentrations of what appear to be small water drops. Again, it is difficult to unequivocally classify these images as either water or ice. The 2 second averages of calculated reflectivities are noisier here than in Fig. 3.1.1 probably as a result of the smaller sample volumes.

Here the 2 second volumes sampled are between 1 and 4 litres. Again, average reflectivities are computed over the whole sampled volume (30 litres). These calculations suggest that the acquired radar signal is coming from particles whose densities are greater than that of recently frozen water drops. In this case, we may be looking at a volume of mixed liquid and frozen water drops. If these measurements are accepted, then these precipitation embryos cannot have ice-crystal origins.

The next small image example is a pass through a seeded plume (Fig. 3.1.3). This cloud was seeded with dry ice at -10°C, then re-penetrated 3 minutes later at a temperature of around -17°C. The cloud top was observed to rise about 1000 m between the seed and the post seed pass or around 5 to 6 m/s. This compares well with the average updraft speed of 6.3 m/s computed from the aircraft vertical velocity measurement system on the post-seed pass. The radar signal and seeded plume correspond well in Fig. 3.1.3 , indicating that the correct time lag has been used to bring the radar and the 2D measurements into spatial congruence. What is surprising is the apparent density of the particles that comprise the seeded plume; somewhere between 0.8 and 0.9 g cm^{-3}.

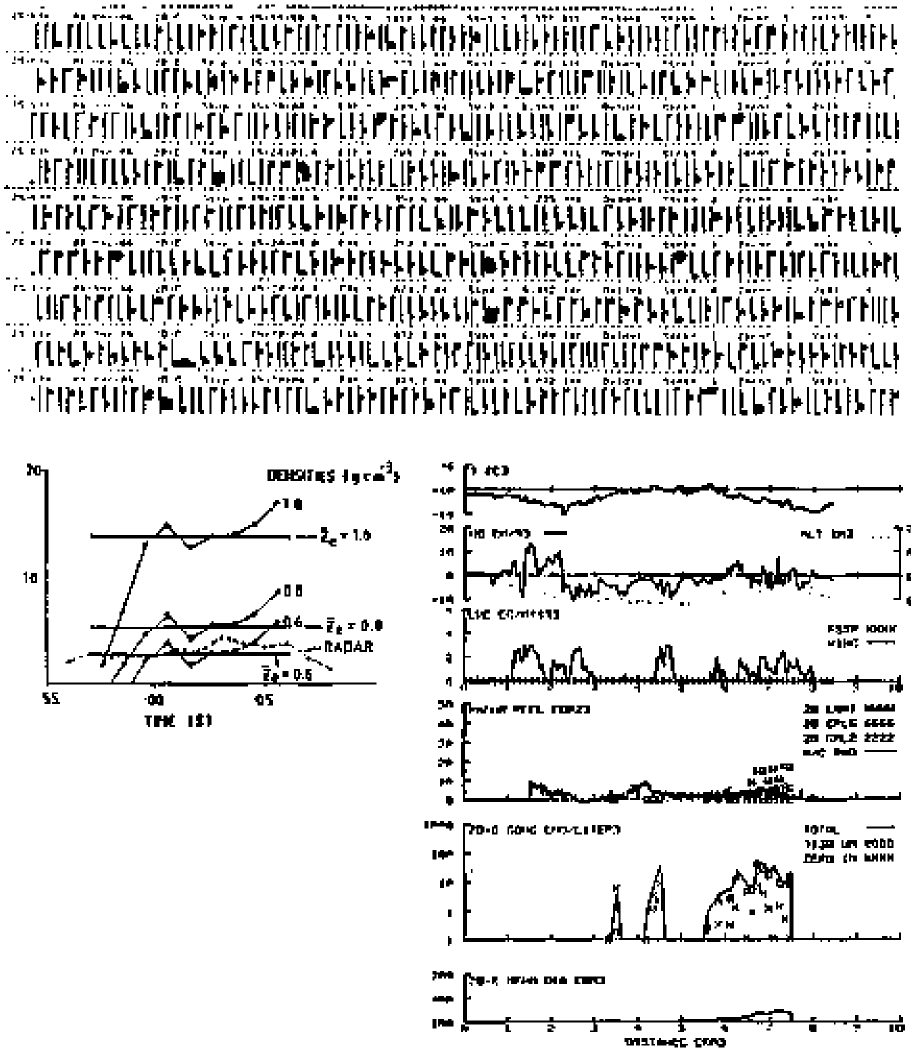

Fig. 3.1.1. Time histories of equivalent radar reflectivity factors measured by the Learjet's 3 cm radar and computed from the 2D-C images shown at the top of the figure, assuming particle densities of 0.6, 0.8 and 1 g cm^{-3} (water). Time bars (vertical lines separating each image) are 1.12 mm long. Post flight analysis records of pertinent microphysical measurements are also shown. Images appear to be of small ice and graupel particles. The time histories from top to bottom are: static temperature (T), true vertical gust velocities (WG), cloud liquid water measured by the King-CSIRO hot wire and a PMS FSSP laser probe, reflectivities, 2D probe concentrations and diameters.

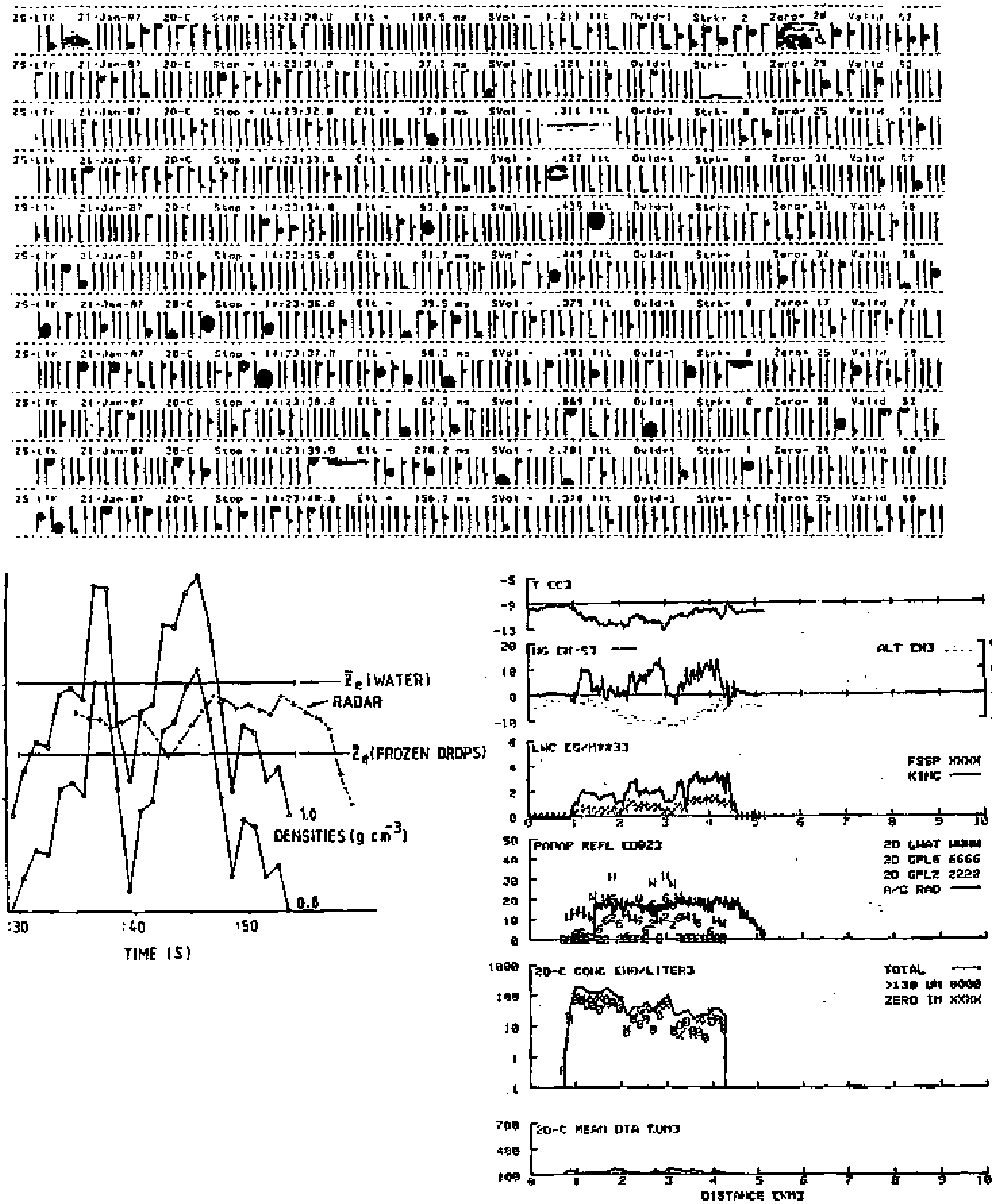

Fig. 3.1.2 Same as in Fig. 3.1.1 except here, the recorded images look more like small water drops.

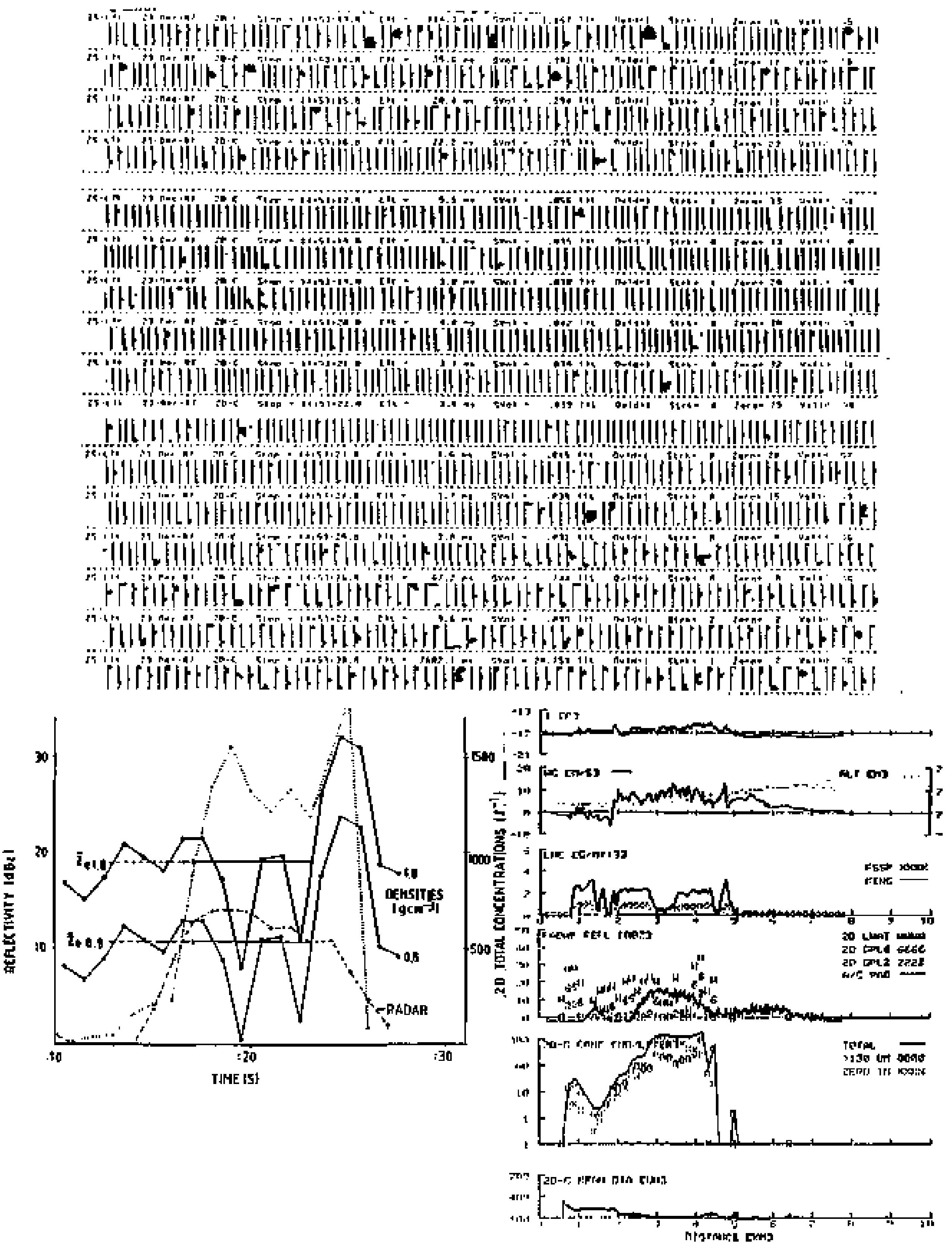

Fig. 3.1.3 An analysis of a traverse through a seeded plume. This cloud was seeded with dry ice 3 minutes before the pass shown above. The dotted line (.....) superimposed upon the radar reflectivity comparisons represents total 2D concentrations (note concentrations axis on the right side of this panel).

Ice crystals collected by the South African Weather Bureau Aerocommander 690A in seeded plumes lend support to these measurements (see Bruintjes et al., 1987 for details of the Aerocommander's instrumentation). Figure 3.1.4 shows a view of short, fat columns which are a typical product of dry ice seeding. This type of crystal has never been found in untreated (natural) clouds in the Bethlehem area. The density of these crystals, estimated to be around 0.9 g cm^{-3}, should result in riming growth rates that are comparable to frozen drops of the same dimensions (Johnson, 1987).

Fig. 3.1.4 Photograph of ice crystals collected on an oil coated slide in a cloud seeded with dry ice. This photograph was provided by courtesy of R. Bruintjes, South African Weather Bureau.

(ii) Larger images, approaching and exceeding 1 mm in diameter.

The first example presented here is a penetration through a storm in the Johannesburg area, close to the central interior of the subcontinent (Fig. 3.1.5). Here, graupel images appear to dominate. However, there are a few circular images towards the centre of the pass, precisely where the radar signal rises towards the reflectivities calculated on the assumption that the acquired 2D images are of water drops. These drop-like images also occur where the updraft is strongest. The importance of an updraft in accelerating coalescence is well known (Leighton and Rodgers, 1974). The measurements in this cloud suggest that the dominant precipitation formation process is of the 'coalescence-freezing' variety described by Braham (1986).

Contrast the above example with the one shown below (Fig. 3.1.6). This is one of several passes flown through turrets growing on the western flank of a storm north of Bethlehem in the Free State. Although the concentrations are lower, the 2D images in this example do not look all that different from those of the previous example, yet they produced no detectable radar echo. This result was so surprising that equipment failure was suspected, and the radar was recalibrated immediately upon returning to Nelspruit. Oil-coated slides exposed in the Bethlehem 690A, which was flying co-ordinated cloud penetrations with the Learjet on this storm, tell the story. Loose, moderately rimed crystals with sector-like branches similar to those illustrated in Fig. 3 of Bruintjes et al., (1987) were collected on the slides (estimated densities of 0.2 g cm^{-3}). This example dramatically illustrates the advantages of using the radar to aid in deciphering the habit of images collected by the 2D-C probe.

(d) Discussion

A major problem with these measurements is the large particle sampling problem. In both pass-averaged reflectivities shown in Fig. 3.1.1 and 3.1.2, the largest particles account for more than 50 percent of the computed Z_e. Increasing the sample size by combining data from other runs is not a realistic solution to the problem for the reasons argued by Smith (1982). Briefly, he states that there is no assurance that additional samples will be drawn from the same population.

The graphical presentation used in Figure 5 of the Smith paper is used here to display cumulative distributions of computed Z_e versus drop size, normalized by dividing by the mass-weighted mean diameter (D_m). Cumulative distributions from the examples shown in Figs. 3.1.1 and 3.1.2, calculated from 2 second reflectivity averages, are plotted in Fig. 3.1.7. These cumulative distributions approach an ordinate value of 1.0 in a reasonably smooth manner, indicating that, at least in these two examples, the large particle sampling problem may not be too acute. This may be the best that can be done at present since a method of estimating the population value of Z_e does not appear to exist.

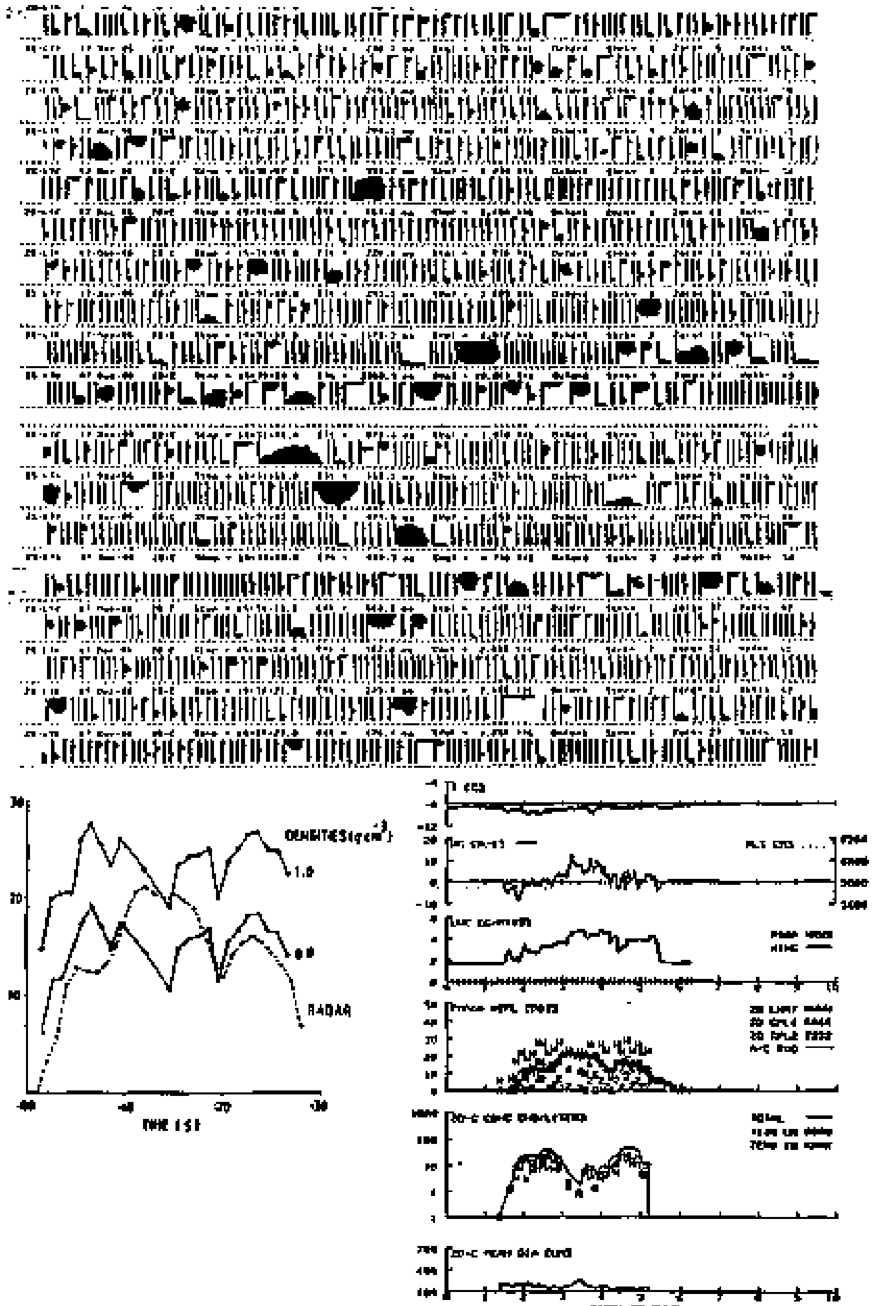

Fig 3.1.5 A pass through a growing cloud turret that appears to contain drops and recently frozen riming drops (dense graupel). The DC offset in the King measurement of liquid water is caused by an erroneous application of the dry-air correction term.

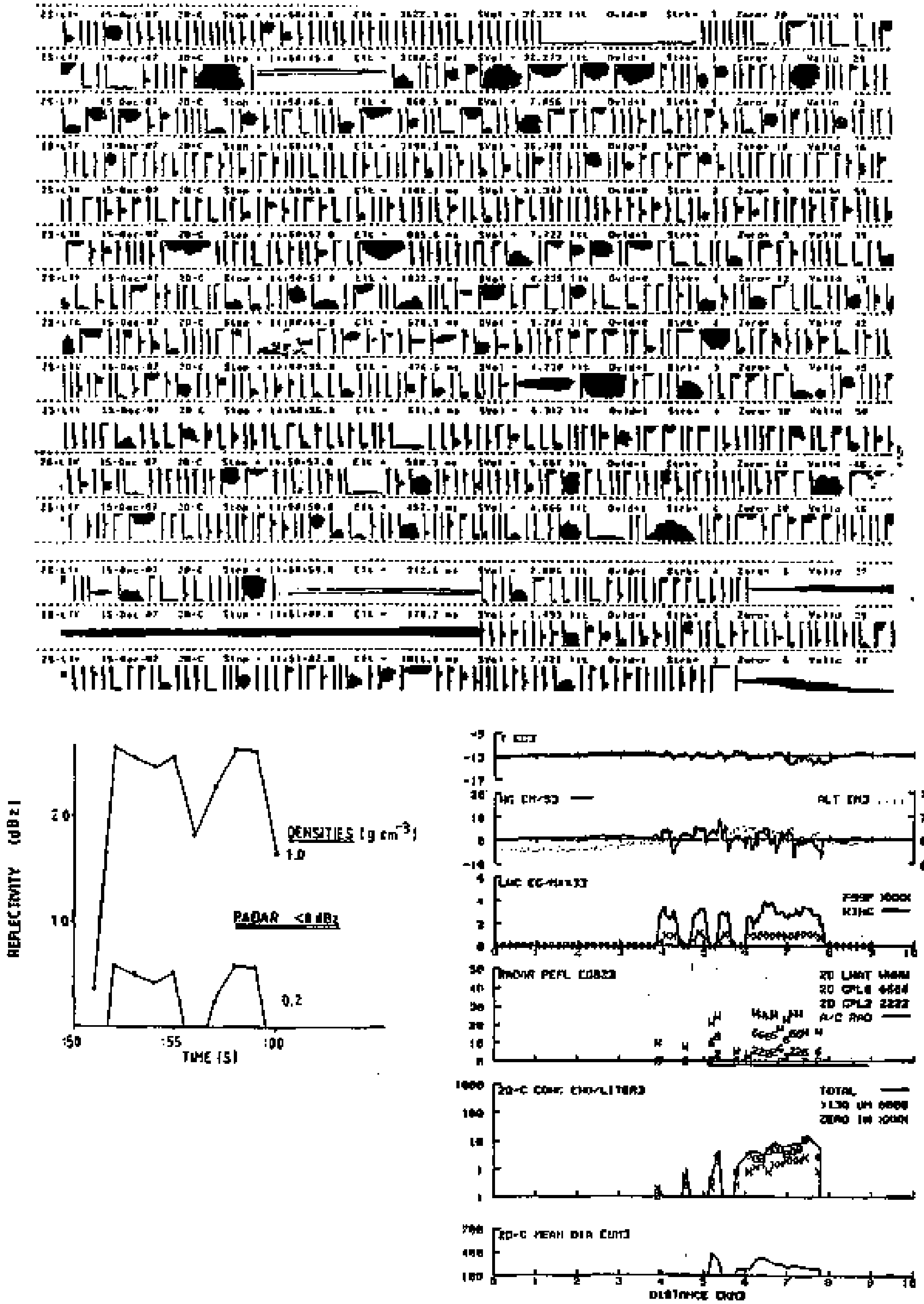

Fig. 3.1.6 An example of a traverse through a cumulus tower growing on the western flank of a thunderstorm just north of Bethlehem, Orange Free State. Note the complete absence of any radar return from the images encountered on this pass.

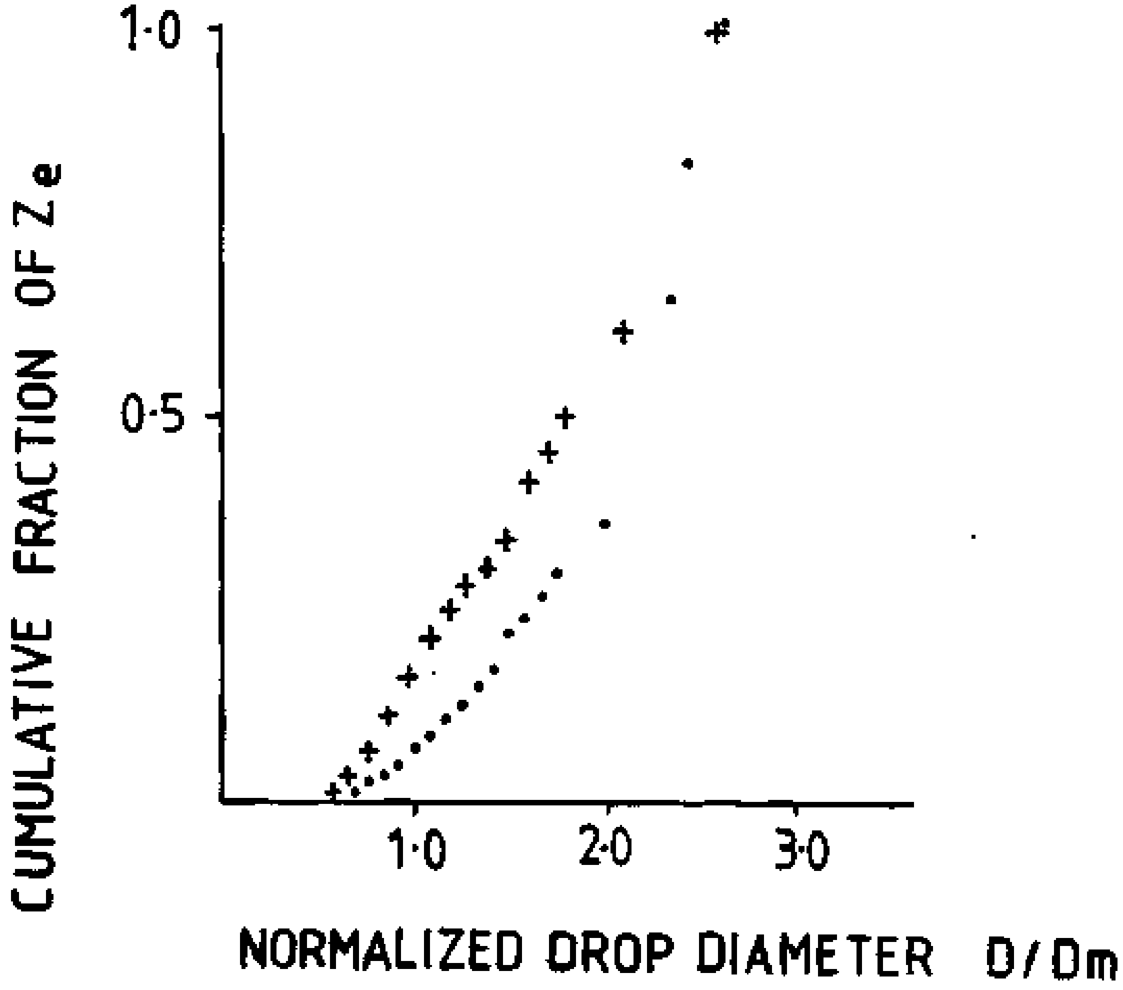

Fig. 3.1.7 Comparisons of distributions of cumulative reflectivities computed from the images shown in Fig. 3.1.1, and 3.1.2 above. The crosses and the dots on the figure represent the small graupel of Fig. 3.1.1 and the small drops of Fig. 3.1.2 respectively. The distributions are normalized by dividing by D_m, the mass-weighted mean diameter.

What may rescue this scheme from producing nonsense results is the nature of the particles that we are looking at. The density differences between drop or even frozen drop and ice crystal precipitation embryos are usually large (except apparently in cases when the ice has been produced by dry ice seeding). Thus, the system is not required to discriminate, say, between densities of 0.6 and 0.8 g cm^{-3} (2 to 3 dB). Also, according to the model of Pflaum and Pruppacher (1979) developed from wind tunnel studies, a small frozen drop of an initial density of 0.9 g cm^{-3} and a diameter of 300 µm rimes to become a chunk of graupel with a diameter of 1 mm and a density of 0.25g cm^{-3} in a little over 2 minutes. So, if we encounter ice particles in a newly developing (non-precipitating) cloud approaching 1 mm in diameter, they are usually either recently frozen drops or well-rimed graupel.

The measurement system described here has been found very helpful in identifying the dominant precipitation formation mechanism in the Nelspruit area of the Eastern Transvaal. Density comparisons of the type described above indicate that the embryos in most of the area's developing rain clouds that have been sampled to date show densities of greater than 0.8 g cm^{-3}, indicating drops and graupel with recently frozen drop centres. These measurements indicate that a precipitation formation process described by Braham (1986) as a "coalescence-freezing" mechanism appears to be the dominant precipitation formation mechanism in the medium to large size convective storms in the research area. What is intriguing is the apparent microphysical difference between the clouds in the Bethlehem area and those around Nelspruit, clouds separated by just 300 km.

Almost all cloud physics samples at Nelspruit are from rapidly rising cloud turrets on the flanks of convective complexes, many of which are almost unmixed (close to adiabatic liquid-water contents) at the most common penetration level of around -10°C. Such an unmixed region stands a good chance of containing a volume of homogeneous early precipitation growth. Perhaps the best measure of this is steady 2D-C concentrations across the sampled volume. Steady values across the interiors of clouds of the reflectivity-weighted densities calculated from the 2D-C images and the radar measurements of equivalent reflectivity factors suggest that this is the case in many of the clouds sampled around Nelspruit. That such steady comparisons have been found, despite the disparity in sample volumes, is an important result of this work. The tiny pinhole sample made by the aircraft's 2D probe through a cloud can be considered representative of a much bigger cloud volume (seen by the radar), at least in the initial stages of precipitation growth.

This is good news indeed for cloud modellers, who can perhaps use aircraft data in their numerical models with a little more confidence.

3.2 Aircraft-produced ice particles

(a) Introduction

Observations of aircraft produced ice particles (APIPs) in clouds were first observed and reported by Rangno and Hobbs (1983). Noted characteristics of these APIPs were high concentrations of uniformly sized ice crystals in plumes whose diameters expanded to about 300 m some 5 minutes after the initial aircraft penetration. The seeding 'signal' produced by the APIPs was found to be so similar to that produced by dry ice that it was difficult to distinguish between the two. The paper also warns about the possibility that APIPs may have contaminated past seeding experiments by producing significant quantities of ice crystals in the 'unseeded' group of clouds in the experiment. This was one of the reasons that the PAWS seeding experiment split the no seed category in two: clouds that were sampled and not seeded, and clouds that were neither sampled nor seeded.

The preliminary statistical analysis of this subclass (Galpin, 1988) indicates that the clouds sampled by the aircraft are from a different population from those clouds in which no measurements were taken (the null hypothesis was rejected). This strongly suggests that the aircraft by itself may be producing a seeding effect. It should be noted that this was not the anticipated (or even the desired) outcome of this experiment.

This result was the motivation behind dedicating one research flight to the search for APIPs. What follows is a report on these measurements.

(b) Flight results

APIPs flight, 23 December 1987. This flight was specifically dedicated to a search for APIPs. Flight procedures were to pick a reasonably isolated but rapidly rising cloud turret, penetrate the turret as it ascended through the $-10^{o}C$ level, then follow the turret up, re-penetrating at right angles to and some 3 to 5 minutes after the initial penetration.

Cloud 1. This cloud was first penetrated close to the $-10^{o}C$ level at 14:23. The second (orthogonal) penetration occurred some 3 minutes later at 14:26. Figure 3.2.1 shows a time history of the total particle concentrations measured by the 2D-C probe with a panel showing images encountered during this APIPs encounter. Note that the 2D probe is suffering from electrostatic interference on either side of the peak in ice crystal concentrations. This example corresponds closely to those reported in the Rangno and Hobbs paper, in that:

- a sharp momentary spike of high (> 1000 l^{-1}) concentrations of ice crystals was recorded

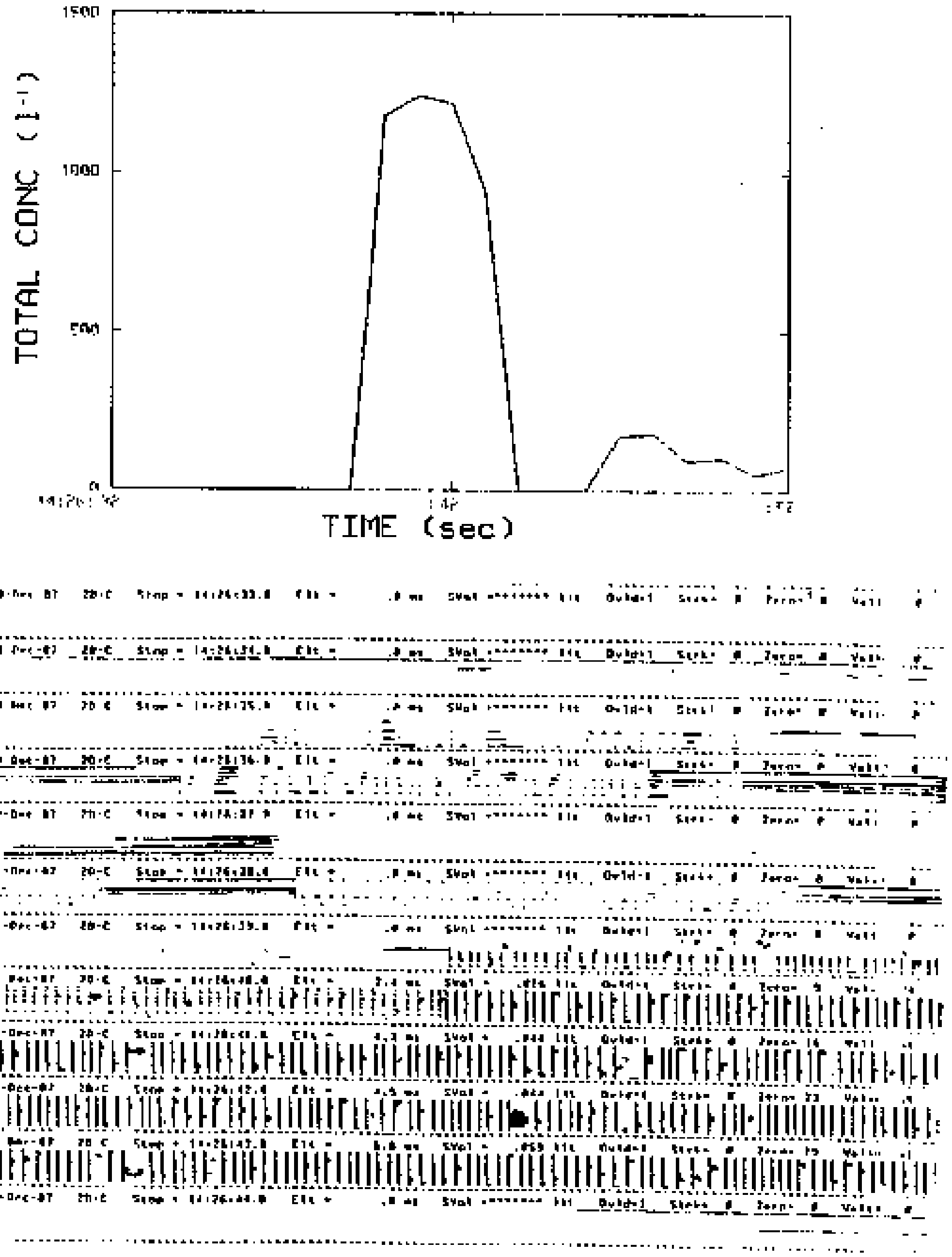

Fig. 3.2.1 A plot of total 2D-C concentrations versus time and the associated 2D images.

- the ice crystals in the plume have a relatively uniform size distribution

- the plume has a diameter of around 300 m (in this case 480 m).

Cloud 2. This cloud was first penetrated at the -10°C level at 14:31. The second pass through the cloud (at 14:35) failed to detect any signs of APIPs. However, the third pass (at -17°C, 6 minutes after the first pass), encountered two separate peaks of high ice crystal concentrations (>1000 l^{-1}). The distance between the peaks suggests that the high concentrations may be contained in the decaying wing tip vortices left by the Learjet. This possibility deserves further attention, as the theory of wing tip vortices is well established. For example, the spread of the vortices with time, at least in still air, can be adequately predicted. (This bimodal structure is not unusual in an APIPs encounter).

Fig. 3.2.2 shows the two ice crystal peaks detected by the 2D-C probe and the accompanying panel shows the usual distributions of small, uniformly-sized ice particles, associated with an APIPs encounter.

Cloud 3. It is interesting to compare the dry ice and APIPs seeding signatures. This cloud was seeded at 14:50, close to the level of the -8°C isotherm. Re-penetration was at 14:53 at -16°C. Fig. 3.2.3 shows the seeded plume and the associated 2D images. They indeed look similar to the APIPs images. However, the seeded plume is much wider. Assuming that the second penetration was orthogonal to the first, this plume is almost 1300 m wide 3 minutes after seeding (compared to ~300 m for a typical APIPs plume). Note that this plume is also bimodal. Is it possible that the ice crystals are being concentrated in the wing tip vortices?

The final example shown here was discovered after looking through the data collected in Italy (June to September, 1988). A number of isolated towering cumulus were being sampled and one in particular was sampled twice to try and follow the precipitation development in the cloud.

21 August 1988. This cloud was first penetrated at 11:15, then re-penetrated at 11:19, 4 minutes later. Both penetrations were around the -10°C level in the cloud. We were alerted to the possible presence of APIPs by the abrupt increase in 2D particle concentrations from around 2 to over 500 per litre (Fig. 3.2.4). The panel accompanying Figure 3.2.4 shows once again small, uniformly distributed ice particles.

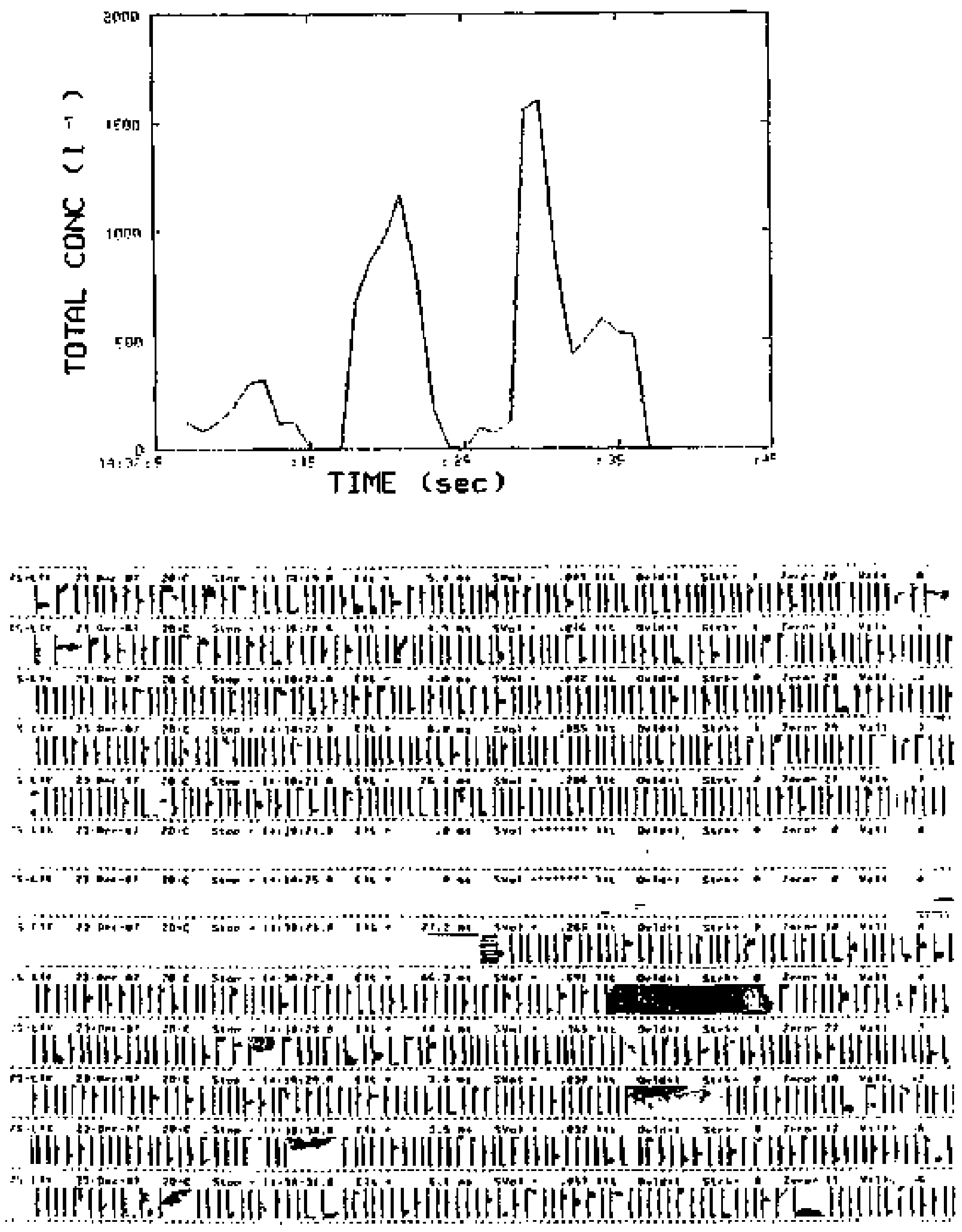

Fig. 3.2.2 A plot of total 2D-C concentrations versus time and the associated 2D images.

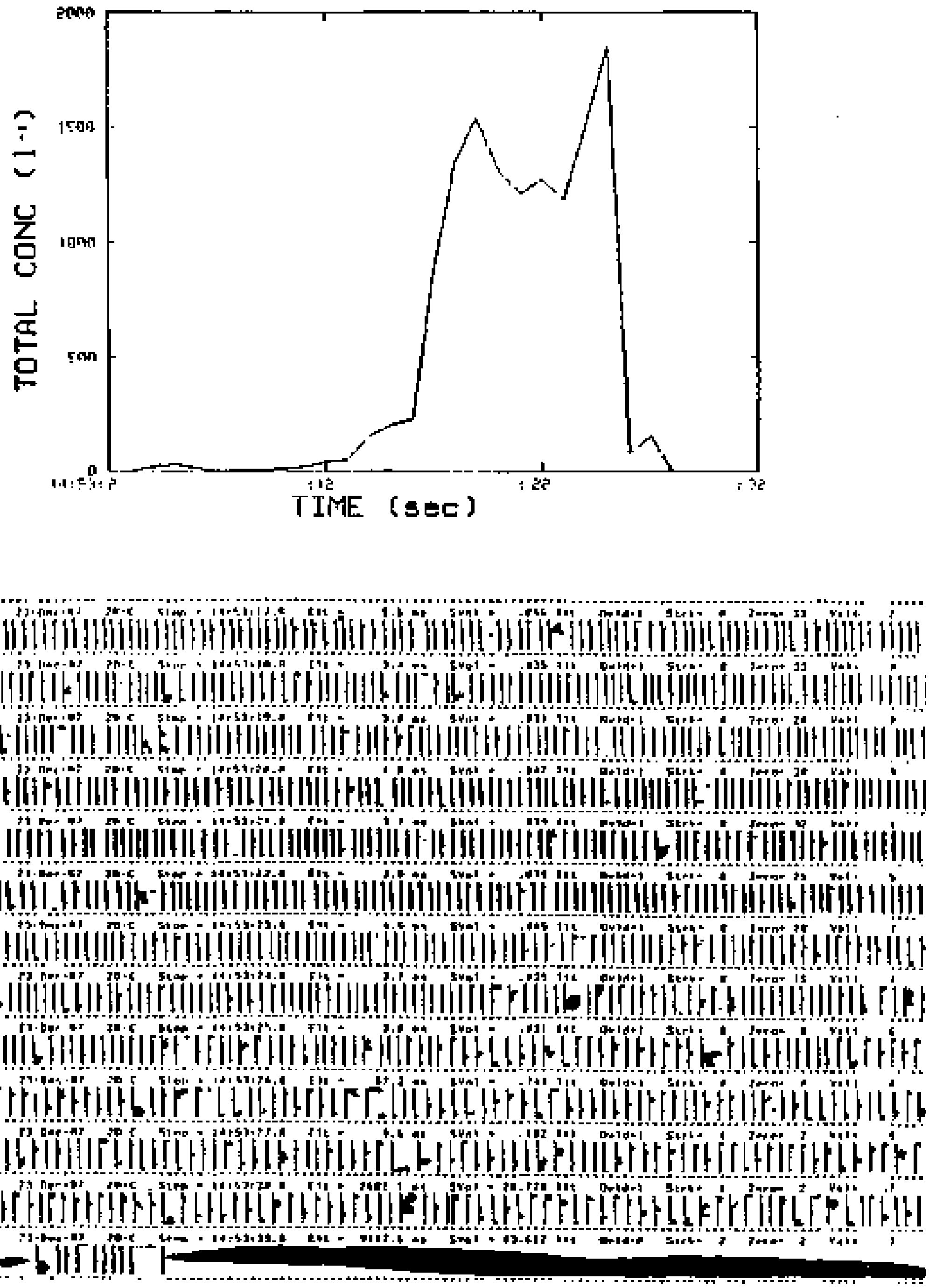

Fig. 3.2.3 Same as in Fig. 3.2.1. This cloud was seeded with dry ice.

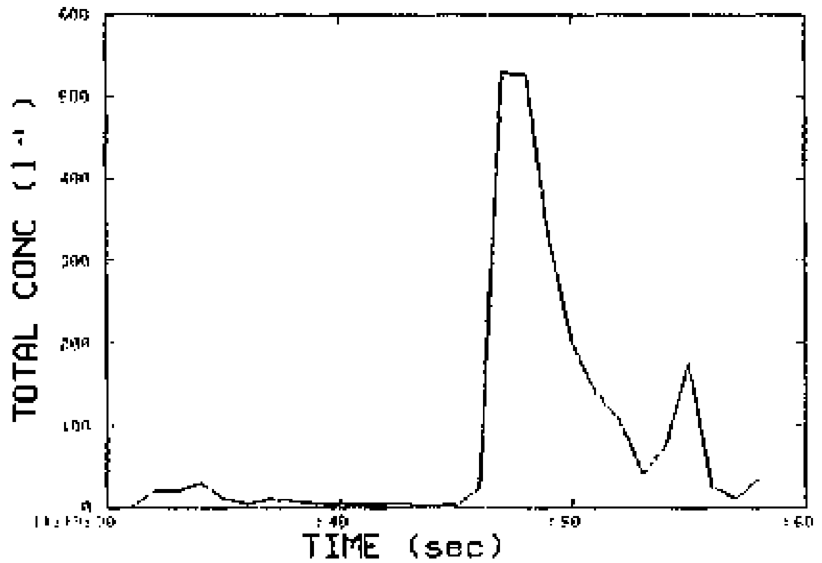

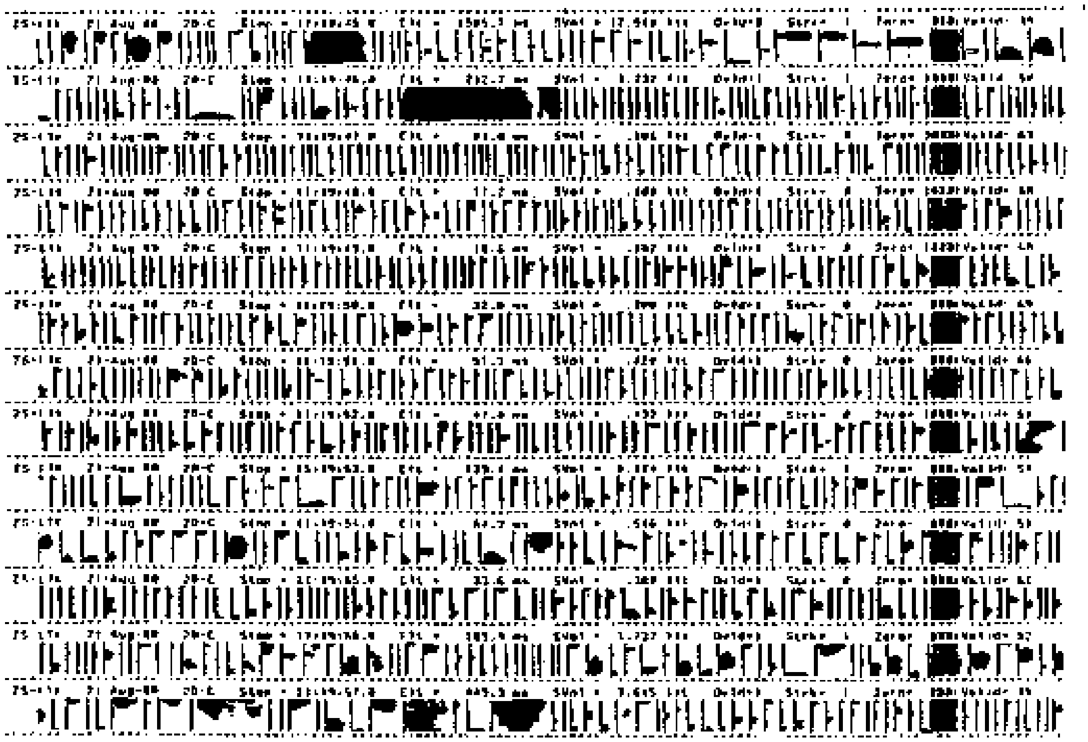

Fig. 3.2.4 Same as in Fig. 3.2.1. This measurement shows an accidental encounter with what appear to be APIPs during the Italian cloud sampling programme.

(c) Discussion

There can no longer be any doubt that high concentrations of ice crystals are produced by an aircraft flying through a cloud containing supercooled water. Some of the as yet unsolved problems raised by this phenomenon are:

- do some aircraft produce fewer ice crystals than others, do jets differ from turbo props in their APIPs signatures?

- what is the primary mechanism(s) responsible for the production of APIPs?

- do APIPs significantly affect the natural precipitation formation mechanisms?

This last question is the most important one of all, since an affirmative answer would have a profound impact upon the design of future seeding experiments.

3.3 Precipitation growth rates experiment

(a) Introduction

The objective of this experiment was to measure any acceleration of precipitation growth rates caused by seeding using the Learjet's instrumentation system. The key sensor in this exercise was the Learjet's 3 cm radar, utilizing a 5.8 km range gate.

Briefly, the exercise was an extension of the current experiment using the same three way randomization scheme. The "double-blind" scheme that was developed for the 1986/87 season was used so that neither the pilots nor the data analysts were aware of the treatment until the end of the experiment.

Experiment I

The pilots were instructed to choose a reasonably isolated cloud turret on the flanks of an isolated multicell storm, the same type of cloud that had been the seeding target over the 3 year seeding experiment. The same manoeuvres were performed for both the seed/sample and no seed/sample categories. The pilots flew through the cloud at around -10^{o}C, sampling and perhaps seeding.

Succeeding passes were flown at about 3 minute intervals. Each post "seed" pass was initiated in the normal manner, with the aircraft lined up for a penetration and the instrumentation system turned on a minimum of 20 seconds (3 km) from the near cloud boundary. Just prior to entering cloud, the run was broken off. The only relevant data recorded were temperature, pressure, airspeed and radar reflectivity values from the flying range gate 5.8 km ahead of the aircraft. A total of four post "seed" passes were attempted, covering a time interval of about 12 minutes after the first penetration. Post "seed" runs were flown with the aim of maximizing the chances of intercepting the seeding plume.

In cases of a no seed/no sample draw, the first pass was also broken off before cloud entry. Succeeding passes were flown as above.

The designated response variable was the rate of the change of pass-averaged and maximum radar reflectivities, i.e.

$$dZ_{mean}/dt \text{ and } dZ_{max}/dt$$

In seed and no seed/sample cases, pre-seed microphysical measurements were available so that the pre-treatment state of these cases could be described.

Experimental results were evaluated using standard re-randomization techniques.

Experiment II

In order to collect microphysical data on post-seed passes and to search for such effects as tower-to-tower contamination and APIPs, an additional experiment was designed. This differed from Experiment I in that the first pass as well as any subsequent passes on a selected tower included, if possible, cloud penetrations. This experiment was carried out on the first selected tower of a given complex (as in Experiment I) or on subsequent towers.

(b) Results

The designated response variables were the rates of change of pass-averaged and maximum radar reflectivities, i.e.

$$dZ_{mean}/dt \text{ and} \quad (1)$$

$$dZ_{max}/dt \quad (2)$$

We have evaluated the differences in the means of the above for penetrations 1 and 2 and 1 and 3 for Experiments I and II using standard re-randomization techniques. These results are listed in Tables 3.3.1 and 3.3.2.

Table 3.3.1 - Experiment I

Penetrations	1 to 2		1 to 3	
Cases (S/NS)	5/8		5/8	
Response Variable	(1)	(2)	(1)	(2)
Difference (%)	0	-37	88	70
p values(%)	49	36	68	64

Table 3.3.2 - Experiment II

Penetrations	1 to 2		1 to 3	
Cases (S/NS)	14/14		14/12	
Response Variable	(1)	(2)	(1)	(2)
Difference (%)	-60	-52	-117	-116
p value (%)	9	12	0	1

The results from Experiment I show an increase in the aircraft radar reflectivities from seeded versus unseeded clouds by the third pass (some 5 to 10 minutes after the first pass). However, this difference is not significant (the sample size is small). The results from Experiment II show exactly the opposite trend - by the third pass, reflectivities from the seeded clouds are on average 116 percent less than the untreated clouds, at a significance level of less than 1 percent. Recall however, that the second experiment was not double blind.

There are a number of possible explanations for this mixed result:

(1) In the smaller clouds, the seeding may be enhancing precipitation growth rates which cause the precipitation embryos to turn around sooner (not reach such heights) in the life of the cloud.

(2) The freezing of supercooled water drops. Turning this water into ice would result in lower radar returns.

(3) Insufficient sample size.

(4) The real explanation is probably a sampling problem. It is almost impossible for one aircraft to consistently sample the volume of a cloud where the changes caused by the seeding are taking place. The aircraft's sample volume capabilities are just too small compared to the volume of the affected cloud.

This is when the ground based radar operating in volume scan mode must take over. The need for such large volume sampling capabilities is illustrated in the following example. The Learjet seeded a cloud north of Carolina on 17 March, 1988 at 14:13 with about 5 kg of dry ice (a 26 second seeding run). The pass was close to the -10^{o}C isotherm at a height of 6662 metres (above mean sea level). A second, post-seeding penetration was made at 14:21, some 8 minutes later, at a height of 7055 metres. This penetration, orthogonal to the first, picked up clear signs of the microphysical seeding signature. Run-averaged radar reflectivities also show an increase (from 13.5 to 17.5 dBz). However, the whole story can only be captured by the ground based radar. Some of the variables calculated by the storm tracking programme are shown in Fig. 3.3.1. The radar picks up track on the target storm at 14:05. The Learjet seeded this storm at 14:13 (see circle at the top of Fig. 3.3.1 indicating height and time of seeding run). Around 14:17, the radar picked up a sudden jump in the height of the maximum reflectivity (Z_{max}). This is followed sequentially by increases in maximum reflectivity, rain rate, and finally rain flux, which reaches a maximum some 15 minutes after the seeding run.

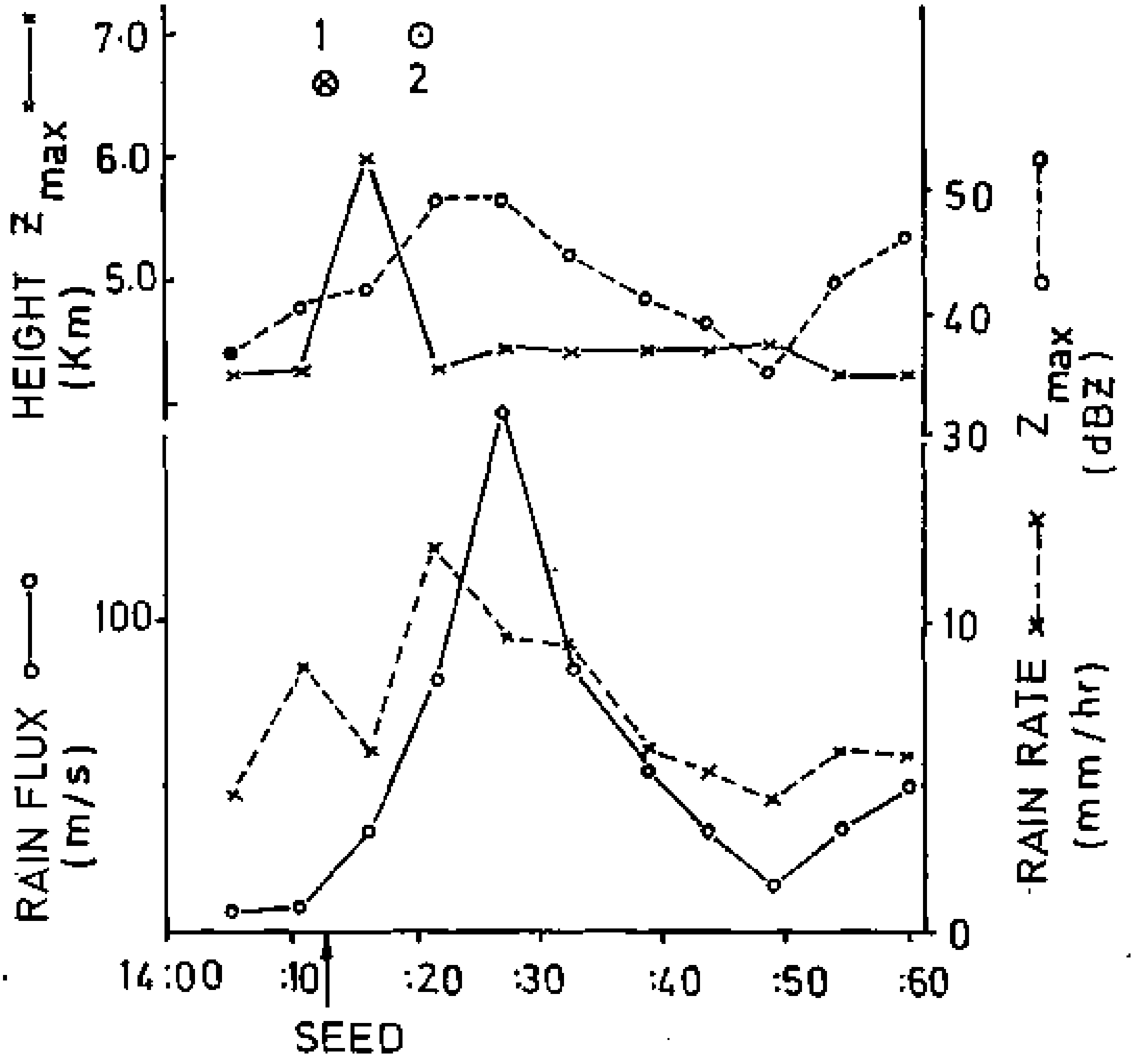

Fig. 3.3.1 Selected storm track variables plotted against time for a seeded and sampled cloud. Note the positions and times of the seed (1) and the sample (2) runs.

If the aircraft had descended below 6 km immediately after the seeding run for an orthogonal post-seeding pass, the sudden rise in the height of the maximum reflectivity might have been recorded. As it was, the second pass at around 7 km (see Fig.3.3.1) was well above the main precipitation growth region in this cloud.

To put things in perspective: the volume of the storm as measured by radar at the time of the second pass was 71 cubic kilometres; the volume measured by the Learjet's 2D probe on this pass was less than one cubic metre!

Three more studies of interest were conducted on the data from these experiments. The first repeats the result shown in Table 3.3.1 and 3.3.2, but in a more graphic form. We asked the question: "Did the maximum reflectivities between passes increase or decrease?"

Table 3.3.3 Radar reflectivity changes between passes

CLASS	MAXIMUM REFLECTIVITY	PENETRATION 1 - 2	2 - 3	3 - 4	%
SEED	UP	6	2	0	36
	DOWN	3	9	2	64
NO SEED SAMPLE	UP	5	2	1	62
	DOWN	1	3	1	38
NO SEED NO SAMPLE	UP	4	5	2	73
	DOWN	1	1	2	27

Between first and second passes in seeded storms, two thirds of the test clouds show increases, one third decreases (Table 3.3.3). In the no seed/sample and no seed/no sample clouds, just one cloud in each category shows a decrease in this interval. Between second and third passes, 9 out of 11 seeded clouds show decreases in reflectivities. Three out of 5 and just 1 out of 6 show decreases in no seed/sample and no seed/no sample clouds respectively. Over all, 36 percent of seeded clouds show increases in reflectivities between passes, 64 percent show decreases. These proportions are almost exactly reversed for no seed/sample clouds (62 percent show increases, 38 percent decreases). In the no seed/no sample category, 73 percent of the clouds show increases in reflectivities between passes whereas just 27 percent show decreases. The trends shown in Table 3.3.3 could be explained if seeding is indeed enhancing precipitation growth rates, leading to the earlier and more rapid development of precipitation products which now follow lower growth trajectories through the cloud. This result does not suggest that the seeded clouds have been invigorated by the sudden release of the latent heat of freezing - the dynamic seeding hypothesis. This exercise then, may have advanced our knowledge slightly about how cloud seeding works, leading us a little closer to the day when we can formulate a coherent seeding hypothesis.

There are two additional results that emerged from this experiment that confirm some of our earlier work. Average and maximum particle concentrations measured over each run by the 2D probe are listed in Table 3.3.4. In at least 10 of the 14 seeded clouds, the second penetration has intercepted the seeded plume. The medians are calculated for purposes of comparison, since two observations of anomalously high particle counts, Case 24 and Case 25 in the no seed/no sample and no seed/sample categories respectively would produce unrealistically high arithmetic averages in such small samples. The explanation for the high particle counts in Case 24 is not known; in Case 25, APIPs might be a possible explanation.

Table 3.3.4 Comparison between first and second passes of particle concentrations measured by the 2D probe

SEED					NO SEED / SAMPLE					NO SEED / NO SAMPLE	
Case	1st Pass		2nd Pass		Case	1st Pass		2nd Pass		Case	2nd Pass	
No	2D Concentrations (l^{-1})				No	2D Concentrations (l^{-1})				No	2D Concentrations (l^{-1})	
	Mean	Max	Mean	Max		Mean	Max	Mean	Max		Mean	Max
5	0	0.3	257	673	1	0.8	1.5	2.1	9.4	10	0	0.3
6	0	0.7	1.2	3.4	2	0.3	0.4	1.1	1.5	11	0.9	1.1
8	0	0	2.0	2.9	9	0.1	0.3	3.2	14.3	19	4.1	9.4
13	5.3	9.4	184	542	16	0	0.1	4.7	23.5	24	67	616
14	14.1	17.0	76	441	25	0.2	0.2	24.3	122.7			
15	0.5	1.6	13	98								
17	0	0	83	463								
18	25.4	156.4	370	600								
20	4.3	19.1	9	151								
21	0	0	8	43								
22	0	0	144	514								
23	0	0	0	0.1								
26	1.3	4.4	269	1640								
28	0	0	53	243								
Medians	0	0.5	79	342		0.2	0.3	3.2	14.3		2.5	5.2

Most clouds show very low particle concentrations on first passes. Since this first pass takes place at around -10°C, this indicates that most clouds are relatively ice-free at this temperature, a necessary but not a sufficient condition for a glaceogenic seeding potential.

The second result comes from a comparison of the temperature at the convective condensation level (T_{ccl}) and the temperature difference between a pseudoadiabat through the T_{ccl} and the environmental temperature at 500 mb (ΔT_{500}) calculated from the

Lear atmospheric sounding measured prior to each experiment. The ratio of $T_{ccl}/\Delta T_{500}$ and the maximum reflectivity recorded on each pass are compared in Table 3.3.5. Shown here is a clear tendency for low reflectivities to be associated with low values of the $T_{ccl}/\Delta T_{500}$ ratio.

Table 3.3.5 - Comparison of the $T_{ccl}/\Delta T_{500}$ ratios and first pass maximum reflectivities

	MAXIMUM REFLECTIVITIES (dBz)					
$T_{ccl}/\Delta T_{500}$	0-4.9	5-9.9	10-14.9	15-19.9	20-24.9	25+
1.5-1.79	13	3	1			
1.8-1.09	1		1			
2.1-2.39	4	2				
2.4-2.69	5	2	2	1	1	2
2.7-2.99						
3+	2		1			

This confirms the results reported in Mather et al., 1986; the higher the value of this ratio the greater the likelihood of encountering coalescence products (supercooled drops, recently frozen riming drops) around the -10°C level in the local clouds.

(c) Summary

Although the experiment did not produce the anticipated results, much was learned in terms of the volume sampling capabilities of the Learjet. The Learjet is an excellent aircraft for delivering the seeding agent to the right place at the right time, a vital function in any seeding experiment. It is also able to "tag" the cloud microphysically at a critical phase in its growth; at the onset of precipitation development (liquid water content, updraft profile and speed, dominant precipitation formation mechanism, etc). Once the seeding has taken place, it is almost impossible for a single aircraft to follow the effects of the treatment on the evolving precipitation formation mechanisms. A simple example will indicate why. Three minutes after seeding the cloud analysed in this section, the seeded plume had spread out to fill a volume of around 15 km^3! Where in this rather large volume is the aircrft, with its very limited volume sampling capability, going to sample next?

The development of post-seeding precipitation and its effects on the dynamics of the cloud systems are going to have to be traced by remote sensors, such as radars. It is unlikely that a full formulation of a seeding hypothesis can be completed without major inputs from these devices.

3.4 Cloud water budget calculations

(a) Introduction

The addition of three systems to the Learjet's cloud physics measurement capabilities has resulted in the ability to assess how the water in a growing cloud is distributed between cloud water and growing precipitation particles, and how this total cloud water content compares to adiabatic values. A brief description of the instruments that have made these estimates possible follows.

CSIRO-King liquid water content probe: This instrument was developed by Dr Warren King at the CSIRO in Australia, and is built under license by Particle Measuring Systems (PMS), Boulder Colorado. The device is a hot wire anemometer, whose sensor element is maintained at a constant temperature. The power required to maintain this constant temperature in a wet (cloud) environment is proportional to the liquid water content of that environment for drop sizes less than 100 µm and liquid water contents less than about 5 g/m^3. This instrument is superior to the Johnson-Williams hot wire anemometer that it replaced on the Learjet. It has a wider dynamic range and responds to larger drop sizes, making it a more suitable instrument for estimating cloud liquid water contents in the moist, warm-based convective clouds found around Nelspruit.

Lyman-alpha hygrometer measurements of the vapour content of air tapped off the eighth stage compressors of the Learjet engines: This technique is described in detail in Section 9, Vol IV of the PAWS Phase I Final Report (WRC 133/4/88). Briefly, the aircraft engines are used as huge evaporators which vaporize all the water in a cloud, including that contained in precipitation particles (water or ice). The humidity of this air is then measured, using a Lyman-alpha hygrometer, giving an estimate of total cloud water content.

Flying radar range gate: This technique is fully described in Section 3.1 of this report. The aircraft's 3 cm radar (standard equipment) is utilized for this measurement. Prior to cloud penetrations the radar is locked facing forward (approximately 0 degrees azimuth and elevation with respect to the aircraft flight path) by a switch on the instrument console. A single radar range gate 1800 m ahead of the aircraft is sampled 10 to 11 times each tenth of a second. The peak reflectivity during this period is recorded and 10 of these estimates are averaged to produce a reflectivity estimate each second of flight path (~150 m). Measurements of these equivalent reflectivity factors are compared to reflectivities calculated from images acquired by the 2D-C probe over a range of assumed particle densities. Matching the calculated and measured reflectivities gives an estimate of the densities and therefore the water content of the imaged particles.

(b) Results

There are four basic conditions that we have looked at with these three instruments.

Condition I : Cloud liquid water less than 4 g/m^3, no 2D images.
- King and Lyman-alpha agree

Condition II : Cloud liquid water exceeds 4 g/m^3, no 2D images.
- King saturates, Lyman-alpha measurement of cloud liquid water content accepted.

Condition III : Cloud liquid water content less than 4 g/m^3, 2D images, no radar echo.
- images are low density graupel particles containing little cloud water, King and Lyman-alpha measurements should be close.

Condition IV : Cloud liquid water content less then 4 g/m^3, 2D images, radar echo.
- under these conditions a match is sought between the equivalent radar reflectivities (Z_e) measured by the radar and the reflectivities calculated from the 2D images using a range of density assumptions. With this match, an estimate of the water content of the growing precipitation particles can be made. This water plus that measured by the King (provided that it does not saturate) should equal the total cloud water content minus the saturation mixing ratio at that level, measured by the Lyman-alpha hygrometer.

Examples of these conditions are shown in the following figures.

Fig. 3.4.1 shows Conditions I and II occurring on the same penetration. In the first cloud turret (between 1 and 2.5 km) the Lyman-alpha and King measurements of cloud water follow each other well. In the second cloud (4 to 7 km) the King output shows the typical "top hat" profile of an instrument that is saturating and in the comparison between the King and the Lyman-alpha, the latter measurement exceeds the former by more than 1 g/Kg. Table 3.4.1 summarizes these two events. (The data are taken from the cloud event statistics summaries computed by the Learjet data analysis software).

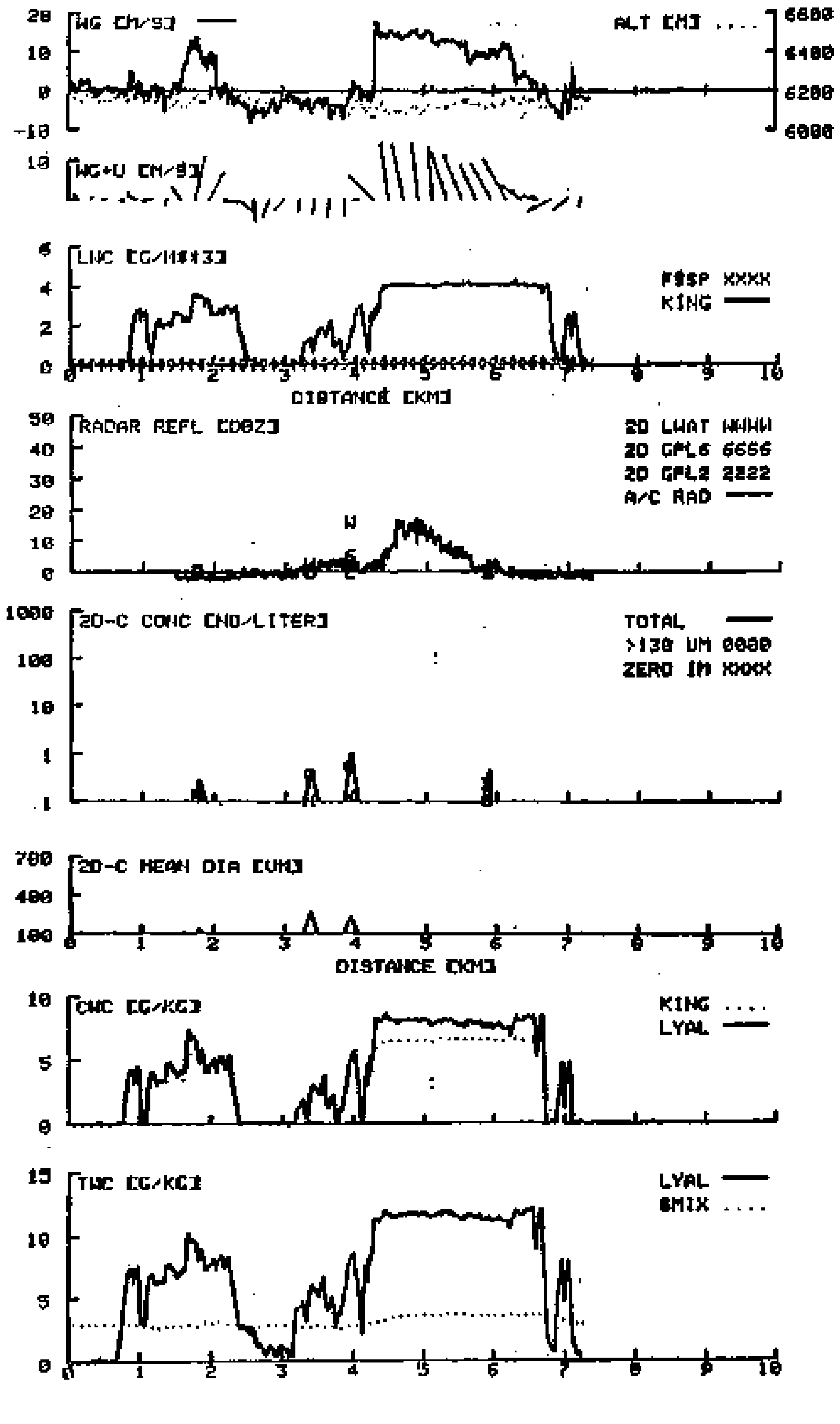

Fig. 3.4.1 Time histories of some of the variables measured on cloud penetrations. Conditions I and II-correspondence of King and Lyman-alpha and saturation of King, no 2D images.

Table 3.4.1 CONDITION I AND II

	Condition I	Condition II
King (g/m^3)	2.31	3.14
Lyman-alpha (g/m^3)	2.31	3.56
2-D conc (l^{-1})	0	0.6
Radar return (dBz)	-1.1	3.5

Condition III is illustrated in Fig. 3.4.2. Here we have lots of 2D activity, but the lack of a radar return from these particles indicates that their densities and therefore their water contents are very low. Table 3.4.2 summarizes the numerical calculations from this cloud.

Table 3.4.2 Condition III - 2D particles, but no radar echo

King (g/m^3)	3.38	Diff = 0.06		
Lyman-alpha (g/m^3)	3.44			
Radar return (dBz)	-2.2			
Computed 2D return (dBz) and water contents for assumed densities of:			dBz	g/m^3
		1.0 (water)	23	0.28
		0.8 (graupel)	15	0.22
		0.6	12	0.17
		0.4	9	0.11
		0.2 g/cm^3	3	0.06

Condition IV is illustrated in Fig. 3.4.3. Here, a significant portion of the cloud water is contained in the precipitation particles. The radar and 2D reflectivity comparisons suggest average particle densities of around 0.8 g/cm^3 whereas the best match between the difference between the Lyman-alpha and King cloud water measurements (0.89 g/m^3) would be for graupel particles with densities around 0.6 g/cm^3.

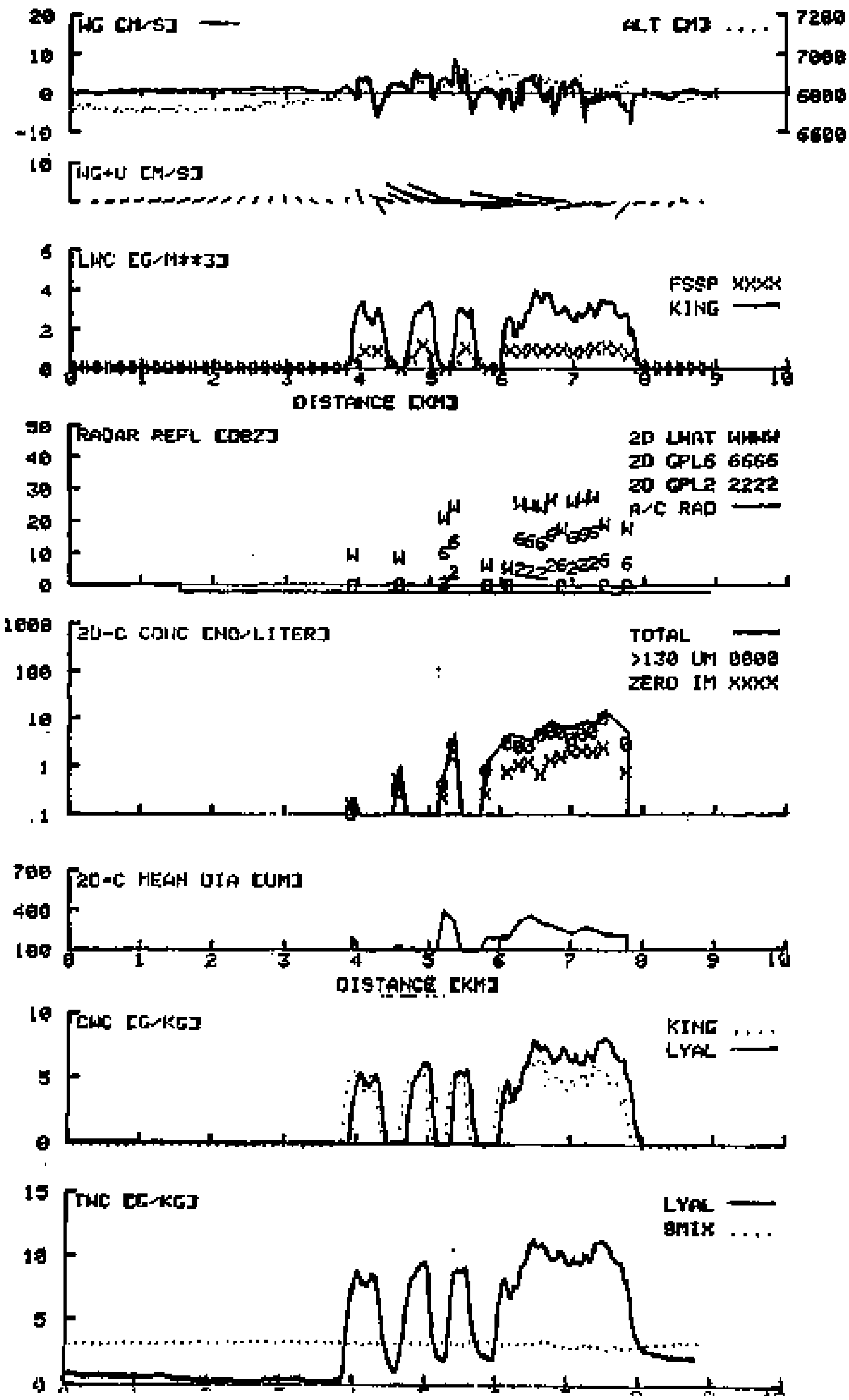

Fig. 3.4.2 Same as in Fig. 3.4.1, for Condition III - King and Lyman-alpha agree, 2D images of low density graupel.

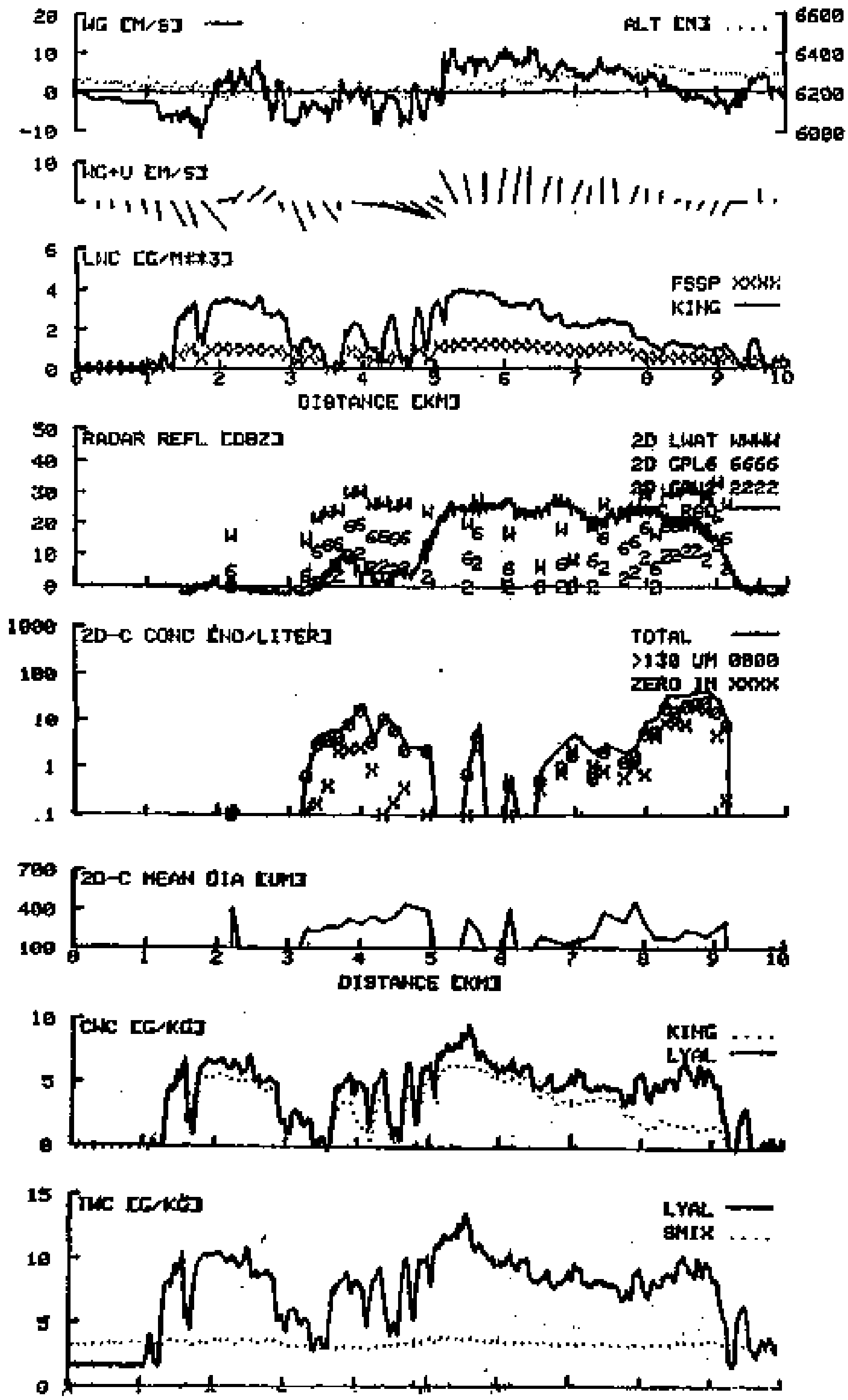

Fig. 3.4.3 Same as in Fig. 3.4.1, for Condition IV - Lyman-alpha exceeds King liquid water measurement, 2D images account for difference.

Table 3.4.3 Condition IV - 2D particles showing a radar echo

King (g/m^3)	2.09	Diff = 0.89	
Lyman-alpha (g/m^3)	2.98		
Radar return (dBz)	18		
Computed 2D return (dBz) and water contents for assumed densities of:		dBz	g/m^3
	1.0 (water)	24	1.42
	0.8 (graupel)	16	1.13
	0.6	14	0.85
	0.4	10	0.57
	0.2 g/cm^3	4	0.28

A variation on Condition IV can occur when many of the particles imaged by the 2D probe exceed 1 to 2 mm in diameter (Fig. 3.4.4). The software truncates all the large particles to 1 mm diameter circular images for reflectivity computations, but no truncation is used when computing particle water contents. This condition is illustrated in Table 3.4.4. The radar reflectivity (27 dBz) exceeds any of the reflectivities calculated for the 2D images.

Table 3.4.4 Variations on Condition IV - large 2D particles showing a radar echo

King (g/m^3)	2.09	Diff = 1.56	
Lyman-alpha (g/m^3)	3.65		
Radar return (dBz)	27		
Computed 2D return (dBz) and water contents for assumed densities of:		dBz	g/m^3
	1.0 (water)	17	1.41
	0.8 (graupel)	8	1.13
	0.6	6	0.85
	0.4	2	0.57
	0.2 g/cm^3	-4	0.28

Using the relation between reflectivity and liquid water content (Brown and Braham, 1963):

$$Z_e = 380 \ M^{1.46}$$

where

Z_e = equivalent radar reflectivity (mm^6/m^3),

M = liquid water content (g/m^3)

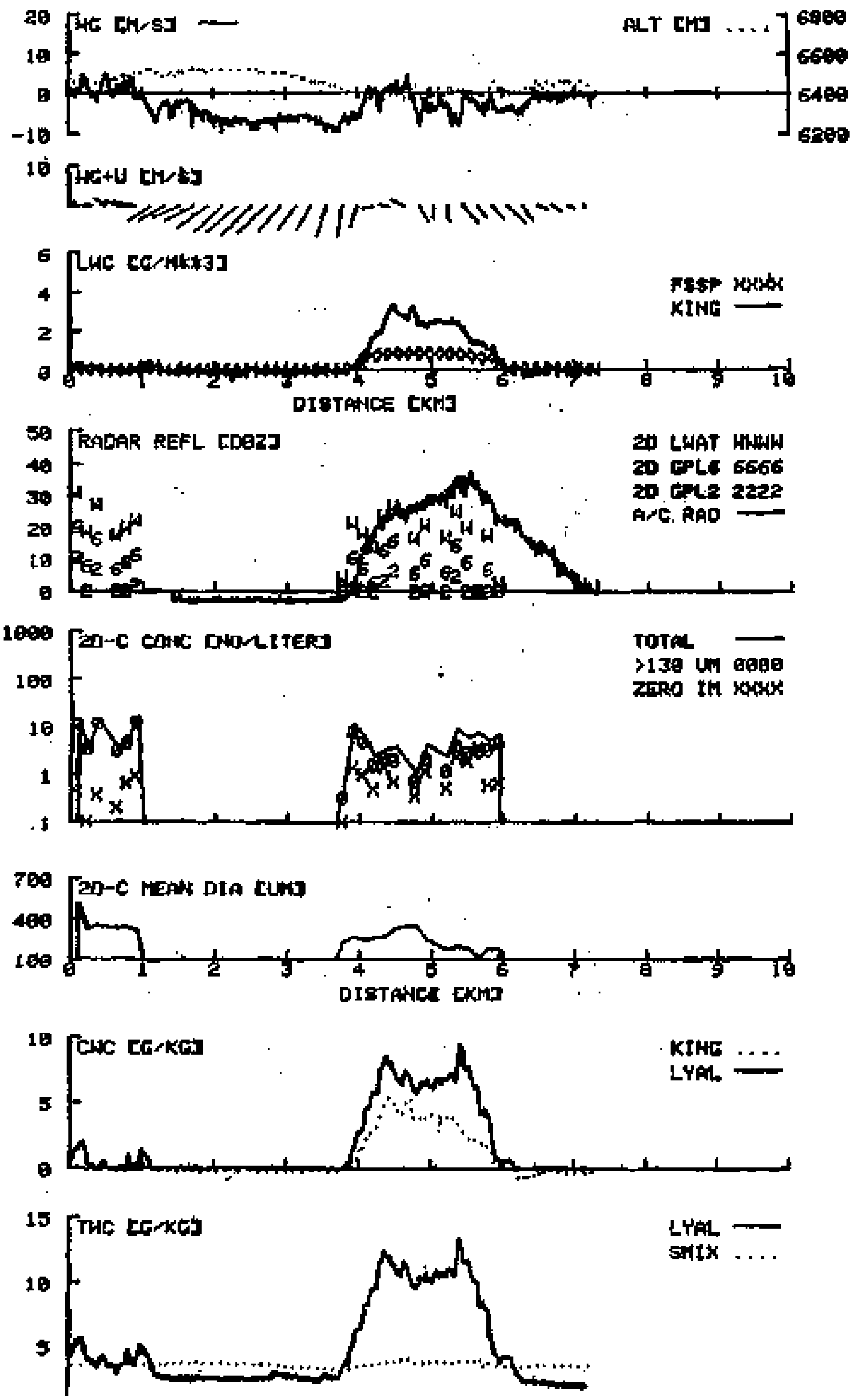

Fig. 3.4.4 Same as in Fig. 3.4.1, a variation of Condition IV. Lyman-alpha exceeds King measurements, radar and 2D liquid water measurements account for balance.

the liquid water content measured by the 2D probe (1.41 g/m^3) corresponds to 28 dBz which is close to the signal measured by the radar (27 dBz). This measure of water contained in the precipitation particles is not far off the difference between the King and the Lyman-alpha (1.56 g/m^3).

These exercises, which demonstrate an internal consistency in the aircraft measurements, are of the sort that build confidence in these instruments and their outputs. Only with such confidence can inferences be made about the microphysical processes that these measurements reveal.

3.5 Coalescence enhancement - a method of augmenting rainfall from convective storms?

(a) Introduction

A lot of work has been done over the past few years by the Nelspruit instrumented Learjet, penetrating fresh elements of convective clouds (usually on the flanks of thunderstorms) at levels around -10°C. This work has revealed that a "coalescence-freezing" mechanism (Braham, 1986) appears to be the dominant precipitation formation mechanism in the storms over the eastern escarpment region of the Transvaal (Mather et al., 1986). While most of the clouds in this area exhibit drops or frozen drop embryos at penetration levels, clouds in other areas of South Africa show either an absence of any particles or riming ice crystals at around -10°C (Kraus et al., 1987). Examination of the thermodynamic environments in which these clouds form indicates that the transition zone between one state of precipitation growth and the next may be quite a narrow one. This implies a potential instability which might be exploited for rain augmentation purposes. That such exploitation takes place inadvertently will be demonstrated below.

Observations are presented here that were made in a thunderstorm growing in the vicinity of a large paper mill. The microphysical measurements around the -10°C level departed so radically from what was expected at that level that some explanation for the errant behaviour of this storm had to be found. It will be shown that all the observations are consistent with an unusually active coalescence mechanism which modified the characteristics of this storm.

(b) Results

The most notable differences between the paper mill storm and others that have been sampled in similar thermodynamic environments are listed below:

- liquid and partially frozen large drops exceeding 4 mm in diameter
- high (twice normal) concentrations of small droplets as measured by a forward scattering laser probe (FSSP 100)
- almost complete conversion of cloud water to precipitation.

Eleven penetrations were made 4 to 6 minutes apart on new cloud turrets growing on the western to northwestern flank of this storm. Table 3.5.1 is a summary of the salient microphysical measurements from one representative penetration. A summary of the near-storm sounding conducted by the Learjet just west of the storm and immediately after the 11 penetrations is listed at the bottom of this table. Fig.3.5.1 shows selected time histories as well as some of the images collected by the 2D laser imaging probe on this pass.

Some of the more important observations from this table and the accompanying figure are:

- the dimensions of this cloud, a reasonably homogeneous cloud turret 5 to 6 km in diameter
- the high radar reflectivities recorded from the "flying" range gate 1800 m ahead of the aircraft (Mather, 1989), which exceed 40 dBz for almost 3 km and reach a maximum of over 52 dBz. It should also be noted that there was no hail encountered on any of the penetrations
- the Lyman-alpha time history shows this measurement just exceeding the adiabatic liquid content calculated from the

Table 3.5.1 A summary of microphysical and environmental measurements in and around the storm growing in the vicinity of a paper mill, 20 December 1988.

Property	Mean	Max	Min	Units
Pressure	431	444	421	mb
Static Temp	-10.8	-9.3	-13.0	^oC
Updraft Speed	11.9			m/s
True Airspeed	155	170	147	m/s
Lyman-a CWC	4.22	6.12	1.86	g/m^3
Lyman-a TCWC	11.33	14.74	6.43	g/kg
Reflectivity (Radar)	39.0	52.4	14.7	dBz
		2D-C		
Mass weighted D	2.16	4.72	0	mm
Reflectivity (Water)	25.1	35.0	0	dBz
LWC	3.44	29.43	0	g/m^3
		FSSP		
Concentrations	477	619	261	cm^{-3}
Mass-weighted D	16	18	14	µm
LWC	0.48	0.70	0.21	g/m^3
		CLOUD THERMODYNAMIC PROPERTIES		
Cloud Base Temp	13.0			^oC
Buoyancy at 500 mb	5.5			^oC
Saturated Mixing Ratio	13.2			g/kg

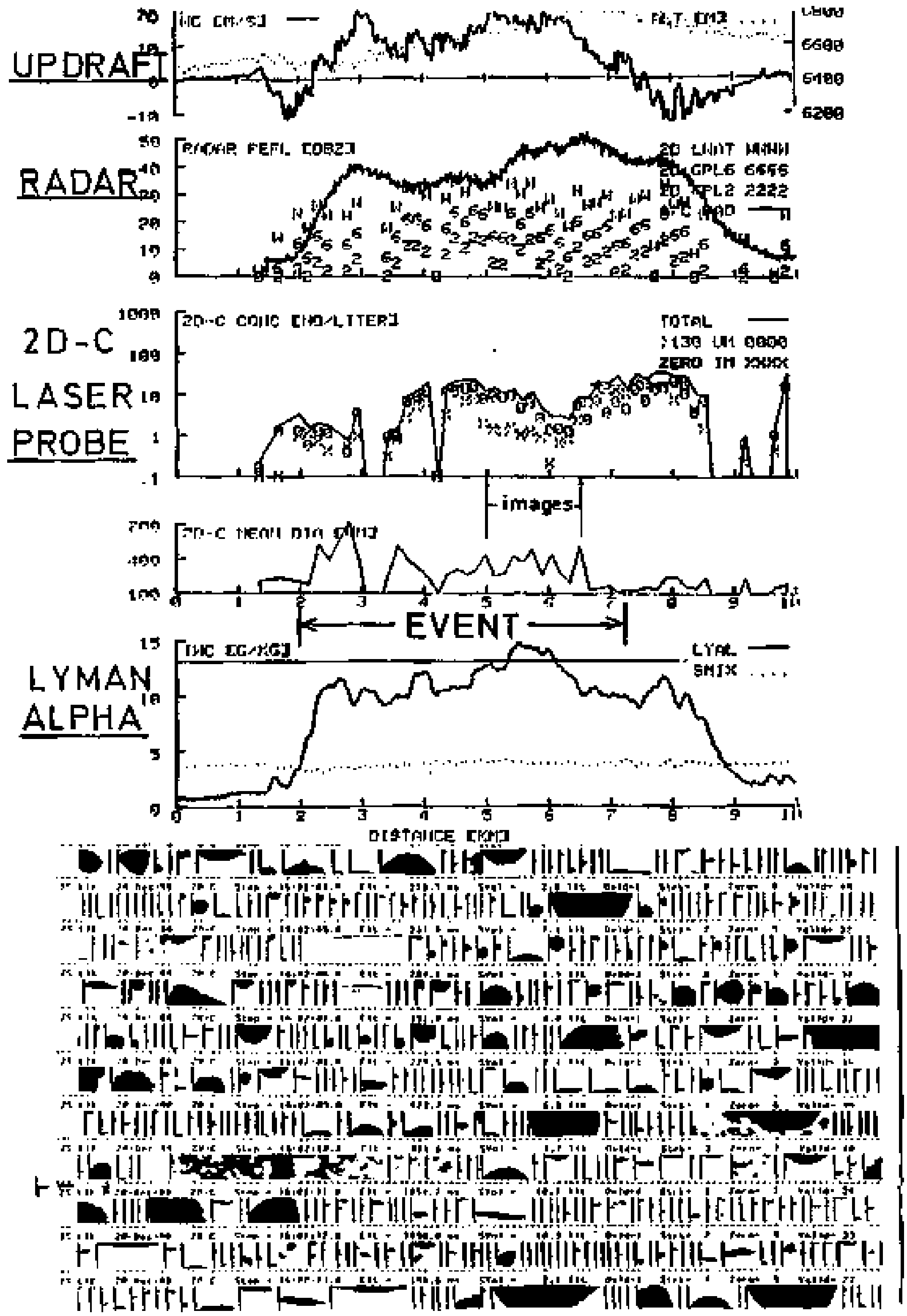

Fig 3.5.1 Time histories of cloud physics measurements from a penetration through a turret on the western flank of a storm growing in the vicinity of a large paper mill. Traces from the top downwards are: true gust velocity, measured and calculated (from 2D-C probe) equivalent radar reflectivities, 2D-C concentrations, mean diameters and finally the Lyman-alpha measurements of total water content. A portion of the 2D-C images recorded on this pass appears at the bottom of the figure.

sounding for a distance of less than a kilometre, but generally staying just below this value. Comparisons of 2D-C calculated water content (3.44 g/m^3) and Lyman-alpha cloud water content (4.22 g/m^3) indicate that, on average, all but about 0.8 g/m^3 of cloud water has been converted into precipitation-size drops. (The 2D-C probe measures only the water content in the rain drops using a circle-fit procedure (Heymsfield and Parrish 1978). The Lyman-alpha measures total cloud water content, i.e. vapour plus cloud water plus precipitation)

- the updraft velocity (11.9 m/sec) and the terminal velocity of a 4.7 mm drop (about 9 m/sec) are close so that an accumulation or "big` drop zone" in which cloud water contents locally exceed adiabatic values might be anticipated

- the pass-averaged mass-weighted mean diameter and droplet concentration measured by the forward-scattering laser probe (FSSP-100) would, according to Table 2 in Mather et al., (1986), place this cloud a long way from the coalescence threshold, indicating an unusual droplet spectrum for a cloud in which large drops are found at -10°C.

A further indication of the unusual nature of this storm is based upon a variation of the classification technique in which cloud base temperature and buoyancy at 500 mb were used to discriminate between the absence or presence of an active coalescence mechanism that produced drops around the -10°C level in new cloud development on the flanks of thunderstorms. Images from a 2D laser probe were used to judge whether drops were present or not, a somewhat subjective process. The use of the return from the flying radar range gate 1800 m ahead of the penetrating Learjet turns out to be a much more unequivocal measurement. If coalescence is active at around -10°C, there will be a strong radar return even if the drops are recently frozen and growing as dense graupel; if only ice crystals are present radar returns will be an order of magnitude less. This is well illustrated in Fig. 3.5.2. Here, the medians of the maximum equivalent reflectivities measured by the aircraft radar from multiple passes through storms on 7 different days are plotted versus temperatures of the convective condensation levels (T_{ccl}) and 500 mb buoyancies (T_{500}) computed from near storm soundings. Also plotted on the same figure is the median of the maximum reflectivities computed from the 9 passes through the paper mill storm (47.0 dBz). In the thermodynamic environment in which this storm grew, the ratio of its cloud base temperature to 500 mb buoyancy (2.36) places it just over the coalescence threshold (defined in Fig. 3.5.2 as a ratio of 2). In this position, its high radar reflectivity is clearly anomalous when compared to the other points on this plot. It should also be noted that the band separating those storms exhibiting coalescence growth from those that are not is a narrow one. It would appear that a degree or two of change in cloud base temperature and/or buoyancy can push a cloud from an ice crystal into a coalescence precipitation growth mode.

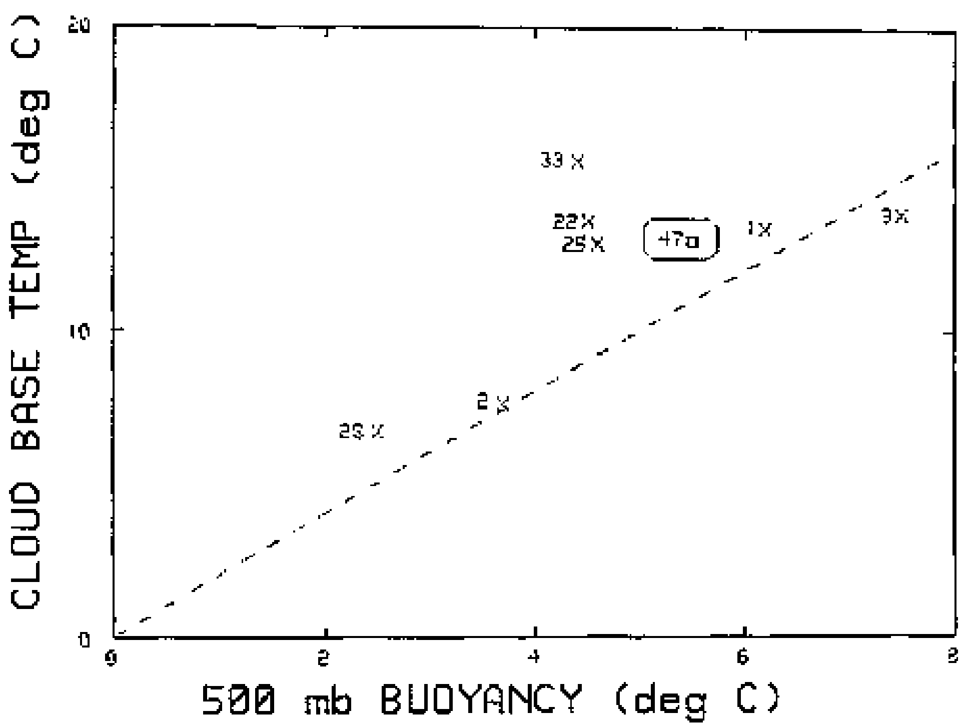

Fig. 3.5.2 The medians of the maximum equivalent radar reflectivities recorded from serial penetrations through new cloud development on the flanks of seven storms recorded on seven different days plotted against cloud base temperatures and buoyancies at 500 mb. The boxed value is for the paper mill storm.

The next bit of evidence to indicate that this was indeed an unusual storm comes from radar data collected on that day. The Nelspruit Project radar operates in a volume scan mode on all experimental days, recording the raw radar data on magnetic tape. These tapes are processed and storms are objectively tracked using software based upon an algorithm developed by Mader (1979). Each storm can be described by its track properties which in turn can be compared to other storms occurring on the same days. On December 20, a total of 65 storms were tracked (not including the sampled storm). Table 3.5.2 lists the means and the maxima of pertinent storm track properties computed for all other storms tracked on this day as well as the track properties of this unusual storm.

Table 3.5.2. Selected storm track properties calculated for the paper mill storm and averages and maxima for all other storms tracked on that day (66).

Track Property	66 storms Mean	66 storms Max	Paper Mill storm	Units
Max radar top	8267	14662	13862	M
Volume Time Integral	53	697	787	Km^3hr
Area Time Integral -1.5^o	11	116	121	Km^2hr
Area Time Integral - 6 km	10	119	147	Km^2hr
Rain Mass -1.5^o	79	948	1238	KTONS
Rain Mass -6 km	74	948	1738	KTONS
<u>Mean Mass</u>				
Rain mass	0.54	3.64	0.22	
Rain Rate	7.1	8.2	10.2	mm/hr
Max dBz	43	55	59	dBz
Duration	.55	1.55	1.57	Hrs

While the radar echo top of the sampled storm does not exceed the maximum recorded on that day, the volume and area-time integrals as well as the radar estimated rain masses of this storm exceed, and in many cases by a wide margin, the maximum values recorded from other storms on this day. The storm in question also lasts longer, rains harder and reaches the highest recorded reflectivity. All this is achieved by a storm whose ratio of storm mass (radar computed) to radar-estimated rain mass is considerably LESS than the mean for all storms recorded on that day, indicating that this large storm is raining in an efficient manner (efficiency defined here as the amount of rainfall produced per unit storm mass).

The last evidence that is presented in this section confirms the alterations in cloud drop spectra reported by Eagan et al., (1974 (a) and (b)), in clouds growing in the vicinity of a paper mill and a forest fire. Table 3.5.3 shows results from 4 runs at about 150 m above the bases of small to medium size (non-raining) cumuli in the vicinity of the paper mill. Run 1 is clearly through a cloud ingesting particles from the paper mill plume.

Table 3.5.3 Summary of measurements of droplet spectra made close to the bases of small non-raining cumuli in the vicinity of a paper mill and a forest fire

Run	1 Vicinity Paper Mill	2 Well West	3 South	4 Forest Fire	Units
Mean	1049	237	314	1013	cm^{-3}
32 um	0.01	0	0	0	cm^{-3}
Mean dia.	6.6	4.7	5.7	6.7	µm
Mass weighted mean dia.	9.7	6.3	8.2	9.9	µm
Dispersion	0.40	0.29	0.31	0.42	

Total droplet concentrations are 3 times higher than background counts (Runs 2 and 3) and the mean and, in particular, the mass-weighted mean diameters are larger. The measurement of importance here is the early appearance of relatively large droplets (32 µm) in the cloud growing in the paper mill plume in average concentrations of 10 per litre. These should lead to the early growth of precipitable drops by means of the coalescence mechanism. Note that the cloud growing near the forest fire has about the same droplet concentration and diameter as the paper mill cloud but shows no sign of the presence of droplets 32 µm.

This absence of the "large droplet tail" in clouds growing in the vicinity of forest fires was also noted by Eagan.

(c) Discussion

Examination of many convective cloud seeding programmes indicate that modest annual increases in rainfall of between 5 and 15% may be achieved in certain circumstances. Since it is not feasible to attempt to seed all storms (seeding 25% would be a good score), increases of around 100 percent per storm must be achieved to increase the annual precipitation by the above amount. Current seeding hypotheses just do not seem able to alter storm behaviour sufficiently to produce this required twofold increase in rainfall. The best clue to date of what will be required of a successful convective rain augmentation programmme may come from Metromex. A summary of the results of this experiment that have a strong bearing on this work are:

(i) Urban first echoes were found to have lower base heights than their rural counterparts

(ii) Urban-influenced cloud droplet spectra showed increased concentrations, reductions in mean drop sizes and increases of more than a factor of two in concentrations of large ($d > 20$ µm) droplets

(iii) There was strong evidence for urban deactivation of ice forming nuclei

(iv) Radar studies showed increases in heights as the echoes crossed the urban areas as well as increases in frequencies of very large echoes one to two hours wind travel downwind of the city

(v) Rain cell analysis showed that most of the rain cells responsible for the nocturnal anomaly came from cells that were exposed to the urban environment. The areas, volumes and intensities of these rain cells were much larger than those found in surrounding rural areas

(vi) Metromex results strongly suggest that at least the nocturnal anomaly was a result of urban influences affecting a few of the heavier rain events (Changnon et al., 1986).

The storm described in this paper fits the description of the type of storm thought to be responsible for the major portion of the positive rainfall anomaly downwind of St. Louis. It has a larger volume and area, rains harder and lasts longer than any other storm observed in the area on that day. These attributes are brought about by an unusually active coalescence mechanism which is documented by cloud physics measurements made by the Nelspruit Learjet at around the -10°C level. The anomalous behaviour of this storm is believed to have been caused by the alteration of cloud base droplet spectra by the effluent from a large paper mill. Measurements indicate that these droplet spectra are very similar to those found in clouds forming over the St. Louis urban-industrial complex (Changnon et al., 1981).

3.6 Airborne rainfall measurements using the Nelspruit cloud base aircraft.

(a) Introduction

The CRAWS cloud base aircraft (ZS-IZN) has been equipped with a cloud physics measurement system which includes a 2D-P laser imaging probe (range: 0.2 to 6.4 mm diameter). A vertical gust system identical to the one in the project Learjet described in Volume IV of the PAWS I report (WRC 133/4/88), has also been installed. The extra feature that has been added to the cloud base aircraft is the ability to record complete scans from the aircraft's 3 cm radar. The object here is to use the aircraft as a "flying rain gauge". It is believed that this system has the potential for making the best possible estimates of rainfall from isolated convective storms. No feasible network of rain gauges can possibly be expected to match the accuracy of such a system, provided it is calibrated properly and used in an intelligent manner. Cloud base rainfall would thus be considered "ground truth". Rainfall estimates made using the Carolina 5 cm radar would be checked against this standard.

Progress in bringing this system on-line has been slow. It was discovered halfway through the 1988/89 season that the log IF amplifier that is used between the commercial receiver and the recorder had failed. A replacement finally arrived in March.

A study of the data that had been acquired indicated that direct comparisons of the 2D-P and the radar with the radar in scan mode were uncertain since the volume sampled by the 2D-P probe was scanned by the radar just once every 4 seconds. For a more unequivocal comparison, it was decided to lock the antenna facing forward along the flight path, so that the volume being sampled by the probe would be scanned continuously by the radar. A flight was launched on March 13, 1989 and IZN was operated in this configuration on 8 penetrations through showers from isolated storms. The following is an analysis of these data.

(b) Measurement techniques

(i) Radar

The characteristics of the 3 cm radar on the cloud base aircraft are listed below:

Make	: Bendix RDR 1200
Pulse length	: 3.5 µs
PRF	: 99 Hz
Frequency	: 9345 MHz
Power	: 10 Kw Peak
Beam width	: 7^{o}

With the radar locked facing forward along the flight path, the equivalent radar reflectivities from the fourth range gate are compared to reflectivities calculated from the 2D-P probe images ($\sum nD^6$). The middle of the fourth range gate is 1875 m ahead of the aircraft (2 μs skip, 3 μs range gate x 3.5, 150 m per μs). The length of the volume sampled by the radar is 525 m (pulse length 3.5 μs). The number of integrations of the radar signal is 8, so that the radar sample rate is 12.38 samples per second (PRF/8).

Since the volumes sampled by the 2D-P probe are irregular, depending upon rain drop concentration, the comparisons between radar reflectivities and reflectivities calculated from the 2D probe data are controlled by the size of the volume sampled by the 2D probe. The time required for the aircraft to reach the centre of each radar sample from the fourth range gate is calculated (knowing the aircraft's true air speed). The number of these radar measurements that fall within each 2D volume sample is averaged and compared to the equivalent reflectivity computed from the drops within this volume. The following sketch may be of some help in visualizing how the comparisons are made.

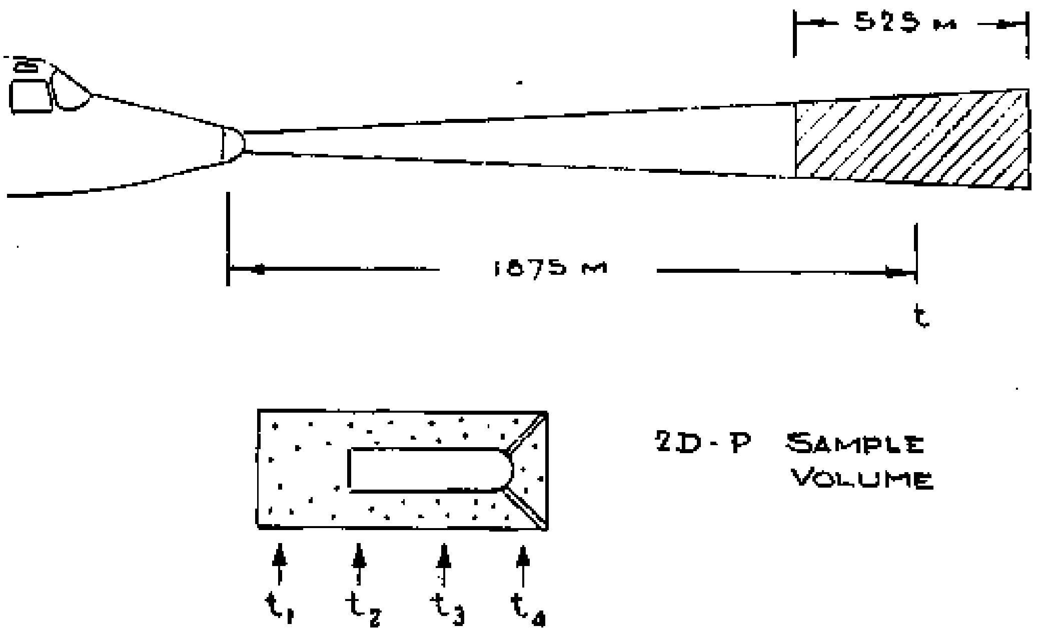

Fig. 3.6.1. Radar and 2D-P geometry for comparisons of radar and computed 2D reflectivities.

ii) Particle size measurements

Rain drop sizes are measured by a 2D-P laser imaging probe. The probe on the Learjet is configured to work in two modes: end reject "on" or "off". With end reject "on", particles intercepting either of the end elements are rejected, which restricts the sampling of the larger particles (effectively reducing the sample volume). Since it is the large particles that are the major contributors to radar reflectivities, liquid water contents and therefore rain rates, a better sampling configuration for the probe is to operate with end reject "off" and recover the dimensions of the partially viewed or truncated particles using a circle-fit procedure (Heymsfield and Parrish, 1978).

Since the 2D-P probe is the most important element of this rainfall measuring system, it is prudent to check on the sampling characteristics of this instrument to ascertain that the measured drop size distributions conform to an accepted standard.

First, the larger rain drops must be corrected for shape distortions to obtain a volume-equivalent diameter, since they tend to "pancake", and the vertically oriented 2D-P probe views the diameter of these pancakes. The method of correction is made following Green (1975), whose aspect ratios are in good agreement with experimental results.

Measured drop size distributions sampled on one pass through a rain shaft falling from a convective storm are listed in Table 3.6.1.

Following Smith (1982), the inverse cumulative distribution, $N_L(D)$ is computed (last column, Table 1) and plotted in Fig. 3.6.2. $N_L(D)$ is related to the Marshall-Palmer exponential size distribution by

$$N_L(D) = \int n_o e^{-\lambda D} dD = (n_o / \lambda) e^{-\lambda D}$$

A least squares linear fit to the points in Table 3.6.1 gives

$$N_L(D) = 677e^{-2D}$$

Table 3.6.1. Observed rain drop distributions in a rain shaft falling from a convective storm.

Channel Number	Average diameter (mm)	No of drops observed	Inverse cumulative distribution	$N_L(D)$ (m^{-3})
1	.241	678	3667	229
2	.439	713	2989	187
3	.637	576	2276	142
4	.835	459	1700	106
5	1.033	386	1241	77
6	1.23	215	855	53
7	1.426	170	640	40
8	1.623	136	470	29.4
9	1.829	94	334	20.9
10	2.027	62	240	15.0
11	2.215	51	178	11.1
12	2.411	22	127	7.9
13	2.608	48	105	6.6
14	2.805	17	57	3.5
15	3.002	8	40	2.5
16	3.2	11	32	2.0
17	3.4	11	21	1.3
18	3.6	5	10	0.6
19	3.8	0	5	0.3
20	4.0	1	5	0.3
21	4.2	3	4	0.25
21	4.4	1	1	0.06

Sample volume: 16.0 m^3, D_m = 2.0 mm, W = 0.27 gm/m^3

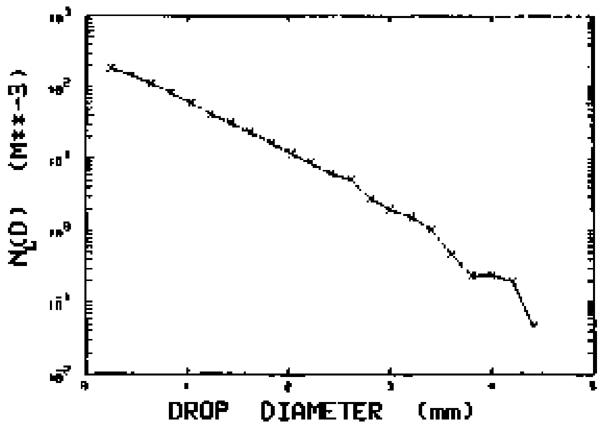

Fig. 3.6.2 Semi-logarithmic plot of the inverse cumulative drop distribution, $N_L(D)$, for the 2D-P sample in Table 3.6.1.

Thus, for an exponential size distribution, the mass-weighted mean diameter,

$$D_m = 4/\lambda$$

and the liquid water content of the precipitation,

$$W = \sigma \pi n_0 D_m^4 / 256$$

where σ is the density of water.

As a further check, $N_L(D)$ is normalized as follows:

$$N_L(D)(\sigma D_m^3 / W) = 64/\pi \, e^{-4D/D_m}$$

The sampled drop distribution, normalized by D_m/W, is plotted against normalized drop diameters (D/D_m) in Fig. 3.6.3. The solid line in the figure is the "universal" exponential function with y intercept equal to $64/\pi$ and a slope of -4. The experimental data agree well with this universal exponential function.

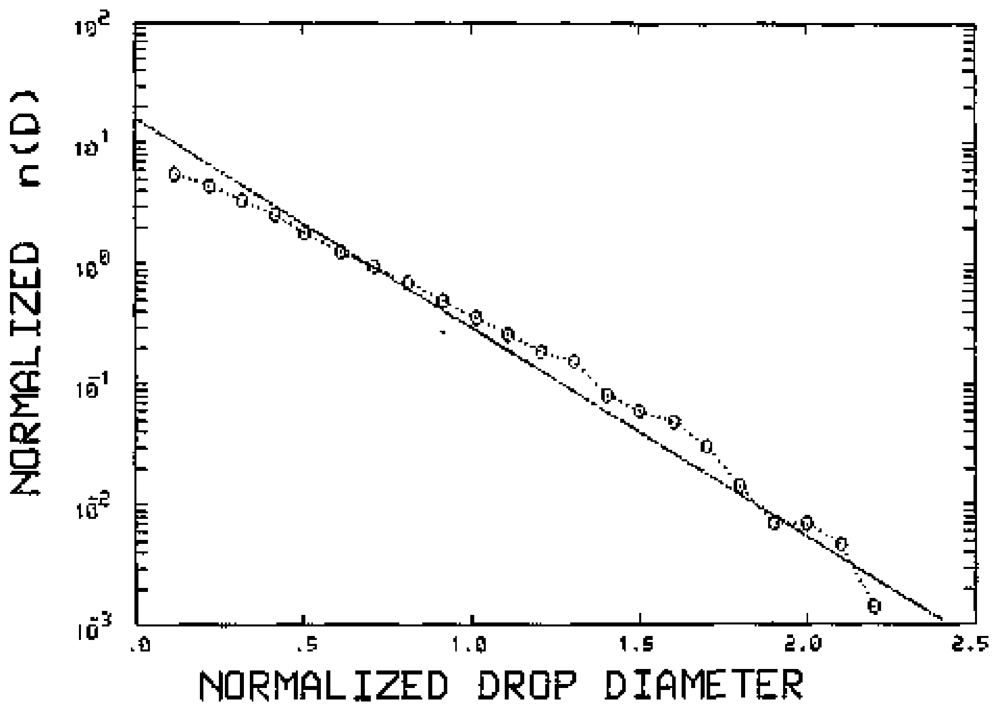

Fig. 3.6.3. Normalized form of the data from Table 3.6.1, showing agreement with the "universal function" represented by the straight line (see Smith, 1982).

A final check on the data, also suggested by Smith, is to plot the cumulative fraction of the liquid water content in the experimental sample. This is done in Fig. 3.6.4. The solid curve in the figure is the cumulative distribution of a continuous exponential function like the Marshall-Palmer distribution. Again it can be seen that the experimental data closely follow the contour of an exponential distribution.

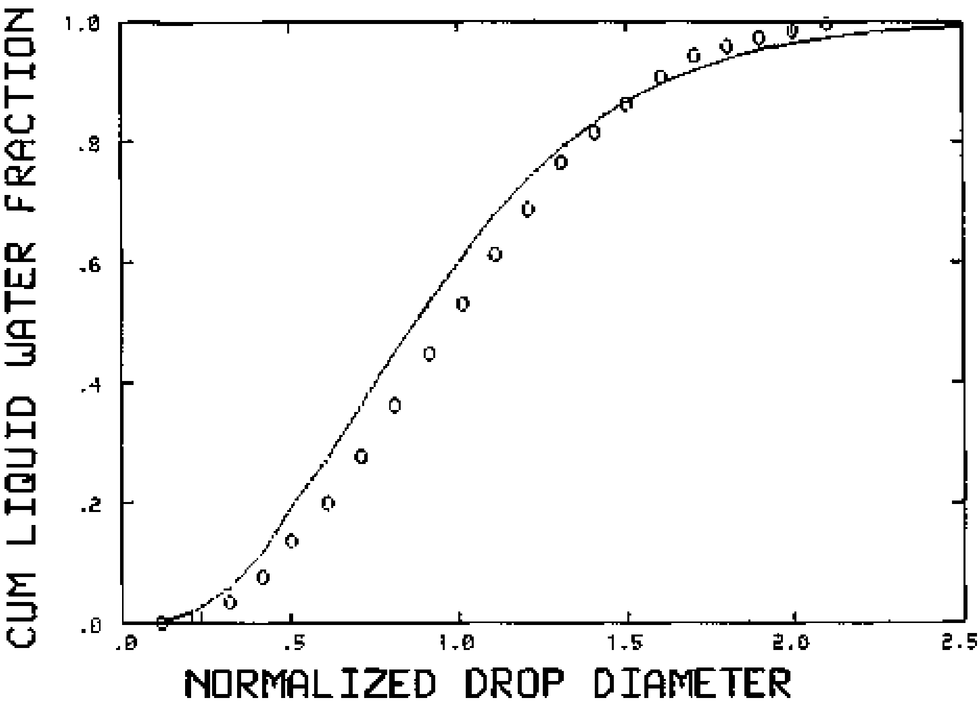

Fig. 3.6.4. Normalized mass concentration versus normalized drop size. The smooth curve is the exponential distribution predicted by a Marshall-Palmer distribution.

If the measured rain drop distribution is truly exponential, mass-weight mean diameters, liquid water contents and equivalent reflectivities calculated assuming an exponential distribution should agree closely with the same quantities calculated over the run using the following formulae:

$$W = (\pi/6)\sigma\Sigma N(D)\ D^3$$

$$Z_e = \Sigma\ N(D)\ D^6$$

Reflectivity, assuming an exponential distribution is computed from

$$Z_e = 0.176\ Dm^6\ N_L(D)$$

The results from these computations are listed in Table 3.6.2.

All the above comparisons and analyses generate confidence in the probe measurements and analysis software.

Table 3.6.2. Comparison of estimates assuming an exponential distribution to those calculated over the pass.

Quantity	Computed over pass	Assuming exp. distribution	Units
Dm	2.10	2.00	mm
W	0.36	0.27	gm/m^3
Z_e	37.9	38.8	dBz

(c) Radar/2D-P equivalent reflectivity measurement comparisons.

If the radar is properly calibrated and the 2D images are corrected for distortion, then any disagreement between measured (radar) and calibrated (2D-P) equivalent reflectivities are probably a result of the disparity in sample volumes of the two instruments. The radar each second views a volume of about 9.7 x 10^8 m^3, while the 2D probe samples just 0.15 m^3. Despite the sample volume mismatch, the two measurements are comparable as is illustrated in Fig. 3.6.5. Here, the unsmoothed 2D-P calculated reflectivities are compared to the radar signal averaged as described in Section (b) above. Perhaps some averaging of the 2D-P signal would improve agreement, but this will be accomplished when calculating the line integral of rain rates along the flight path.

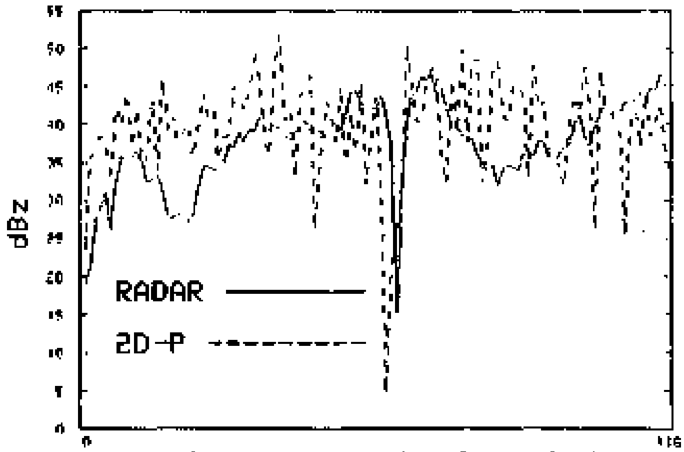

Fig. 3.6.5 A comparison of calculated (2D-P) and measured (aircraft 3 cm radar) equivalent reflectivities acquired from a single pass through a rain shower. The radar signal has been suitably lagged.

(d) Rainflux calculations.

Here, we follow the method outlined by Cooper (1980). Briefly, representative PPI radar displays of storms often resemble a two-dimensional distribution:

$$R(x,y) = \frac{R_o}{2\pi\sigma_x\sigma_y} \exp\left(\frac{-x^2}{2\sigma_x^2} \frac{-y^2}{2\sigma_y^2} \right)$$

Assuming this to be the true distribution, the total rain flux, R_o, would be

$$R_o = \int\int R(x,y)\, dx\, dy.$$

On any one pass through the precipitation, the line integral, L, of the rainfall rate would be

$$L_x = \int R(x,o)dx = R_o/\sqrt{2\pi}\sigma_y$$

or

$$L_y = \int R(o,y)dy = R_o/\sqrt{2\pi}\sigma_x$$

The total rainflux is then

$$R_o = (2\pi L_x L_y \sigma_x \sigma_y)^{1/2}$$

for two orthogonal passes which pass through the centre of the rainfall distribution. The required values of L and σ are computed from the aircraft measurements as follows:

$$L_i = \int R(s)\, ds$$

$$S_i = \frac{1}{L_i}\int s\, R(s)ds$$

$$\sigma_i^2 = \frac{1}{L_i}\int (s - s_i)^2\, R(s)\, ds$$

where R(s) is the rainfall rate at position s along the aircraft flight path.

Fig. 3.6.6 shows a comparison of aircraft and ground based 5 cm radar comparisons of calculated rain flux. Initially, there is close agreement, then the radar-measured flux shows a sudden jump (from 53 to 89 m^3/s) at 12.65 hours which is not mirrored by the aircraft measurements. Careful examination of the low level PPI indicates that the tracking programme incorporated a lot of additional echo (30 to 40 dBz) that was not penetrated by the aircraft.

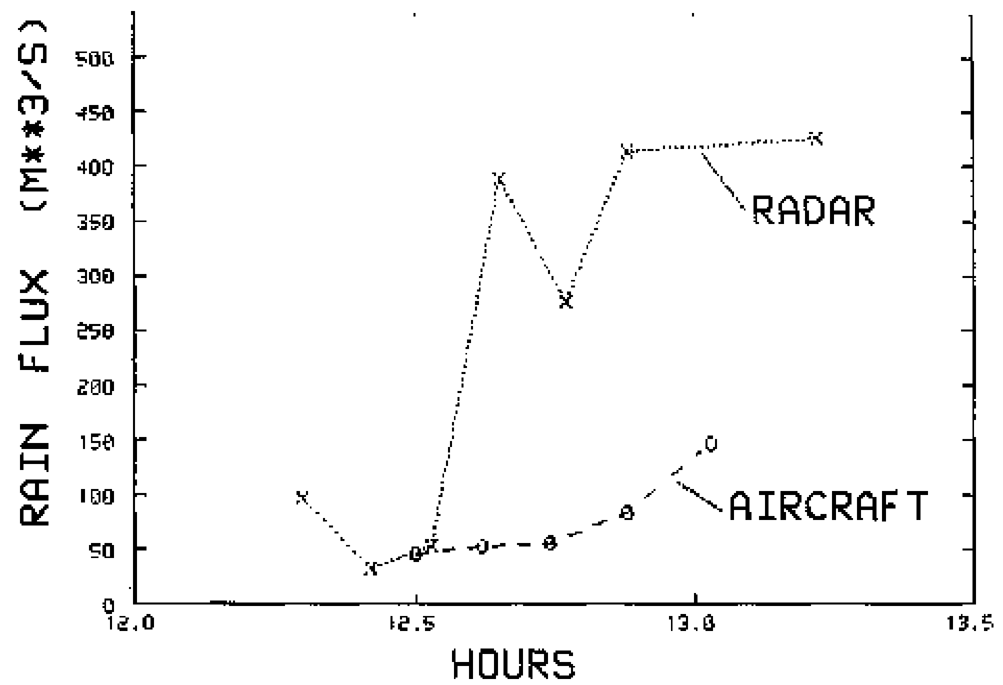

Fig. 3.6.6. Rain fluxes measured by the ground based 5 cm radar compared to fluxes obtained from the 2D-P probe using the method outlined in the text.

(e) Discussion

From this preliminary report, it is clear that this work has just commenced. Techniques for measuring rainfall with the aircraft still have to be perfected. Methods of more fully utilizing the aircraft's 3 cm radar still have to be investigated. Precipitation echo areas and reflectivity distributions can be mapped by this system, which should help bridge the sample volume gap that exists between the 2D-P measurement of rain rates and those of the ground based radar.

The prime advantage of this system, if its potential can be fully realized, lies in its mobility. Experiments do not have to be confined to a surface network, but can take place anywhere within the range of the ground based radar.

3.7 Evidence of an accumulation or "big drop" zone.

(a) Introduction

The possibility of an accumulation or "big drop" zone aloft (above the freezing level) and its implications in terms of hail growth have been a source of speculation for decades (Kessler, 1969; Browning, 1977). The existence of such a zone is the cornerstone of the Soviet hail suppression hypothesis (Sulakvelidze, 1974). Here a clear case of an accumulation zone is reported, persisting over more than 2 km of a penetration through a cloud rising vigorously on the flanks of a multicell storm. New instrumentation on the Nelspruit Learjet convincingly measures the superadiabatic liquid water contents that were found in the cloud.

The storm that is the object of this study was found travelling northeastward towards the western border of Swaziland. The measurements that follow were taken when the storm was just south of the town of Amsterdam, between 15 and 16:00 SAST. Synoptic analyses showed an upper air trough to the west of the area and a cold front moving up the southeast coast, through Durban by 08:00. These conditions produced scattered afternoon thunderstorms along the escarpment west and north of Swaziland.

(b) Instrumentation

The instruments used in this case study have been described in a previous paper (Mather, 1989). For convenience, a list and a brief description of these instruments follows:

(i) Radar flying range gate. The aircraft 3 cm radar is locked in a forward-facing position aligned along the flight path prior to cloud penetration. The return from a single range gate 1800 m ahead of the aircraft is recorded. This signal is suitably lagged during playback of the flight data to coincide with the other microphysical measurements.

(ii) Lyman-alpha engine vapour technique. This instrument is fully described in Morgan et al., (1989). Air is tapped off the eighth stage of the Learjet compressor. The water vapour content of this air is measured using a Lyman-alpha hygrometer. This is a measurement of total cloud water content, since it includes water vapour, cloud liquid water plus the water stored in precipitation particles, all of which are evaporated by the jet engine compressors.

(iii) CSIRO-King liquid water probe. Although at Lear speeds this sensor saturates at around 4 g/m^3, it has provided reliable measures of cloud water up to this limit. The probe also has a large droplet size limit. Response to liquid water contents with median volume diameters of greater than 100 μm is significantly diminished (Biter et al., 1987).

(c) Measurements

Fig. 3.7.1(a) portrays selected time histories and Fig. 3.7.1(b) some of the images from the laser cloud probe that were collected on this run. The 2D probe suffers from electrostatic interference initially, but recovers shortly after the 3 km distance marker. The start of the event over which averages are computed is set to commence at 3.49 km into the run and end at 5.76 km. Table 3.7.1 is a summary of some of the means calculated over this event. Of great interest here is the close correspondence between the 2D probe and Lyman-alpha measurements of the water content of the precipitation particles. The Lyman-alpha estimate is obtained by subtracting the saturation mixing ratio (at the level of penetration) and the King measurement of liquid water from the Lyman-alpha total cloud water content measurement. (It should be noted here that the Lyman-alpha and King measurements of cloud liquid water content correspond closely when there are no particles larger than about 100 μm present and the King does not reach saturation). The 2D probe measurements are extracted from the images using a circle-fit procedure (Heymsfield and Parrish, 1978) and the assumption that the particles are supercooled water drops.

The laser imaging probe on the Learjet is a Particle Measurement Systems 2D-C with a resolution (distance between diodes) of 35 μm. The images appearing in Fig. 3.7.1(b) have not been processed in any way (i.e. artifacts such as splashers and streakers removed, smoothing of drop images, etc).

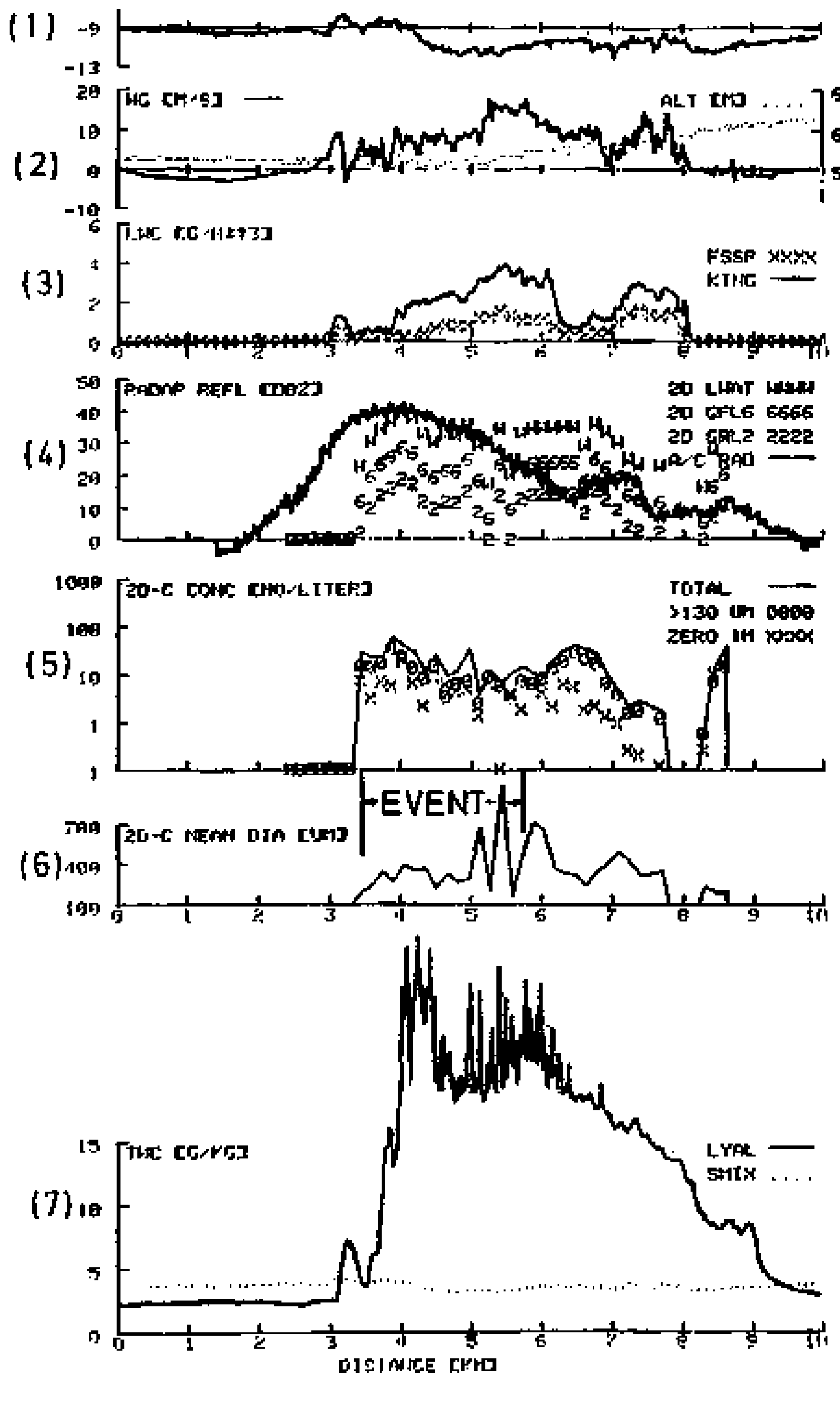

Fig. 3.7.1 (a) Time histories, recorded during a penetration through an accumulation or "big drop" zone. Time histories from the top of the figure down are: static temperature (1), true vertical gust velocities (2), King and FSSP cloud liquid water (3), equivalent radar and calculated 2D-C reflectivities (4), 2D-C concentrations (5) and mean diameters (6), and finally, total cloud water measured by the Lyman-alpha humidiometer (7).

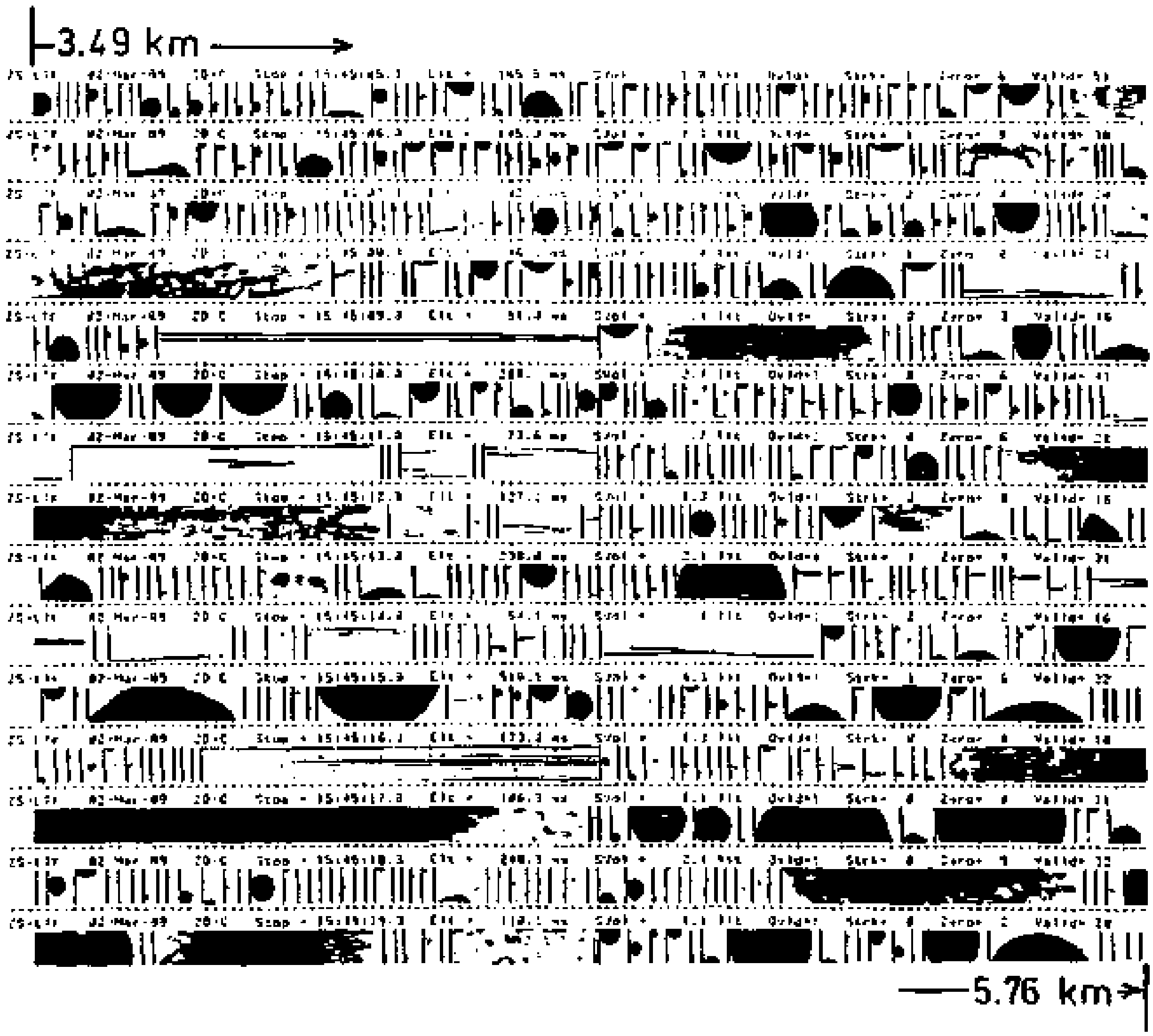

Fig. 3.7.1 (b) Drop images from the 2D particle size spectrometer recorded over the event marked in Fig. 3.7.1(a). The vertical dimension of the time bars separating the images is 1.12 mm. The ragged images (e.g. line 4 and 5, the end of line 7 and the beginning of line 8, the end of line 12 and the beginning of line 13) are produced by splashing drops and are rejected as artifacts before computing liquid water contents and reflectivities.

Table 3.7.1 Summary of cloud physics and environmental measurements.

Measurement	Sensor	Average over event	Units
Cloud water content	King	2.3	g/m^3
Cloud water plus precipitation	Lyman-alpha	11.8	g/m^3
Precipitation water content	(L-A)-(King)	9.5	g/m^3
Precipitation water content	2D probe	9.2	g/m^3
Total cloud water	Lyman-alpha	22.0	g/Kg
Adiabatic limit	Sounding	15.4	g/Kg
Reflectivity	Aircraft radar	34.2	dBz
Reflectivity	2D probe	31.7	dBz
Updraft speed	Angle of attack vane, rate gryo and accelerometer	9.2	m/s
Cloud Base Temperature	Rosemount Probe	17.3	^oC

The spikes in the Lyman-alpha time history are presumably caused by the extremely large drops that are encountered on this penetration. The average equivalent radar reflectivity calculated from the 2D images (assuming water drops) underestimates the reflectivity recorded from the aircraft radar by about 2.5 dB. This is not surprising since drops over 1 mm in diameter are truncated to this size for the 2D reflectivity computations (see Mather, 1989). No such truncation takes place when calculating precipitation water contents.

The calculated updraft speed across this event is 9.2 m/s which is capable of supporting drops of about 6 mm in diameter.

(d) Discussion

Given warm cloud bases and sufficient buoyancy, an active condensation-coalescence mechanism exists in convective clouds in the Eastern Transvaal. This is revealed by the appearance of large supercooled water drops at around the -10^oC level in these clouds. From this observation to the development of accumulation zones would merely require the right updraft profile.

Of what significance are such accumulation zones to the production of rain and in particular hail? This will, of course, depend upon their frequency and volume. It is not surprising that they are encountered so seldom by instrumented aircraft, given the sampling limitations of these systems (both in time and space). Good radar data should be able to detect such zones as enclosed volumes of high reflectivity aloft (> 50 dBz).

3.8 Further development of the engine compressor technique for measuring total and condensed water mixing ratios in clouds.

(a) Introduction

The new technique for measuring water quantities using the jet engine compressors as evaporators has been a component of the Learjet instrumentation for several years. Development of the technique continues, however, and, during the 1986-87 season, progress was made in understanding the errors induced by non-isokinetic flow into the engine inlets. The effective volume flow in the engine compressor was also established.

(b) Non-isokinetic effects

The principles and techniques involved in performing the jet engine measurements are described in detail in Vol. IV section 9 of the WRC Report 133/4/88; here we will discuss only the problems under study.

Ideally, a jet engine should take in all air geometrically intercepted by its intake. This is realized only under particular conditions of power setting, true air speed and altitude. Under more general conditions the engine will either reject air from the geometrically intercepted flow tube or draw air from outside it. Thus the flow near the engine inlet is distorted and particles of differing sizes will be sampled from different volumes of air.

This source of sampling error has been examined by installing a static pressure sensor in the nacelle of the port engine and monitoring the "spill fraction" (S.F), as defined below.

$$S.F. = 1 - F_N/F_G = 1 - 0.92\ V_N/TAS$$

where F_G is the flux of air intercepted by the engine inlet, F_N is the flux of air in the nacelle, V_N is the airspeed in the nacelle and TAS is aircraft true airspeed.

The spillage effect produces no error in the measurement if the droplets are small enough to follow the air. For the present evaluation we estimate the change in mixing ratio for drops so large as to not respond at all to the airflow, and so estimate an upper limit to the error.

The true mixing ratio, W_p, will be

$$W_p = W_{PN} \times V_N \times S_N / TAS \times S_I$$

where

S_I and S_N are the air interception cross-sectional area of the inlet and the cross-sectional area of the inlet where the pressure was measured, respectively ($S_I = 0.14$ m^2, $S_N = 0.129$ m^2) and W_{PN} is the mixing ratio in the nacelle.

Fig. 3.8.1 shows estimates of S.F. made on a test flight. Spill fraction can be seen here to be an increasing function of airspeed and pressure and a decreasing function of power setting (for constant airspeed).

The smallest particles in the cloud follow the air motion closely and so, for them, there is no non-isokinetic error in the mixing ratio. The liquid water mixing ratio for the cloud droplets must be subtracted from the condensed water mixing ratio before applying a correction for the spill effect. Thus, the estimated true value, W of condensed water mixing ratio will be

$$W = W_{KING} + (1 - S.F.)(W_C - W_{KING})$$

where W_C is the condensed water mixing ratio measured by the engine-compressor technique. As an example, for a pressure of 486 mb and a TAS of 150 m sec^{-1}, the S.F. is approximately + 0.25. If the engine measurement was 6 g/kg and the King hot wire yielded 3 g/kg, the estimated true value would be 3+(1-0.25)(6-3) or 5.25 g/kg, an error of 12.5 percent. This is, again, an upper limit estimate of the error.

Since performing this study it has been decided to reduce the penetration speed of the aircraft well below 150 m sec^{-1} in order to keep this type of measurement error below 10 percent.

(c) The sample volume; mixing in the compressor

The compressor is designed to direct the air through the engine without developing swirl. Air is sampled at one point on the circumference of the last compression stage. Water entering the opposite side of the engine would not be sensed if mixing were not thorough. A simple test was performed to check for complete mixing of the air in the compressor. With the engine running at 88 percent rpm a garden hose was directed into the engine at its outer edge near the compressor face. This narrow water source was then moved, in steps of 45 degrees, completely around the outer rim and data from the Engine-Vapour system recorded on tape. No variation of the total water mixing ratio with position of the hose could be detected. Mixing in the tangential sense is complete and the volume sampling rate is the total volume flow through the engine.

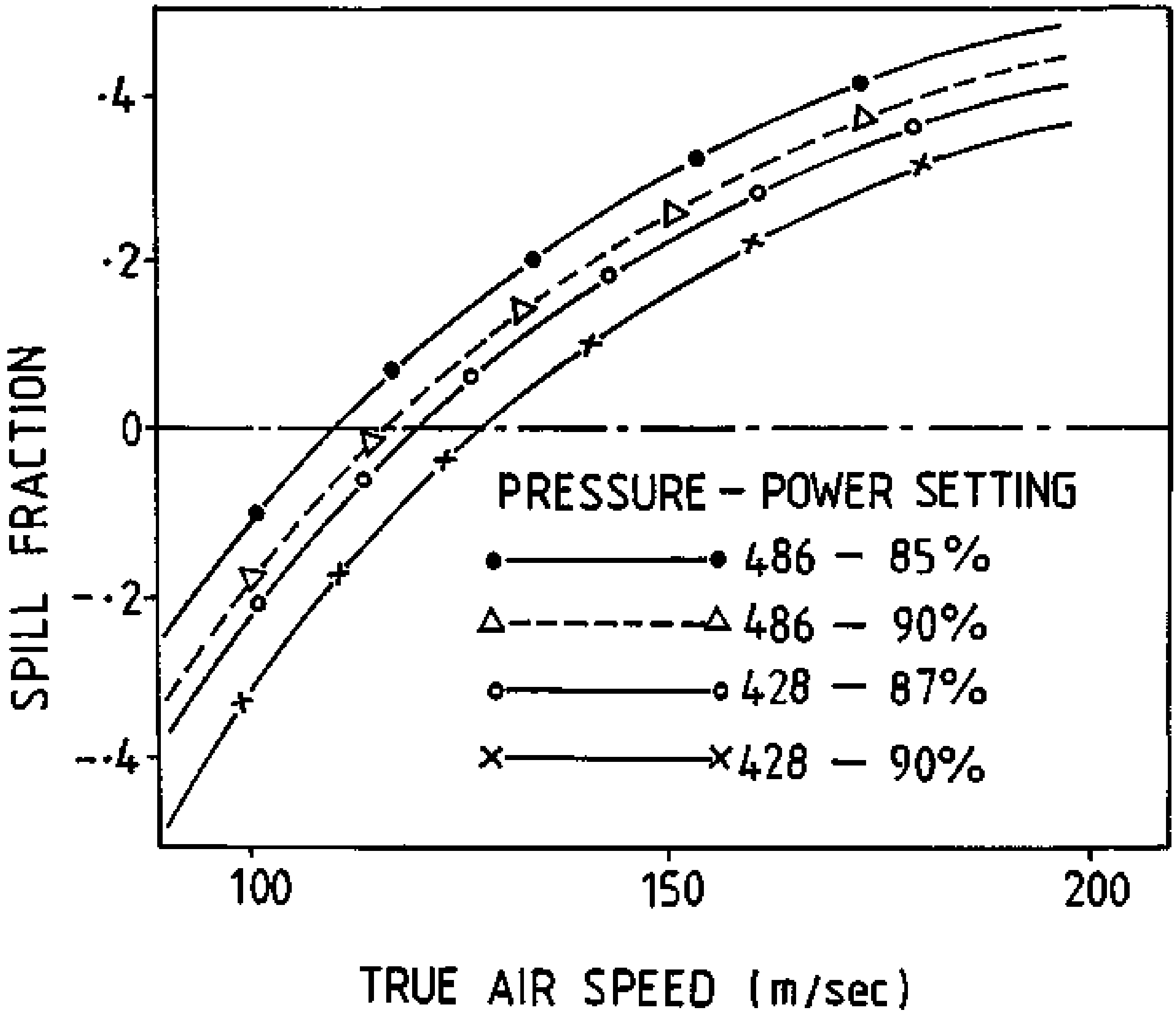

Fig. 3.8.1 The Spill Fraction (S.F.) as a function of True Air Speed (TAS), for four trials at constant power settings.

4.0 PROJECT RADAR

4.1 Radar move to Carolina

The Nelspruit radar was moved to Carolina for two reasons. First, the location at the Nelspruit airport site was far from ideal for rainfall measurements. Surrounding terrain forced the use of a 3 degree low level scan, but even at this elevation there was terrain blocking the radar beam from the southern around to the northwestern quadrant. The second reason was supplied by the Department of Water Affairs who were asked the question, "If a successful rain augmentation technology was to be developed, where would it first be used?" Their answer was in the region south and west of Carolina, where the Komati, Usutu and Vaal rivers have their headwaters. This is also the area where many of the country's inter basin transfer schemes are located.

The search for a new radar site centred around the town of Carolina, which is perched almost on top of the continental divide that separates rivers that flow east into the Indian Ocean and west into the Atlantic. A site at the local airport was finally chosen as the best compromise between an ideal radar site and the logistical problems of supplying power and communications. The new site will permit a low level scan of around 1.5 degrees.

Once the site had been selected permission to erect the radar on the airport had to be obtained from the Carolina Town Council. A meeting was held in the Town Hall in Carolina on September 15, 1987 at 14:00 hours. In attendance were the Carolina Town Council, representatives from the WRC and from CloudQuest. Permission in principle was obtained at this meeting. The next step was to survey the site and submit plans for approval to the Carolina Town Council and the Department of Civil Aviation. A professional surveyor from Ermelo was hired for this job. A copy of his survey is on file at Nelspruit.

Supplying power to the site was arranged through the Carolina Municipality. Three phase power was brought from the sewage plant about 900 m north of the airport via underground cables.

The move of the radar/computer system from Nelspruit to Carolina required careful planning. It was decided to move the radar and computer into a "kwikjak" mobile office unit being used as additional office space at Nelspruit. This unit, with 3 x 10 metres of floor space, had sufficient space for the radar, a small workshop and an office. The radar and computer, the airconditioners and all the associated internal and external wiring were installed by the end of January (1988). The Kwikjak, along with the radar antenna and pedestal were loaded onto a large flatbed and transported to Carolina.

The most important aspect of the site preparation at Carolina was the requirement for lightning protection for the sensitive solid state components in the radar and computer. The National Electrical Engineering Research Institute (NEERI) was consulted concerning the problem and they sent Mr David Meal to Carolina to take soil conductivity measurements. Armed with these measurements, he returned to Pretoria to design the required grounding network. Because of the relatively low conductivity of the soil at the site, a grid of copper ribbon was required, which was layed in metre-deep trenches that criss-crossed the site. This grounding plane was bonded to stakes driven into the soil as well as to the security fence that was erected around the site.

A tower for the radar antenna was erected, construction commencing in mid December. The tower was designed by a local engineer and contained one innovative feature; a built-in gantry which can lift the radar pedestal and antenna into position on the tower. This feature will greatly simplify radar antenna and pedestal maintenance.

The new site became operational in mid March of 1989. First radar data were acquired on March 16. A further 3 days of radar data were recorded during the remainder of the season. An initial comparison of these data to the radar data acquired at the Nelspruit site has not revealed any major differences between the two sets of data. One advantage of the new site is the ease with which the two project aircraft can be tracked. Such tracking, especially west of the radar, was always a problem at Nelspruit particularly at the lower heights at which the cloud base aircraft operates.

4.2 Comparisons of Storm Statistics - the Nelspruit versus the Carolina radar site

Because of the hydrological importance of the area south and west of Carolina and the poor radar site at Nelspruit, it was decided to move the project radar to Carolina. The move took almost a season to accomplish, the radar finally coming on line at its new location in March, 1988. The 1988/89 season, then, was the first full season with the radar operating at Carolina.

In the following, comparisons are made between storm track properties computed from the volume scan operations at Nelspruit during the seeding experiment (1984/85, 85/86, 86/87), and those computed from the scans retrieved at Carolina during the 1988/89 season. This work has an important bearing on the seeding experiment, in which radar-derived track properties of seeded and unseeded storms were compared. Any large discrepancies between the Nelspruit and Carolina radar data that is site related could cast doubts upon the validity of the Nelspruit radar data set and the results of the seeding experiment.

The first analysis presented here compares certain critical storm track properties acquired at Nelspruit to those acquired during the first season at Carolina. These are shown as cumulative frequencies (with the exception of storm direction of movement) in Fig. 4.2.1 (a) to (j). The surprise here, if any, is how similar the two sets of track properties are. Storms move a bit faster on the highveld (Fig. 4.2.1 (c)), have higher radar tops in the lowveld (Fig. 4.2.1 (d)), slightly greater volumes on the highveld (Fig. 4.2.1 (e)), seem to produce the same rain amounts as seen from either site (Fig. 4.2.1(g)), have slightly higher reflectivities, on average, at Nelspruit (Figs. 4.2.1(h) and (i)), but show distinctly higher maximum reflectivity heights when viewed by the radar located at Nelspruit (Fig.4.2.1 (j)). It is unlikely that the last result is site related. The radar at Nelspruit could be viewing more storms in which the coalescence precipitation formation mechanism is active. If this is the case, then we are sensing microphysical differences between predominantly lowveld and highveld storms. This may be an important result, since it is likely that cloud seeding techniques will be closely related to the microphysical characteristics of the storms that are to be treated.

The next analysis looks at certain critical track properties in 10 km annuli (Fig. 4.2.2(a) to (i)), to see how these change as a function of range from the radar. The number of tracks used in this exercise, along with the area and the track numbers normalized with respect to the 10-20 km annulus, are listed in Table 4.2.1.

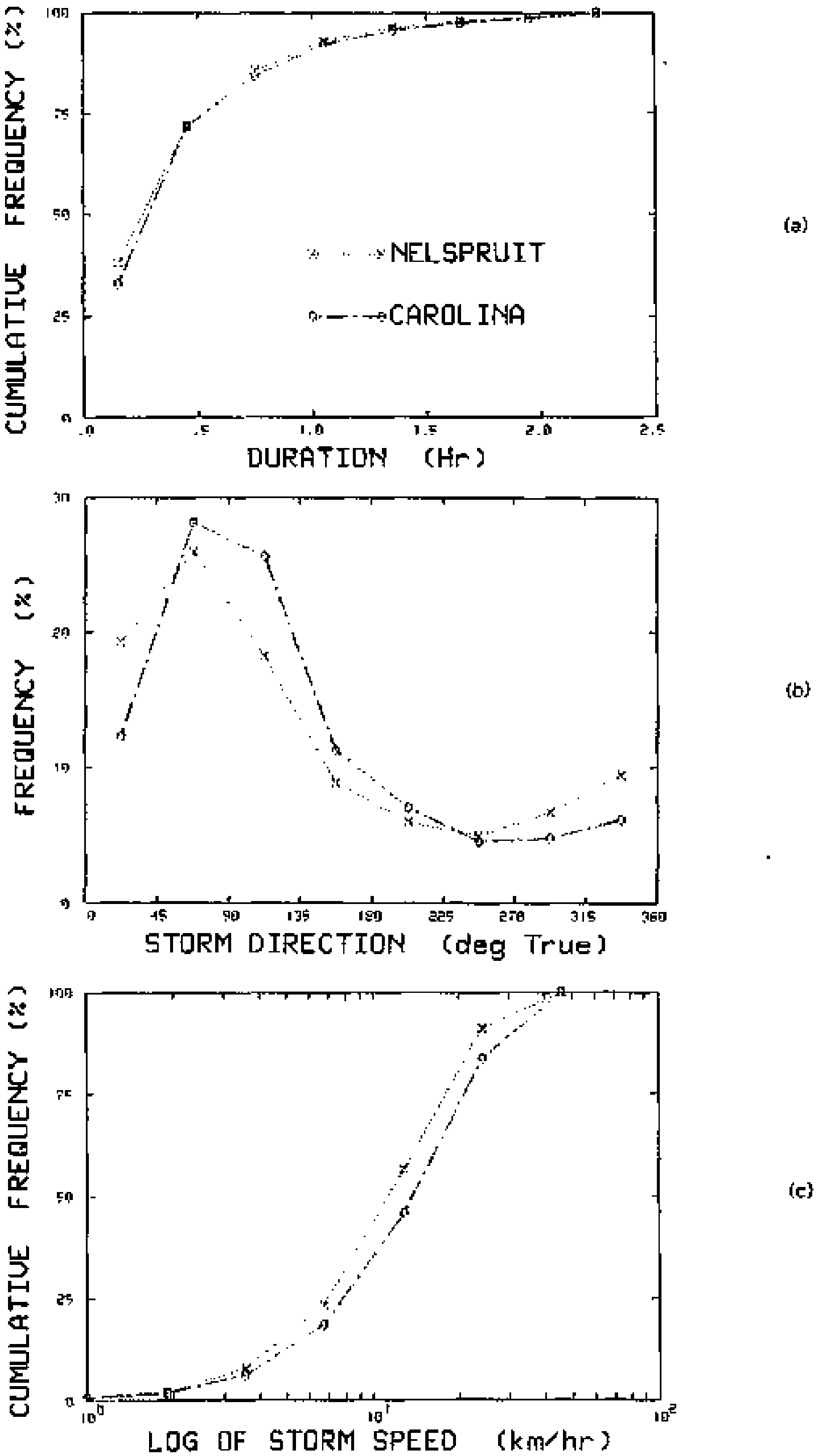

Fig. 4.2.1 A comparison of average storm track properties computed from radar data acquired at the Nelspruit and Carolina sites.

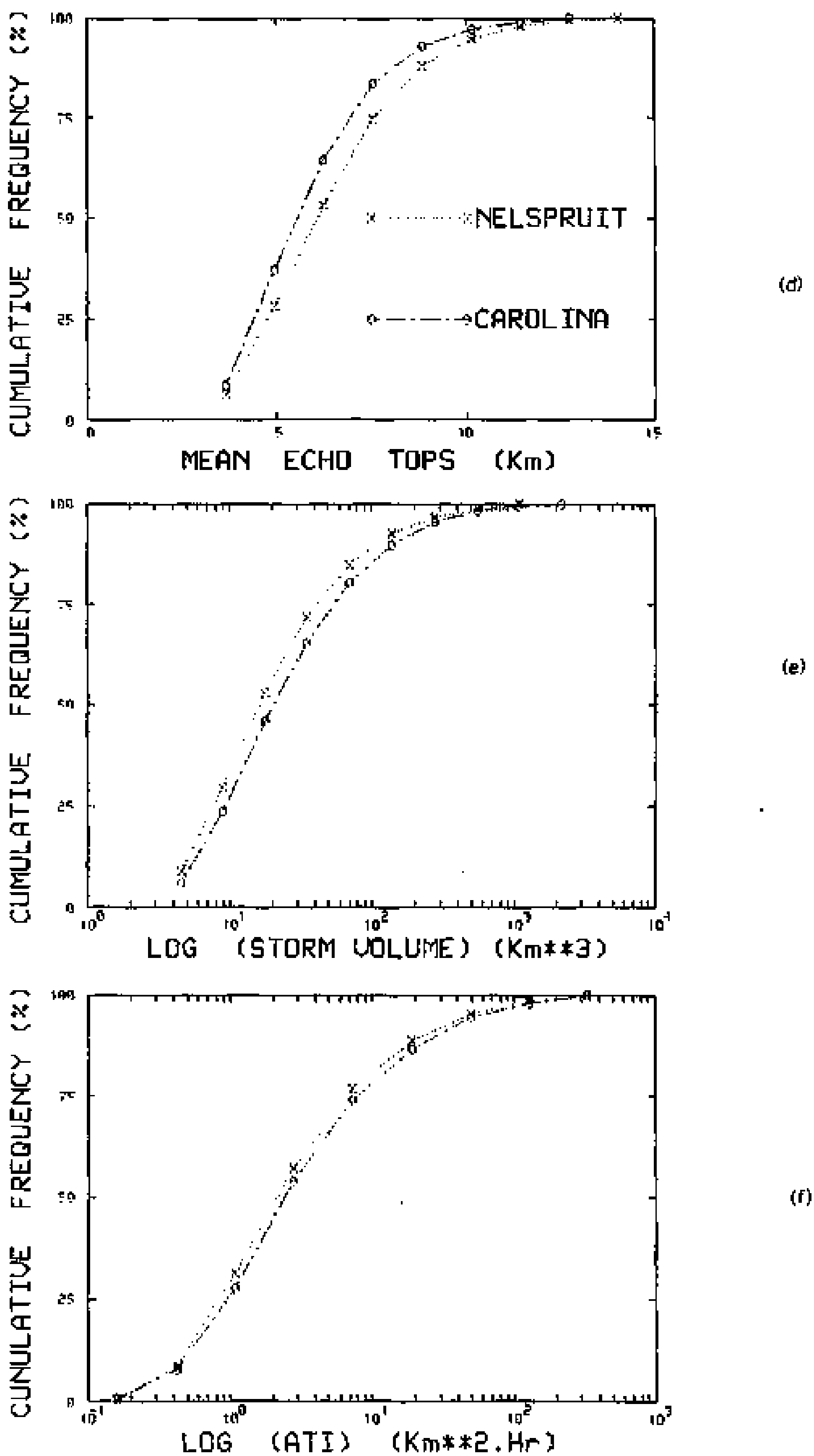

Fig. 4.2.1 continued

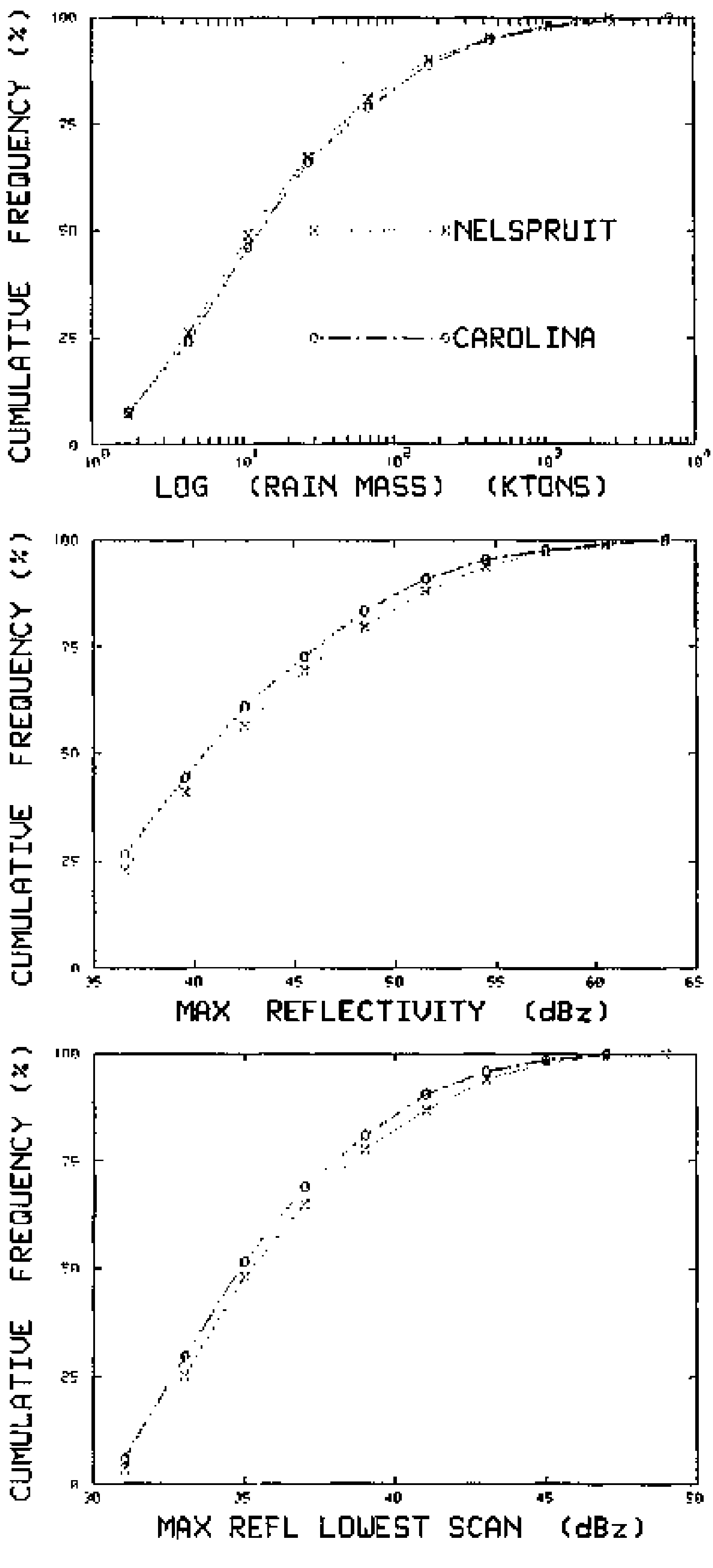

(g)

(h)

(i)

Fig. 4.2.1 continued

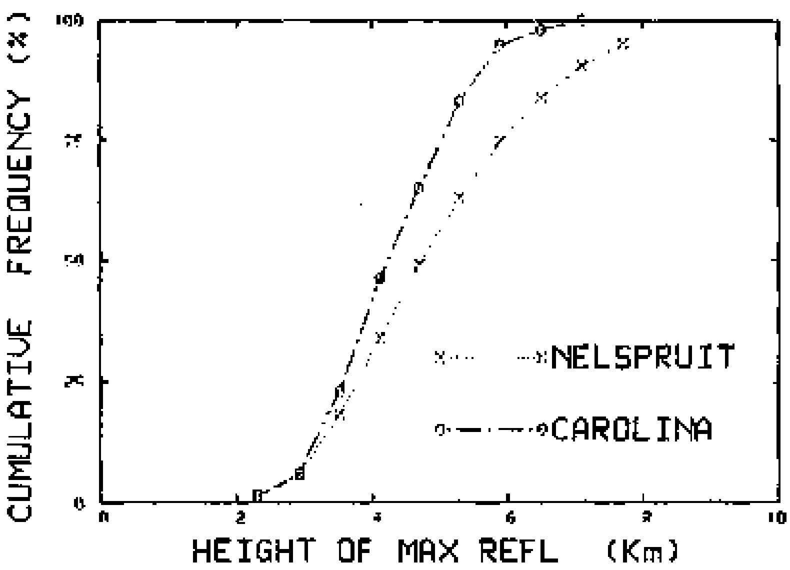

(j)

Fig. 4.2.1 continued

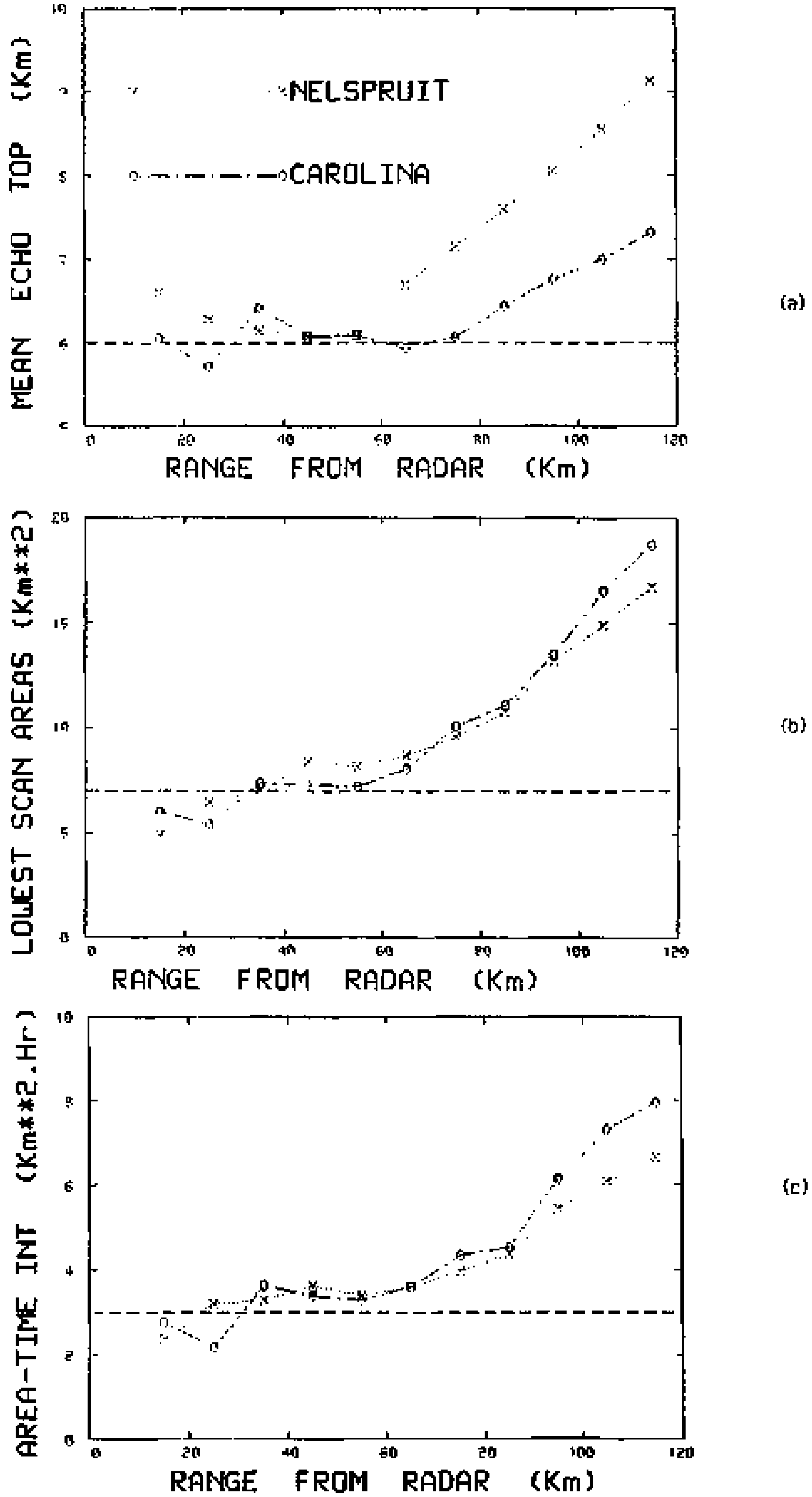

Fig. 4.2.2 The effects of distance from radar on average storm track properties acquired by the radar at Nelspruit and Carolina.

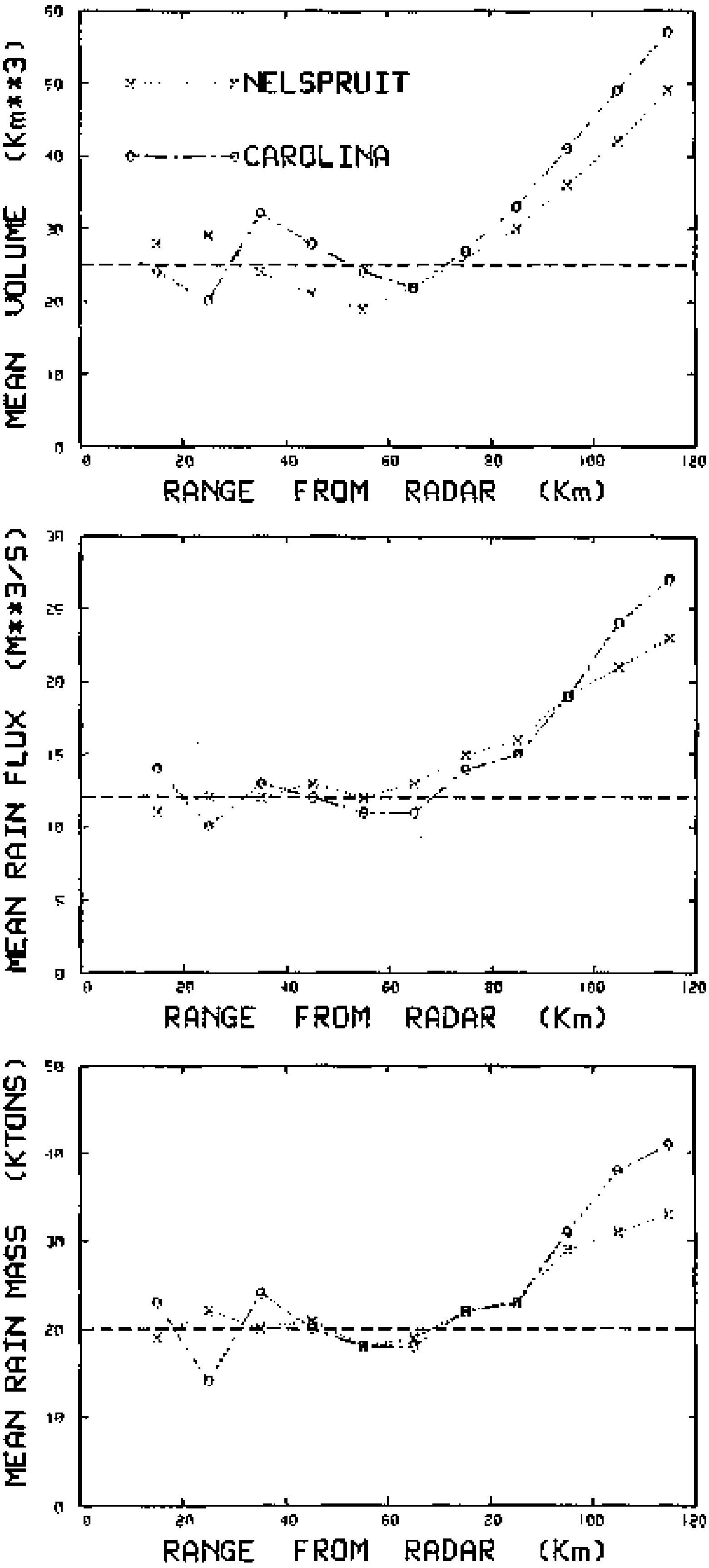

(d)

(e)

(f)

Fig. 4.2.2 continued

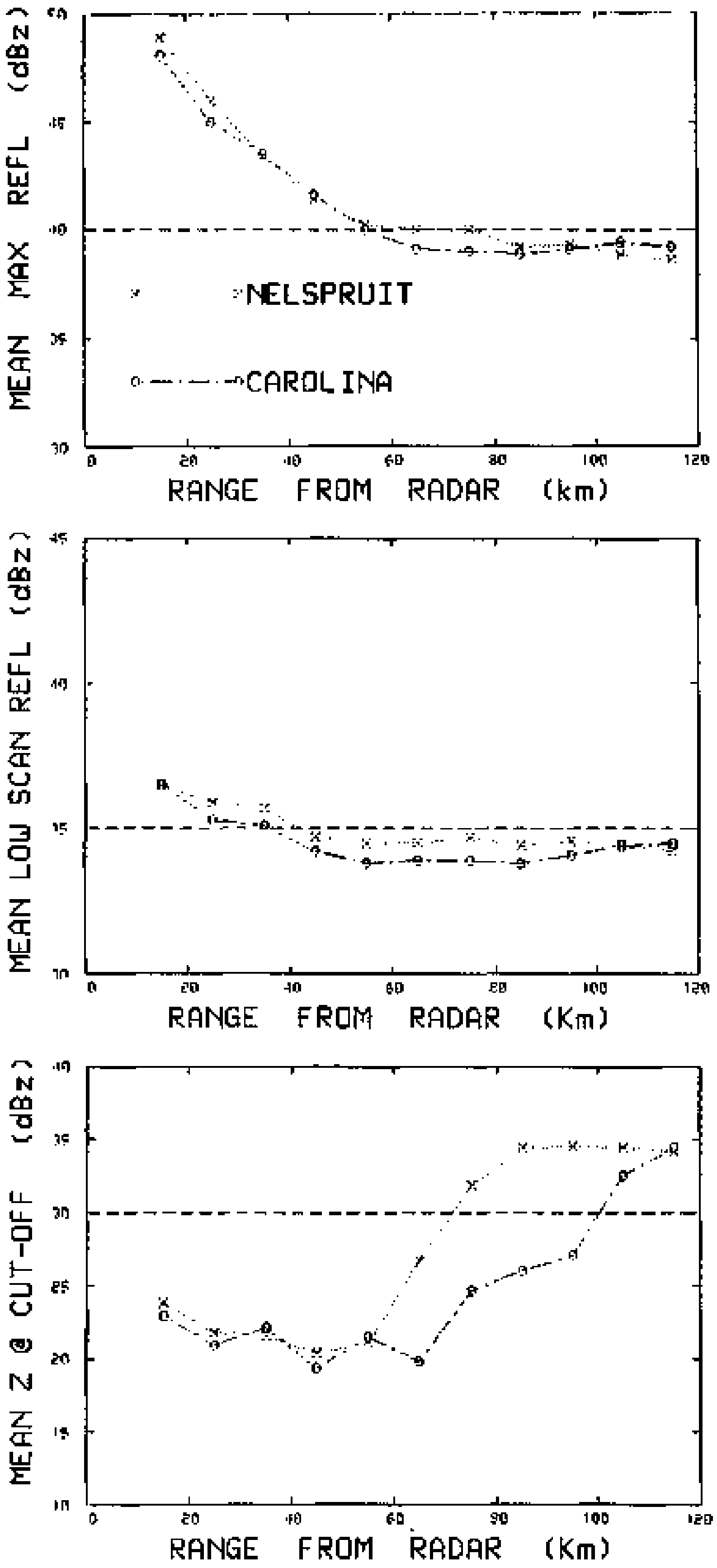

(g)

(h)

(i)

Fig. 4.2.2 continued

Table 4.2.1. Number of storm tracks per annulus

	NELSPRUIT			CAROLINA	
Annulus (Km)	Tracks	Norm Area	Norm Tracks	Tracks	Norm Tracks
10-20	312	1	1	94	1
20-30	487	1.7	1.6	125	1.3
30-40	793	2.3	2.5	154	1.6
40-50	1284	3.0	4.1	249	2.6
50-60	1468	3.7	4.7	328	3.4
60-70	1326	4.3	4.3	389	4.1
70-80	1261	5.0	4.0	378	3.9
80-90	980	5.7	3.1	328	3.4
90-100	723	6.3	2.3	306	3.2
100-110	540	7.0	1.7	285	3.0
110-120	372	7.7	1.2	266	2.8
TOTALS	9546			2900	

The storms used in this analysis represent 97 percent of all storms tracked at Nelspruit (9546/9856) and 93 percent of all tracks at Carolina (2900/3124). Another interesting statistic is that the average number of storms tracked at Nelspruit per operational day is 94 and at Carolina 174. This suggests that the radar is "seeing" more storms at Carolina, a result commensurate with the improved radar site. The most notable differences in the comparisons are mean echo top with height (Fig. 4.2.2(a)) and mean reflectivities at cut-off level (Fig. 4.2.2(i)). The apparent greater tendency at Nelspruit to overestimate storm heights as ranges increase beyond about 60 km from radar may result from the fact that more severe thunderstorms are viewed from Nelspruit than from Carolina (see Battan, pg 170). Another effect, common to both data sets, is the tendency to overestimate storm areas, volumes, rain fluxes and masses as range from the radar increases. This is especially evident beyond about 80 km. It is believed that this is caused by beam filling problems at the greater ranges which are solely a function of the geometry of the beam (beam width) and thus are common to both sites.

The reason for increases in intensities of the mean reflectivities at the cut-off level beyond 60 km for the Nelspruit data and 70 km for the Carolina storm set is not known.

It would appear from this exercise that a cautious approach to the analysis of storm track data from both sites would be to restrict the average range of storms from radar to 80 km or less.

5.0 THE BERG-EN-DAL WORKSHOP

(a) Introduction

One of the most important events of the past 3 years was the Workshop, held at the Berg-en-Dal camp in the Kruger Park from 21 to 23 August, 1989. The purpose of this workshop was to review the current status of rainfall augmentation research in South Africa, to assess the scientific needs and to recommend future short and longer term research objectives.

The workshop was attended by scientists, administrators and managers from the CSIR, the Weather Bureau, CloudQuest, the Department of Water Affairs and the Water Research Commission. Four scientists, tops in their fields, were invited from overseas. These were:

Dr Terry Clark	-	numerical modelling
Dr W A Cooper	-	cloud physics and instrumentation
Dr G Brant Foote	-	cloud physics and dynamics
Dr Paul L Smith	-	meteorological radars

(b) Recommendations

Only those recommendations by the overseas experts that directly affect the PAWS effort will be reviewed here.

(i) Field and analysis efforts are not in balance. More efforts should be devoted to:

- analysis of data
- construction and application of models
- publication of results

(ii) The state of the art of modelling is reaching the stage were it can make a significant contribution to experiments

- explore the possible use of a 2D model for Nelspruit, using realistic forcing effects including terrain
- expand collaborative efforts
- centralize modelling efforts

(iii) A shift in emphasis is needed. The results from the PAWS seeding experiment should be viewed as likely indicators of a seeding potential, but the most productive course at present is to <u>concentrate on understanding the physical processes involved</u>

(iv) Top priority for facilities should be to improve radar capabilities

- better sensitivity
- higher scan rates
- better resolution
- improved displays of data
- introduction of doppler and polarimetric capabilities where possible on existing radars

(v) There is a need to design and conduct experiments to clarify the following concepts:

- the dominance of the daughter or the feeder cell mechanism in multicell convective complexes. Such clarification is needed before seeding hypotheses can be formulated

- secondary ice production and attendant early glaciation

- large particle effects (from anthropogenic sources) upon the coalescence process

- the origins of natural ice, nucleation

- precipitation efficiencies, perhaps estimated by studying storm total water budgets

(vi) Organizational structure. It is difficult to be specific in this area, except that it is clear that people are a scarse resource in this field in South Africa. To keep the people already in the field, and to keep them productive requires an organizational structure that they will find comfortable. The structure should also be designed to attract top graduate students and other scientists to this important field of research.

(c) Summary

The Berg-en-Dal Workshop was a success from many angles. The calibre of the participation from the overseas scientists was excellent. It was an ideal opportunity for communication between the PAWS and the BPRP research efforts. Key administrators became aware, perhaps for the first time, of the progress and problems in the field of rainfall augmentation research. The awareness that South Africa has now become a world leader in this field of research was brought to the surface at the workshop by the invited scientists. Lastly, the venue was excellent. The Kruger Park camp was sufficiently isolated from the outside world that the usual interruptions experienced at conferences just did not occur. This kept the vital communications between the participants at a high level throughout the workshop.

6.0 DRAFT SEEDING HYPOTHESES - NELSPRUIT

(a) Introduction

At the recent Berg-en-Dal workshop it was pointed out that no matter how often an experiment is repeated and a statistical result obtained, the results of the experiment will not be fully accepted until the physical mechanism driving the observed (statistically significant) change is understood. It was decided that the confirmatory seeding experiment at Nelspruit should be suspended until a seeding hypothesis could be formulated and tested. The purpose of this note is to formulate such an hypothesis and to propose a method, using radars and instrumented aircraft, to test its validity.

There are two criteria that the seeding hypothesis must meet:

- it must be physically realistic, supported if possible by numerical cloud models

- the serial response of the storms after seeding should not be at odds with the pattern deduced from the statistical analysis of the 3 year randomized seeding experiment conducted at Nelspruit.

Years spent sampling thunderstorms in the Nelspruit area have led to the conclusion that a viable rain augmentation technology will be based upon increasing the efficiency of the existing rainfall processes. Qualitative observations indicate that much of the water vapour processed by local thunderstorms is lost to the anvil, since precipitation growth rates are not rapid enough to harvest much of the water vapour during the finite lifetimes of the rapidly rising cells which combine to form the multicell storms that are common to the region. Seeding technology should thus be focused on increasing the collection rate of the available supply of supercooled water by any means possible, such as:

- increasing precipitation growth rates
- introducing ice crystals earlier in the growth phase of convective cells
- initiating or enhancing coalescence
- others

(b) The Nelspruit seeding hypothesis

The proposed seeding hypothesis for Nelspruit has evolved from extensive microphysical measurements in the local clouds and from the results of the 3 year randomized seeding experiment. The pertinent results of this experiment will be briefly reviewed here.

Microphysical measurements in the Nelspruit clouds often reveal the presence of large (- 1 mm diameter) drops at $-10^{o}C$, indicating the presence of an active coalescence mechanism. It was discovered that the absence or presence of coalescence products at $-10^{o}C$ could be roughly defined by a ratio of the cloud base temperature to cloud buoyancy at 500 mb. The cloud base temperature is defined by the temperature at the convective condensation level (T_{ccl}) and the buoyancy at 500 mb is measured by the difference between a pseudoadiabat through the T_{ccl} and the environmental lapse rate (ΔT_{500}). When the ratio of the two ($T_{ccl}/\Delta T_{500}$) equals or exceeds 2.0, the probability is high that precipitation is forming via a condensation-coalescence process.

After the second season of the seeding experiment, this observation was applied experimentally to stratify the radar-acquired storms, eliminating those storms from the analysis which were unlikely to develop precipitation via the coalescence process ($T_{ccl}/\Delta T_{500} < 2.0$). The results were dramatic. Many of the radar-measured variables that are believed to indicate a seeding effect showed marked increases (decreases) in probability levels. Table 6.1, which contains the full three season data set, illustrates this result. (The following three tables from Section 2 of this report are repeated here for ease of reference).

Table 6.1 Results using the cloud base temperature/buoyancy ratio to stratify the radar data from the seeding experiment. Stratification - Range 10-80 km,
- Volume at decision time: 0-750 km^3

Mean	-10 to 0	0 to 10	10 to 20	20 to 30	30 to 40min
Rain flux	4	-3	-12	-18	17
Storm Volume	1	-3	-15	-11	8
Storm area	2	-4	- 8	- 6	15%
<u>Cases</u>					
Seed	47	51	49	47	38
No Seed	60	63	62	61	52

Stratification - Range : 10 - 80 km
- Volume at decision time : 0 - 750 km^3
- $T_{ccl}/\Delta T_{500}$: > 2.0

Table 6.1 (cont.)

Mean	-10 to 0	0 to 10	10 to 20	20 to 30	30 to 40 min.
Rain flux	27	17	17	32	76*
Storm Volume	20	17	19	26	42*
Storm area	16	7	10	16	43* %
<u>Cases</u>					
Seed	38	40	39	38	31
No Seed	47	49	47	47	39

*Significant at 0.05 or better

All percentages calculated from : $\frac{\text{Seed - No seed}}{\text{No seed}} \times 100$

The division of the storm case tracks into 10 minute time windows as in Table 6.1, produced additional insights. Perhaps the strongest apparent response to seeding (largest difference between seed and no seed storm tracks) occurs in the first 10 minutes following seeding in the radar-observed distribution of storm mass with height (see Table 6.2).

Table 6.2 Differences between radar-observed maximum rates of increase in mean storm mass with height; seed versus no seed storms.

Mass=f(Height)	-10 to 0	0 to 10	10 to 20	20 to 30	30 to 40min
Max.rates of increase	10	129*	66*	-10	3
Max. rates of decrease	-9	6	11	57*	8 %

*Significant at 0.05 or better

What appears to be happening is that the hydrometeors visible to the radar in seeded storms are moving upwards at a faster rate immediately after seeding than those in the untreated storms. There are at least three hypotheses that might explain this observation:

1. The glaciogenic seeding is releasing latent heat from freezing super cooled water drops. This increases cloud buoyancy (updraft) resulting in higher particle trajectories.

2. The addition of ice crystals to a region of the cloud when none exists naturally causes higher radar reflectivities aloft.

3. The freezing of drops in the cloud which now grow much faster as graupel than they would have had they remained unfrozen (Johnson, 1987)

Hypothesis 1 by itself is not likely to produce the observed results. The additional buoyancy is not great, less than $1^{o}C$ and would be released anyway. If the early release of this latent heat were significant, an increase in cloud top heights should be observed, which is not the case.

Hypothesis 2 operates too slowly to lead to radar observed differences between seeded and unseeded clouds within 10 minutes of seeding. Also, application of the cloud base temperature/buoyancy ratio stratification should not affect the signal if mechanism 2 were dominant.

Hypothesis 3 has the strongest appeal. First, it depends upon the existance of small drops and these are assured by the cloud base temperature/buoyancy ratio partition. Freezing the water drops results in higher trajectories for the less dense graupel particles. Modelled trajectories in Johnson's paper show that starting from the same point in a cloud, a drop that freezes and grows as a graupel particle would arc more than 1 km higher in the cloud than would a water drop after 10 minutes. It would also have twice the mass and about the same radar reflectivity. The longer trajectory of the graupel particle in the model cloud means that it reaches the ground some 5 minutes after it would have as a water drop but with about 15 times the mass (more than twice the melted diameter).

Radar measured differences between seeded and unseeded storms affected by hypothesis 3 would, in sequence, appear as follows:

- higher particle trajectories should appear as increases in the rates of rise of radar reflectivities in seeded clouds soon after treatment

- large melted graupel reaching the ground from seeded storms some minutes later than smaller drops from seeded storms would produce higher radar reflectivities at low scan angles (base PPI) some 20 to 30 minutes after seeding

- the higher trajectories would cause greater dispersion of the less dense graupel particles, thus the precipitation from seeded storms would cover larger areas.

All the above differences, predicted to appear in comparisons between seeded and unseeded storms and caused by the differential growth rates of recently frozen and unfrozen drops, are observed in the analysis of the radar results from the 3 year randomized seeding experiment at Nelspruit (see Tables 6.1 and 6.2).

It is important to note here that it is primarily the longer residence time in the cloud that permits the graupel to grow larger than the water drops, and it is this longer residence time that harvests more water from the cloud, thereby increasing the efficiency of the precipitation process. Thus, the proposed mechanism requires large, long lasting clouds.

One of the more curious results from the 3 year seeding programme was that seeded storms appeared to be moving faster than unseeded storms. This curious observation is not at odds with hypothesis 3. The higher trajectories of the graupel created by seeding would send these new particles into regions of higher wind speeds. These particles would then precipitate farther downwind, causing a radar-observed increase in seeded storm speeds.

In summary, then, a Nelspruit seeding hypothesis should not conflict with the results of the 3 year seeding experiment. The hypothesis tested by this experiment was that there would be radar recognized differences between seeded and unseeded storms. The experiment resulted in the rejection of the null hypothesis, that is, there were significant differences measured by radar between the randomly selected seeded and unseeded storm tracks. It was the hope that these differences would be physically revealing, leading us towards the formulation of a rational seeding hypothesis. This we believe has happened. The paper by Johnson (1987) has been of great help to us in this process, forming the sought after link between the aircraft microphysical measurements and the results of the seeding experiment.

The next step is to thoroughly test the seeding hypothesis.

(c) Seeding hypothesis testing

Three tools will be used to test the validity of hypothesis 3 above. These are:

- the Learjet
- the cloud base aircraft
- the 5 cm project radar

The best sampling windows for the aircraft would appear to be in the first 10 minutes after seeding at cloud top and 20 to 30 minutes later at cloud base. The cloud top measurements will concentrate on sampling any graupel produced by the seeding. It will be important to recognize whether the graupel originates from frozen drops or ice crystals. The Lear's capability to measure graupel densities will feature prominently in this exercise. The availability of a second aircraft to penetrate and sample the seeded turret would greatly increase the likelihood of encountering any graupel produced by the seeding.

The longer residence time in seeded clouds should result in the melted diameters of the graupel exceeding the drop diameters from untreated clouds. This should become evident some 20 to 30 minutes after seeding commences, provided the sampling can take place close enough to the melting level, that is, before drop break-up and collisions blur the seeding effect.

Radar will be used in sector scan mode, producing a complete volume scan of the experimental storm in less than 2 minutes. This measurement will concentrate on comparisons of seeded and unseeded storms in efforts to trace any precipitation formation trajectories that are being altered by the seeding.

7.0. CO-OPERATION WITH THE BETHLEHEM GROUP

(a) Introduction

The Nelspruit group participated in a workshop on cloud physics research held at Bethlehem on the 17th and 18th of November, 1987 (See Proceedings, 1987). At this workshop, the offer was made to bring the Nelspruit Learjet to Bethlehem to engage in joint research flights with the Bethlehem project aircraft. This offer was accepted, and a combined research effort was scheduled, to take place at Bethlehem from the 7th to the 18th of December 1987. The log containing the details of the flights flown during this period is shown in Table 7.0.

Table 7.0 Flight Log - Bethlehem flights

Date	Time	Description
8 Dec 87	1:25	Clear air comparisons: LTK and JRA
9 Dec 87	1:10	Tower fly-by
11 Dec 87	1:50	In-cloud comparisons: LTK, JRA, JRB
12 Dec 87	1:10	In-cloud comparisons: LTK, JRA, JRB
14 Dec 87	1:50	In-flight join-up: LTK and JRA
14 Dec 87	:55	Serial cloud penetrations: LTK and JRA
15 Dec 87	1:35	Serial cloud penetrations: LTK and JRA
17 Dec 87	1:25	West-east storm comparisons
18 Dec 87	1:05	APIPs search: LTK and JRA

NOTES: LTK - Nelspruit Learjet

JRA and JRB - Bethlehem Commander 690As

(b) Calibration flights

The clear air comparisons with the Bethlehem Commander and the Nelspruit Learjet are shown in Table 7.1. Except for the dewpoint measurements, the comparisons are extremely close. Static temperatures, a measurement that incorporates airspeed and altitude, are generally within half a degree Celsius. Dewpoints are measured by different sensors and do not agree at the colder temperatures. The Nelspruit Learjet has the Cambridge dewpoint (frost point) system which claims accuracies of plus or minus $0.6^{o}C$ down to $-30^{o}C$, but response is generally slow at the colder temperatures. At warmer temperatures ($> -15^{o}C$) agreement is within about 1.5 degrees.

TRUE AIRSPEED (m/s)			PRESS (mb)			STATIC TEMP (°C)			DEW POINT (°C)		
LTK	JRA	DIFF	LTK	JRA	DIFF	LTK	JRA	DIFF	LTK	JRA	DIFF
110.0	110.4	-0.4	461.8	462.3	-0.5	-7.8	-8.6	0.8	-26.7	-39.1	12.4
105.8	107.5	-1.7	463.3	462.1	1.2	-7.3	-7.7	0.4	-25.4	-35.	10.2
111.5	113.5	-2.0	462.9	462.1	0.8	-8.0	-8.3	0.3	-28.5	-38.8	10.3
120.8	121.9	-1.1	462.0	462.8	-0.8	-8.2	-8.1	-0.1	-28.8	-38.2	9.4
126.6	127.6	-1.0	462.0	462.6	-0.6	-8.4	-8.0	-0.4	-31.0	-38.1	7.1
97.2	99.5	-0.7	569.6	568.5	1.1	1.3	1.0	0.2	-22.5	-28.2	5.7
104.9	105.4	-0.5	569.4	569.0	0.4	1.0	1.0	0	-22.6	-28.0	5.4
109.4	111.2	-1.8	569.5	568.5	1.0	1.0	1.0	0	-22.9	-29.2	6.3
115.9	117.7	-1.8	569.4	568.7	0.7	1.1	1.4	-0.3	-23.7	-31.9	8.2
126.2	126.5	-0.3	568.1	568.5	-0.4	0.7	1.5	-0.8	-24.5	-32.1	7.6
91.0	91.0	0	694.1	695.6	-1.5	10.0	9.8	0.2	-7.9	-9.1	-1.3
99.2	98.4	0.8	693.1	695.5	-2.4	10.2	10.0	0.2	-10.2	-9.0	-1.2
101.7	102.3	-0.6	694.5	695.5	-1.0	10.2	9.7	0.5	-8.3	-6.9	-1.4
108.6	109.6	-1.0	694.0	695.5	-1.5	9.7	10.0	-0.3	-5.9	-6.2	-0.7
116.9	117.5	-0.6	692.9	695.2	-2.3	10.5	10.6	-0.5	-13.9	-15.2	1.3
MEAN DEVIATION		-0.8			-0.4			0.01			5.2

Table 7.1 LTK and JRA clear air intercomparisons

TIME	TEMP (°C)			DEWPOINT (°C)			PRESS (mb)			TAS
SAST	LTK	TOWER	DIFF	LTK	TOWER	DIFF	LTK	TOWER	DIFF	(m/s)
06:23:43	13.0	14.0	-1.0	11.3	12.5	-1.2	828.4	833.5	-5.1	89.6
06:27:53	13.2	14.0	-0.8	11.5	12.6	-1.1	831.1	833.5	-2.4	96.7
06:11:48	13.0	13.7	-0.7	11.4	12.7	-1.3	830.6	833.6	-3.0	89.6
06:15:40	13.1	13.8	-0.7	11.2	12.4	-1.2	830.2	833.7	-3.5	93.8
06:27:50	12.9	13.8	-0.9	11.2	12.6	-1.4	828.6	833.2	-4.6	98.1
06:31:55	13.0	13.9	-0.9	11.2	12.7	-1.5	828.6	833.3	-4.7	113.2
06:35:56	13.5	14.0	-0.5	11.4	12.8	-1.4	829.4	833.3	-3.9	106.3
06:39:39	13.0	14.1	-1.1	11.7	12.7	-1.0	827.4	833.4	-6.0	127.9
06:43:48	13.3	14.3	-1.0	11.3	12.8	-1.5	827.7	833.4	-6.0	122.2
06:47:30	13.0	14.4	-1.4	12.0	13.1	-1.1	825.8	833.3	-7.5	139.3
06:51:05	13.1	14.8	-1.7	11.8	13.0	-1.2	825.2	833.4	-8.2	137.9
06:54:29	15.1	14.8	0.3	11.3	13.2	-1.9	819.9	833.3	-13.4	159.7
06:56:41	14.4	14.7	-0.3	11.2	13.0	-1.8	819.4	833.3	-13.8	159.7
MEAN DEVIATION			-0.8			-1.4			-6.3	

Table 7.2 Tower fly-by comparisons

Results from the tower fly-by flights for LTK are listed in Table 7.2. The Learjet is measuring temperatures on average about 0.8°C colder than the tower, and lower average dewpoints (-1.4°C). Since

$$T_S = T_T \, (P_S/P_T)^{2/7}$$

where:

T_S = static temperature (°K)

T_T = total temperature (°K)

P_S = static pressure (mb)

P_T = total pressure (mb),

it can be shown that a 6 mb error in static pressure measurement under these tower fly-by conditions can lead to an error of about 0.6°C, which would account for most of the average deviations of the aircraft from tower temperatures shown in Table 7.2. However, since the two aircraft measurements (LTK and JRA) of state parameters agree so well in the clear air comparisons (Table 7.1), which are close to the normal operating range of the Learjet when making cloud physics measurements, the application of a correction factor (such as for static position error) is not warranted at this time.

8.0 SUMMARY

One of the most important messages in this report concerns the seeding experiment. The number of different analyses that have been conducted since the end of the experiment and the publication of poorly interpreted and partial results using limited data sets have caused confusion about the outcome of the experiment and seriously blunted the impact that this experiment should be exercising on future research efforts and experimental designs. Section 2 of this report is an attempt to cut through this confusion by reviewing the important features of this experiment and highlighting the initial results, results that were (as they should be) linked to plausible physical changes in the seeded storms. In retrospect, it seems clear that these results should have been published in the reviewed literature as soon as possible after the completion of the experiment. This might have lessened the current confusion concerning the multiplicity of results that are now scattered through several publications.

It is clear that the CRAWS Learjet, as a cloud physics measurement platform, has finally come of age. The mix of instruments on the jet, some of which have been developed locally, are capable of making the sorts of measurements that are required to illuminate the dominant precipitation formation mechanisms operating in specific areas. The system is also capable of accurately assessing local precipitation efficiencies, here defined as the amount of available cloud water that has been converted into precipitation (complete conversion equals 100 percent efficiency). Understanding the local precipitation formation mechanisms and their efficiencies is viewed as a key to developing a successful rain augmentation technology.

It has taken years of effort to build the instrumentation system now flying on the CRAWS Learjet. This facility should be viewed as a valuable National asset.

A possibly important lesson has been learned by a fortuitous encounter with a storm that had been substantially modified by the effluent from a paper mill. We must be very careful not to get locked into a single method or material for cloud seeding. As our knowledge of the physics of clouds expands, we may be able to devise a treatment (or several treatments) uniquely suited to the local brand of storms.

In the short term, future efforts must be concentrated upon:

- learning the best methods of measuring storm rainfall, for it appears as if the multicell storm will be the experimental unit for some time to come. The use of a properly instrumented cloud base aircraft looks like a promising approach to this problem

- develop and validate, by careful physical measurements, a seeding hypothesis. This must be accomplished before proceeding with the confirmatory experiment

- build a structure that is capable of efficiently focusing the limited available assets (personnel and equipment) upon the goal of developing a viable rainfall augmentation technology that can be shown to supplement South Africa's limited water supplies.

APPENDIX I

1. Phase II seeding experiment

The Phase II seeding experiment will be based upon the techniques and experience acquired during the first seeding experiment. Only two changes have been made in experimental design:

(a) The randomization has been changed from a three-way to a two-way design with the elimination of the no-seed/sample category. This has occurred because of the belief that aircraft-produced ice particles (APIPs) are affecting the control (non-seeded) group of storms.

(b) The experimental area has been changed to the area where a successful seeding technology would probably first be applied. This change led to relocating the project's 5 cm radar to a site on the Carolina airport.

Aspects of the new experiment not contained in the experimental rules (Section 2 of this Appendix) are listed below:

(a) Standard volume scan procedures will be used except the radar in its new location has a low level scan of 1.5 degrees, resulting in a slightly different scan sequence from that used in the first experiment.

(b) Since seeding will no longer be "double blind", it will be essential for an analyst, who is unaware of the treatment, to conduct the evaluation of the radar data. Basically, this means selecting the experimental storm tracks, since all the other analytical techniques are in place.

(c) Evaluation will be based upon radar-measured values of rain flux (m^3/sec) and rain mass (Ktons), also called radar-estimated rain volume (RERV).
Analyses of the seeded and unseeded storm track properties will be divided up into 10 minute segments with reference to "decision time" (t=0).
Statistically significant differences between seeded and unseeded storm rain fluxes and rain volumes are expected to appear some 20 to 30 minutes after t=0.

2. Experimental Rules

09:00 Preliminary forecast - on GO and STANDBY, radar operator leaves for Carolina

10:00 BRIEFING and forecast: NO GO, STANDBY, GO

On GO and STANDBY days:

Preflight and DAS check IZN and LTK
Make dry ice

11:00 Commence volume scan at Carolina
Launch IZN when one isolated storm exceeds 40 dBZ
Launch LTK when two separate storms exceed 40 dBZ
Attempt to vector both aircraft to the same storm

Once LTK selects an experimental storm, this decision will be relayed to the radar operator who will then open one of a sequence of envelopes containing randomized seed/no-seed decisions (decision time).

SEED - carry on seeding the target storm for as long as possible. Four conditions will signal termination of the experiment:

- new turret development ceases or becomes obscured in enveloping cloud
- dry ice is consumed
- aircraft low on fuel
- storm moves out of experimental area

NO SEED - aircraft will mark storm by twice orbiting the area in which the new development is occurring, then will seek a second target storm at least 20 nautical miles (storm centre to storm centre) from initial target.

After the last experiment of the flight (no new experiments will be chosen when fuel quantity drops below 2500 pounds) the Lear will descend to cloud base, then complete a near storm sounding to 25 000 feet before returning to base.

16:00 Close down radar if no echoes have been detected all day

17:00 Latest time for launching the Learjet

19:00 Radar shutdown, or earlier if all storm activity ceases.

3. Experimental rules for radar site at Carolina

1. Radar calibrations - every Monday

2. On "Standby" and "Go" forecasts:
   - commence Volume Scan by 11:00 A.M.

NOTES:

This will mean leaving Nelspruit by 09:00 by car, or 10:00 by aircraft.

- phone Nelspruit to confirm status at 11:00 A.M.
- if no radar echoes develop by 16:00 close down operations
- continue volume scan until 19:00 or until all echoes have dissipated (< 40dBZ).

3. Scramble criteria:

   - one radar echo within 60 nautical miles exceeds 40 dBZ, scramble IZN
   - two distinctly separate radar echoes simultaneously exceed 40 dBZ, scramble LTK.

NOTES:

Radar logs and tapes must be brought to Nelspruit the morning following operations and given to Erika Botha. A Carolina log will be retained at the radar site. This log will be used to record all problems experienced at the site, such as equipment failures, power outages, suggestions, complaints, etc.

References

Biter, C.J., J.E. Dye, D. Huffman and W.D. King, 1987: The drop-size response of the CSIRO liquid water probe. J. Atmos. Oceanic Technol. 4, 359-367.

Braham, R.R., Jr., 1986: The cloud physics of weather modification. Part 1: Scientific basis. WMO Bull., 35, 215 - 221.

Brown, N.E., and R.R. Braham, Jr., 1963: Precipitation particle measurements in cumulus congestus. J. Atmos. Sci., 20, 23-28.

Browning, K.A., 1977: The structure and mechanisms of hailstorms. Meteorological Monographs, 16, No 38, American Meteorological Society, 1-60.

Bruintjes, R.T., A.J. Heymsfield and T.W. Kraus, 1987: An examination of double-plate ice crystals and the initiation of precipitation in continental cumulus clouds. J. Atmos. Sci., 44, 1331-1349.

Changnon, S.A., R.G. Semonin, A.A. Auer, R.R. Braham and J. Hales, 1981: METROMEX: A review and summary. Meteor. Monogr. 18, Amer. Meteor. Soc., Boston 181 pp.

-------, and F.A. Huff, 1986: The urban-related nocturnal rainfall anomaly at St. Louis. J. Climate Appl. Meteor., 25, 1985-1995.

Cooper, W.A., 1978: Cloud physics investigations by the University of Wyoming in HIPLEX 1977. Report No AS119, Department of Atmospheric Science, University of Wyoming 29-32.

Eagan, R.C., P.V. Hobbs and L.F. Radke, 1974(a): Particle emissions from a large kraft paper mill and their effects on the microstructure of warm clouds. J. Appl. Meteor., 13, 535-552.

-------, --------- and ----------, 1974(b): Measurements of cloud condensation nuclei and cloud droplet size distributions in the vicinity of forest fires. J. Appl. Meteor., 13, 553-557.

Galpin, J.S., 1988: Preliminary analysis of radar data concerning the Nelspruit cloud seeding experiment. CKOMP 88/7, CSIR, Pretoria, pp 27.

Green, A.W., 1975: An approximation for the shapes of large raindrops. J. Appl. Meteor., 14, 1578-1583.

Heymsfield, A,J., and J.L. Parrish, 1978: A computational technique for increasing the effective sampling volumes of the PMS two-dimensional particle size spectrometer. J. Appl. Meteor., 17, 1566-1572.

----------, and D. Baumgardner, 1985: Summary of a workshop on processing 2-D probe data. Amer. Meteor. Soc., 66, 437-440.

Johnson, D.B., 1987: On the relative efficiency of coalescence and riming. J. Atmos. Sci., 44, 1671-1680.

Kessler, E., 1969: On the distribution and continuity of water substance in atmospheric circulations. Meteorological Monographs Vol 10, No 32, American Meteorological Society.

Kraus, T.W., R.T. Bruintjes, J. Verlinde and A. Kahn, 1987: Microphysical and radar observations of seeded and unseeded continental cumulus clouds. J. Climate Appl. Meteor., 26, 585-606.

Leighton, H.G., and R.R. Rogers, 1974: Droplet growth by condensation and coalescence in a strong updraft. J. Atmos. Sci., 31, 271-279.

Mader, G.N., 1979: Numerical study of storms in the Transvaal. S. African Soc. J. 61, No 2.

Mather, G.K., B.J. Morrison and G.M. Morgan, Jr., 1986: A preliminary assessment of the importance of coalescence in convective clouds of the Eastern Transvaal. J. Climate Appl. Meteor., 25, 1780-1784.

---------, 1989: Estimates of precipitation embryo densities using measurements from an aircraft radar. J. Appl. Meteor., 28, 1089-1097.

Morgan, G.M., Jr., B.J. Morrison and G.K. Mather, 1989: Measurement of total and condensed water mixing ratios in warm based cumulus clouds by a jet engine evaporation technique. To be published in Theoretical and Applied Climatology, Springer and Verlag, Vienna.

PAWS Final Report - Phase I, 1983-86 Vols. I - IV. WRC Report Nos 133/1/88, 133/2/88, 133/3/88 and 133/4/88.

Pfaum, J.C., and H.R. Pruppacher, 1979: A wind tunnel investigation of the growth of graupel initiated from frozen drops. J. Atmos. Sci., 36, 680-689.

Rangno, A.L., and P.V. Hobbs, 1983: Production of ice particles in clouds due to aircraft penetrations. J. Climate Appl. Meteor., 22, 214-232.

Smith, P.L., 1982: On the graphical presentation of raindrop size data. Atmosphere - Ocean, Can. Met. and Ocean. Soc., 20, 4-16.

-------, 1984: Equivalent radar reflectivity factors for snow and ice particles. J. Climate Appl. Meteor., 23, 1258-1260.

Sulakvelidze, G.K., 1974: Progress of hail suppression work in the USSR. Weather and Climate Modification, Edited by W.N. Hess, 410-431.